


Article

Electron Symmetry Breaking during Attosecond Charge Migration Induced by Laser Pulses: Point Group Analyses for Quantum Dynamics

Dietrich Haase ¹, Gunter Hermann ², Jörn Manz ^{1,3,4,*}, Vincent Pohl ² and Jean Christophe Tremblay ⁵ 
¹ Institut für Chemie und Biochemie, Freie Universität Berlin, 14195 Berlin, Germany; dhaase@chemie.fu-berlin.de

² QoD Technologies GmbH, Freie Universität Berlin, 14195 Berlin, Germany; gunter.hermann@fu-berlin.de (G.H.); v.pohl@fu-berlin.de (V.P.)

³ State Key Laboratory of Quantum Optics and Quantum Optics Devices, Institute of Laser Spectroscopy, Shanxi University, Taiyuan 030006, China

⁴ Collaborative Innovation Center of Extreme Optics, Shanxi University, Taiyuan 030006, China

⁵ Laboratoire de Physique et Chimie Théoriques, CNRS-Université de Lorraine, UMR 7019, 57070 Metz, France; jean-christophe.tremblay@univ-lorraine.fr

* Correspondence: jmanz@chemie.fu-berlin.de

Abstract: Quantum simulations of the electron dynamics of oriented benzene and Mg-porphyrin driven by short (<10 fs) laser pulses yield electron symmetry breaking during attosecond charge migration. Nuclear motions are negligible on this time domain, i.e., the point group symmetries $G = D_{6h}$ and D_{4h} of the nuclear scaffolds are conserved. At the same time, the symmetries of the one-electron densities are broken, however, to specific subgroups of G for the excited superposition states. These subgroups depend on the polarization and on the electric fields of the laser pulses. They can be determined either by inspection of the symmetry elements of the one-electron density which represents charge migration after the laser pulse, or by a new and more efficient group-theoretical approach. The results agree perfectly with each other. They suggest laser control of symmetry breaking. The choice of the target subgroup is restricted, however, by a new theorem, i.e., it must contain the symmetry group of the time-dependent electronic Hamiltonian of the oriented molecule interacting with the laser pulse(s). This theorem can also be applied to confirm or to falsify complementary suggestions of electron symmetry breaking by laser pulses.

Keywords: attosecond chemistry; benzene; charge migration; group theory; laser control; Mg-porphyrin; point groups D_{4h} , D_{6h} and subgroups; symmetry breaking



Citation: Haase, D.; Hermann, G.; Manz, J.; Pohl, V.; Tremblay, J.C. Electron Symmetry Breaking during Attosecond Charge Migration Induced by Laser Pulses: Point Group Analyses for Quantum Dynamics. *Symmetry* **2021**, *13*, 205. <https://doi.org/10.3390/sym13020205>

Academic Editor: Alessandro Sergi

Received: 1 December 2020

Accepted: 21 January 2021

Published: 27 January 2021

Publisher's Note: MDPI stays neutral with regard to jurisdictional claims in published maps and institutional affiliations.



Copyright: © 2021 by the authors. Licensee MDPI, Basel, Switzerland. This article is an open access article distributed under the terms and conditions of the Creative Commons Attribution (CC BY) license (<https://creativecommons.org/licenses/by/4.0/>).

1. Introduction

This paper focuses on the interplay of two domains of research in molecular quantum dynamics: charge migration in molecules on the time scale from a few hundred attoseconds ($1 \text{ as} = 10^{-18} \text{ s}$) to few femtoseconds ($1 \text{ fs} = 10^{-15} \text{ s}$), and electron symmetry breaking by laser pulses; the nuclear symmetry is conserved on this time scale. Here, the term “electron symmetry” means the point group symmetry of the observable one-electron density. The complementary term “nuclear symmetry” means the point group of the nuclear scaffold attained at the global minimum structure in the electronic ground state.

The paper should be of interest also to experts and young scientists in neighboring fields, e.g., quantum control and quantum chemistry. Quantum chemists, for example, are familiar with the assignment of the nuclear symmetry to the electronic eigenstates, with corresponding irreducible representations (IRREPs) in the standard time-independent scenario. From this perspective, one may ask how a laser pulse could ever induce different electron and nuclear symmetries, as suggested by the title and the Abstract of this paper. An important purpose is, therefore, to confirm that this is possible indeed. The phenomenon

shall be demonstrated on the ultrashort time scale of laser-driven quantum dynamics when the nuclei still do not move, i.e., they conserve nuclear symmetry. At the same time, however, the electrons may already exhibit laser-induced transitions from the initial ground state to specific superpositions of eigenstates which imply electron symmetry breaking. Moreover, we aim at the derivation of practical rules for assigning the broken symmetries of the relevant one-electron densities of the superposition states which represent charge migration initiated by laser pulses, in co-existence with the conserved nuclear symmetry. The derivations will be presented in a step-by-step manner for two examples, namely for the effects of linearly polarized laser pulses on oriented benzene molecule, and on oriented Mg-porphyrin. The term “oriented” means the specific orientation of the nuclear scaffold with respect to the laboratory frame; the latter may be determined by a linearly polarized laser pulse. Occasionally, we shall also refer to analogous effects of circularly polarized laser pulses in oriented benzene, Mg-porphyrin or other molecules, but without any detailed derivations. The present non-linear model systems are chosen because their high nuclear point group symmetries $G = D_{6h}$ and D_{4h} support two-dimensional (2d) IRREPs for degenerate electronic states. We shall show below that this offers new opportunities for laser control of electron symmetry breaking. The new phenomenon calls for the present significant extension of the previous theory and applications [1–5].

This Introduction starts with a historical overview of the topic. This sets the stage for a list of the next challenges which we try to master in the rest of this paper. The historical overview centers attention on just five publications [1–5]. To the best of our knowledge, these are the only ones that assign different point group symmetries of the relevant one-electron densities of the initial states of the oriented molecules—this is always the electronic ground state, and its electronic symmetry is the same as the nuclear symmetry—and after symmetry breaking by the laser pulse. In retrospect, one may find various other publications that document the phenomenon implicitly, but without any specification of the relevant point groups. We shall refer to some of this implicit evidence in the next Sections.

Electron symmetry breaking by laser pulses, with an explicit comparison of the symmetries before and after the laser pulses, was documented first by Ulusoy and Nest in their fundamental work on quantum control of aromaticity, with application to the benzene molecule with a specific orientation of its nuclear scaffold [1]. For this example, the nuclear point group symmetry is D_{6h} ; the corresponding IRREPs of the electronic ground state S_0 and the first and second excited electronic singlet states S_1 and S_2 are ${}^1A_{1g}$, ${}^1B_{2u}$ and ${}^1B_{1u}$, respectively. The key result of their publication is that the aromaticity of benzene in state S_0 can be extinguished by means of well-designed laser pulses which prepare the non-aromatic $(1/\sqrt{2})(S_0 + S_1)$ (i) or the $(1/\sqrt{2})(S_0 + S_2)$ (ii) superposition states. Ulusoy and Nest noted that in spite of the robust nuclear symmetry D_{6h} , these electronic superposition states transform according to IRREPs of different D_{3d} (i) and D_{3h} (ii) point group symmetries, and they exhibit different types of periodic charge migrations between neighboring CC bonds (i) or carbon atoms (ii), with periods of 520 as and 720 as, respectively [1]. Recent work has demonstrated, however, that these findings do not hold in the molecular reference frame but only in the reference frame of the laser field [6]. With this understanding, Ref. [1] has the full set of the sub-topics of the title of this paper: Electron symmetry breaking $D_{6h} \rightarrow D_{3d}$ (i) or $D_{6h} \rightarrow D_{3h}$ (ii) versus nuclear symmetry conservation (D_{6h}) during attosecond charge migration induced by laser pulses. However, Ulusoy and Nest focused on laser control of aromaticity, without any explicit note of electron symmetry breaking, even though it was clearly documented. They also did not present any rigorous derivations of their assignments of the broken electron symmetries of the non-aromatic superposition states.

The work of Ulusoy and Nest [1] stimulated quantum dynamics simulation of another electron symmetry breaking in oriented benzene, specifically $D_{6h} \rightarrow C_s$, with robust nuclear D_{6h} symmetry, followed by $C_s \rightarrow D_{6h}$ electron symmetry restoration, simply by time-reversed circularly polarized laser pulses with proper phase relations. Refs. [3,4] document the same type of laser-driven electron symmetry breaking, but different strategies for

symmetry restoration. In Refs. [2–4], the electron symmetries D_{6h} and C_s were assigned just by empirical inspection of the relevant one-electron densities. Ref. [5] refers to preparations of electronic superposition states with different IRREPs in oriented molecules by laser pulses, but without explicit quantum dynamics simulations. The superposition states present attosecond charge migration. Ref. [5] has the first rigorous derivation of the point group symmetries of the one-electron densities of the target states. The applications are for rather simple prototypes, namely $D_{\infty h} \rightarrow C_{\infty v}$ electron symmetry breaking and attosecond charge migration in the $\sigma_g + \sigma_u$ superposition state of oriented H_2^+ , with robust nuclear symmetry $D_{\infty h}$, and by analogy for $C_{2v} \rightarrow C_s$ electron symmetry breaking and attosecond charge migration in the $A_1 + B_2$ superposition state of oriented H_2O , with robust nuclear symmetry C_{2v} .

The pioneering papers [1–5] call for the following extensions: (a) Rigorous assignments of electron symmetry breaking in supplementary examples for oriented benzene and for oriented Mg-porphyrin. For this purpose, we design linearly polarized laser pulses that initiate selective types of attosecond charge migration with corresponding electron symmetry breaking while conserving nuclear symmetry. The results are demonstrated by quantum dynamics simulations of laser excitations of electronic superposition states with different combinations of IRREPs. As a constraint, the duration of the laser pulses should be shorter than 10 fs, as in Refs. [2–4], because in this time domain, the nuclear motions may be considered as frozen, i.e., they conserve nuclear symmetry [7,8]. For comparison, the laser pulses which were designed in Ref. [1] take 80 fs or even longer times. (b) Derivation of simple yet rigorous rules for the assignments of symmetries of the relevant one-electron densities of the resulting electronic superposition states in the oriented molecules. These rules (b) will be applied not only to the new examples (a), but they will also be used to check the previous assignments of electron symmetry breaking in Ref. [1]. This calls for a significant extension of the previous rules for superpositions of non-degenerate electronic states with one-dimensional (1d) IRREPs [5] to superpositions of non-degenerate plus degenerate electronic states with 1d plus 2d IRREPs in oriented molecules. The present applications serve as examples that should enable analogous derivations of rigorous rules for the assignments of laser-induced symmetry breaking in electronic superposition states in other oriented systems.

The subsequent Section 2 presents the models, methods and techniques. Section 3 has the results and discussions. The conclusions are in Section 4. Appendix A derives various general theorems for electron symmetry breaking induced by short linearly polarized laser pulses in oriented molecules with arbitrary point groups of the frozen nuclear scaffolds. Appendix B has additional results for the two model systems, benzene and Mg-porphyrine.

2. Models, Methods and Techniques

This section has nine subsections. The first one (Section 2.1) presents a convenient analytical, parametrized expression for the electric fields $\mathcal{E}_p(t)$ of various linearly polarized laser pulses labeled $p = 1, 2, 3, \dots$ which achieve different types of electron symmetry breaking in oriented molecules, ready for applications to the two examples, oriented benzene and Mg-porphyrin. For each system, the “first” laser pulse ($p = 1$) is used for specifying the laboratory frame. Section 2.2 defines the orientations of the nuclear scaffolds with respect to the laboratory frame. The scaffolds have the symmetries of the familiar nuclear point groups G . Section 2.3 specifies the nomenclature for the corresponding symmetry elements and the related symmetry operations—this task is mandatory, in view of two different conventions in the literature, with different assignments of the symmetry operations which yield different IRREPs of some of the electronic states in the laser-induced target superposition states. Section 2.4 defines the electronic Hamiltonian H_e of the oriented molecules and summarizes the methods of quantum chemistry for the evaluations of the electronic eigenstates with the energies, wavefunctions, assignments of IRREPs of G , and the related dipole transition matrix elements. Section 2.5 defines the time-dependent Hamiltonians $H_p(t)$ for the oriented molecules interacting with the

linearly polarized laser pulses labeled p , or two sequential laser pulses, and determines the subgroups $S(H_p(t))$ of G by those symmetry operations of H_e which are conserved in $H_p(t)$. Section 2.6 summarizes the methods of quantum dynamics for the laser-driven time evolution of the electronic states, starting from the electronic ground state. Section 2.7 discovers some symmetry relations of the wavefunctions which are driven by laser pulses with different linear polarizations. The quantum chemical method for calculating the one-electron densities of these superposition states is in Section 2.8. Section 2.9 adds some details for the design of the laser pulses for selective types of electron symmetry breaking.

The order of presentations of Sections 2.1–2.9 is convenient, for the present purpose, but it suffers from the dilemma that several Sections depend on each other in various ways. Unfortunately, there is no unique “logic” or “ideal” order of the presentations which could avoid this problem.

2.1. Linearly Polarized Laser Pulses in the Laboratory Frame

The subsequent applications use several linearly polarized laser pulses. They are labeled by $p = 1, 2, 3, \dots$. The first one ($p = 1$) is used for the definition of the right-handed set of Cartesian coordinates x, y, z of the laboratory frame. All laser pulses—including the first one—propagate along the same direction: this defines the z -direction along the unit-vector \mathbf{e}_z of the laboratory frame. All laser pulses are linearly polarized, with polarization (unit) vector \mathbf{e}_p perpendicular to \mathbf{e}_z . In the present applications, the polarization vector of the “first” laser pulse ($p = 1$) defines the x -direction, $\mathbf{e}_x \equiv \mathbf{e}_{p=1}$. The y -direction is along the unit vector \mathbf{e}_y perpendicular to \mathbf{e}_x and \mathbf{e}_z .

The time-(t)-dependent electric fields $\mathcal{E}_p(t)$ of the linearly polarized laser pulses are modeled as products of the polarization vectors \mathbf{e}_p times scalar fields $\mathcal{E}_p(t)$ with \sin^2 -shapes of the carrier envelopes,

$$\begin{aligned}\mathcal{E}_p(t) &= \mathbf{e}_p \mathcal{E}_p(t) \\ &\equiv \mathbf{e}_p \mathcal{E}_{0p} \sin^2[\pi(t - t_{ip})/\tau_p] \sin[\omega_p(t - t_{ip} - \tau_p/2)] \quad \text{for } t_{ip} \leq t \leq t_{ip} + \tau_p \\ &= 0 \quad \text{else}\end{aligned}\quad (1)$$

Here \mathcal{E}_{0p} denotes the electric field strength, t_{ip} and $t_{ip} + \tau_p$ are the initial and final times of the laser pulse, τ_p is its (total) duration. For applications of a single laser pulse, we set $t_{ip} = 0$. For two sequential laser pulses p and $p + 1$, the second pulse is fired right after the first one, hence $t_{i,p+1} = t_{ip} + \tau_p$. The carrier frequency is denoted ω_p : the corresponding periods, wavelength, and photon energy are $T_p = 2\pi/\omega_p$, $\lambda_p = c T_p$ and $\hbar\omega_p$, respectively; c and $\hbar = h/2\pi$ denote the velocity of light in vacuum and Planck’s reduced constant, respectively. The carrier-envelope phases $\omega_p(t_{ip} + \tau_p/2)$ are fixed such that the $\sin[\dots]$ term is antisymmetric with respect to the maximum of the \sin^2 -shape function. The corresponding maximum mean intensity (i.e., the maximum of the intensity time-averaged over one period) is at $t = t_{ip} + \tau_p/2$. Its value is approximated almost perfectly by

$$I_{mp} = 0.5 \epsilon_0 c \mathcal{E}_{0p}^2, \quad (2)$$

where ϵ_0 is the permittivity of vacuum. In the present applications, the values of the photon energies are in the domain of several eV. The corresponding wavelengths are in the domain of several hundred nanometers—more than four orders of magnitude larger than the size of the molecules. As consequence, the electric fields are almost perfectly homogeneous in the molecular domains, as modeled in Equation (1).

Some methods for the determination of the laser parameters in Equation (1) for control of the electron symmetry breaking and charge migration are presented in Section 2.9.

2.2. Orientations of the Nuclear Scaffolds

The present scenario of the nuclear scaffold of benzene ($^{12}\text{C}_6\text{H}_6$) is adapted from Ref. [1]. The scaffold has the familiar D_{6h} symmetry. It is oriented with respect to the laboratory frame as shown in Figure 1, with its center of mass at the origin. Specifically, the molecular plane is in the laboratory x - y -plane, and two carbon nuclei are on the y -axis.

This scenario has also been used in Refs. [2–4,6,9–12]. An alternative orientation of the nuclear scaffold—i.e., again with the molecular plane in the laboratory x-y-plane, but with two carbon nuclei on the x-axis instead of the y-axis—is considered in Refs. [13,14].

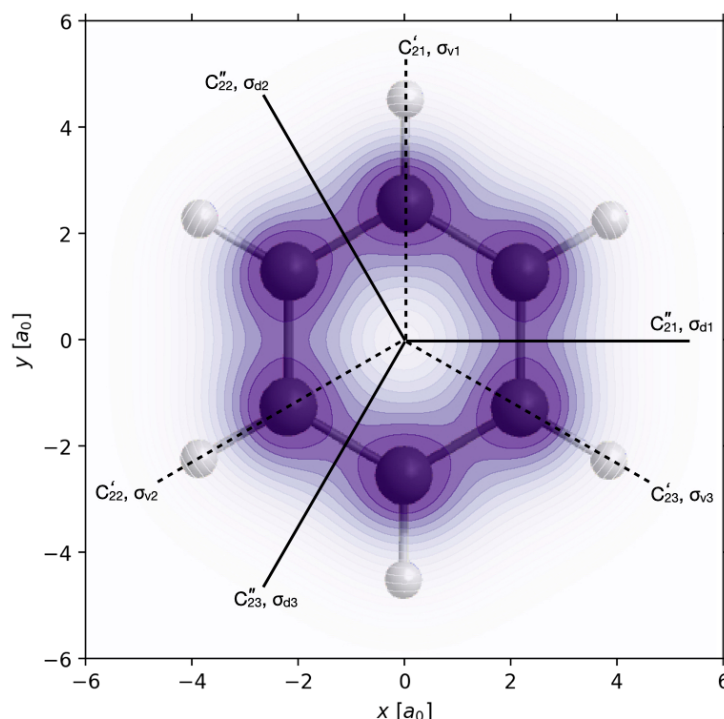


Figure 1. Orientation of the nuclear scaffold of benzene ($^{12}\text{C}_6\text{H}_6$) in the x-y-plane of the laboratory frame, with two carbon nuclei on the y-axis. The scenario is adapted from Ref. [1]. The scaffold has D_{6h} symmetry. The principle axis is along the laboratory z-axis, pointing to the reader. The nuclear center of mass is at the origin. Additionally indicated are some important symmetry elements, in particular, the binary rotation axes C'_{21} , C'_{22} , C'_{23} and C''_{21} , C''_{22} , C''_{23} . They coincide with the lines of intersections of the horizontal symmetry plane σ_h and the vertical and dihedral planes σ_{v1} , σ_{v2} , σ_{v3} and σ_{d1} , σ_{d2} , σ_{d3} , respectively. Additionally shown by colored contours in the x-y-plane is the one-electron density $\rho_0(\mathbf{r}) = \rho_{1A_{1g}}(\mathbf{r})$ of the electronic ground state $|0\rangle = |1A_{1g}\rangle$ integrated over z, i.e., $\int dz \rho_0(x,y,z)$, with D_{6h} symmetry.

The quantum mechanical indistinguishability of the carbon nuclei (bosons), as well as the protons (fermions) implies that one cannot assign individual nuclei to any specific sites of the nuclear frame. Instead, the probabilities of occupying the carbon and proton sites are the same ($=1/6$) for all carbon nuclei and protons, respectively [6]. This renders the presentation of the results rather easy, e.g., one can talk about charge migration from the “left” ($x < 0$) to the “right” ($x > 0$) CC bonds, or from the “bottom” ($y < 0$) to the “top” ($y > 0$) domains of carbon nuclei, without labeling the individual carbon nuclei.

For the nuclear scaffold of oriented Mg-porphyrin ($^{24}\text{Mg}^{14}\text{N}_4^{12}\text{C}_{20}\text{H}_{12}$) we adapt the scenario of Ref. [15], also used in Ref. [16]. It has the familiar D_{4h} symmetry. It is oriented with respect to the laboratory frame as shown in Figure 2, with its center of mass at the origin. The molecular plane is again in the laboratory x-y-plane, and the four nitrogen nuclei are on the x and y-axes.

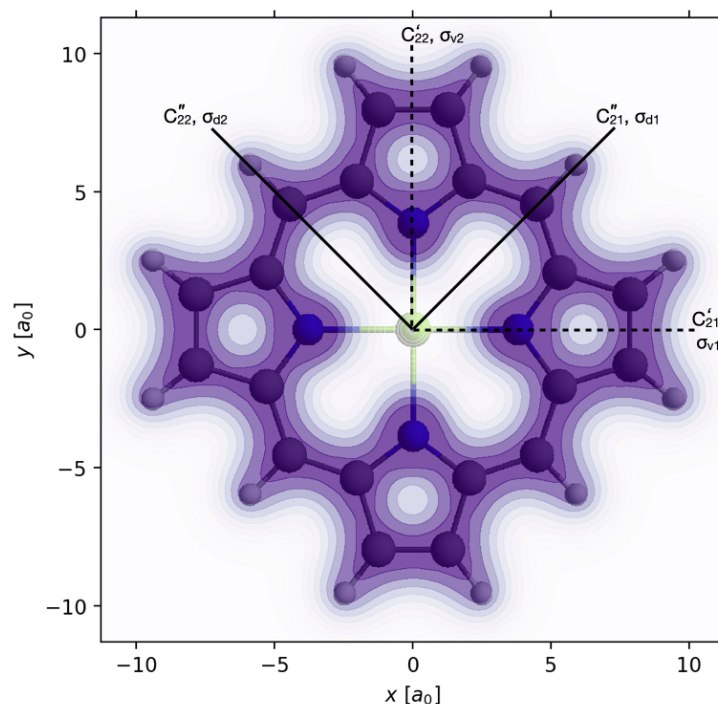


Figure 2. Orientation of the nuclear scaffold of Mg-porphyrin ($^{24}\text{Mg}^{14}\text{N}_4^{12}\text{C}_{20}\text{H}_{12}$) in the x-y-plane of the laboratory frame, with the nitrogen nuclei on the x and y axes. The scenario is adapted from Ref. [15]. The scaffold has D_{4h} symmetry. The notations are as in Figure 1, in particular for the binary rotation axes C'_{21} , C'_{22} and C''_{21} , C''_{22} , for the associated vertical and dihedral planes σ_{v1} , σ_{v2} and σ_{d1} , σ_{d2} , respectively, and for the one-electron density of the electronic ground state $|0\rangle = |1A_{1g}\rangle$ integrated over z , i.e., $\int dz \rho_0(x,y,z)$, with D_{4h} symmetry.

2.3. Nomenclature of Selected Symmetry Elements, Symmetry Operations and Subgroups of the Point Groups D_{6h} and D_{4h} of the Oriented Benzene and Mg-Porphyrin

The laser pulses (Section 2.1) shall be designed (Section 2.9) to break the original electron symmetries of the oriented molecules, i.e., from D_{6h} for benzene and D_{4h} for Mg-porphyrin (Section 2.2) to selective subgroups. Here, we explain the nomenclature for some important symmetry operations which are necessary to specify those subgroups. The related symmetry elements include the inversion center which coincides with the center of mass at the origin, the horizontal symmetry plane σ_h which coincides with the laboratory x-y-plane, and few others which are illustrated in Figures 1 and 2. Specifically, benzene (analogous results for Mg-porphyrin are in brackets) has three plus three (two plus two) axes for binary rotations C'_{21} , C'_{22} , C'_{23} and C''_{21} , C''_{22} , C''_{23} (C'_{21} , C'_{22} and C''_{21} , C''_{22}). These coincide with the lines of intersections of the horizontal plane σ_h and the vertical and dihedral planes σ_{v1} , σ_{v2} , σ_{v3} and σ_{d1} , σ_{d2} , σ_{d3} , (σ_{v1} , σ_{v2} and σ_{d1} , σ_{d2}), respectively. The symmetry elements correspond to symmetry operations which may be written with the same notations, i.e., binary rotations C'_{21} , C'_{22} , C'_{23} and C''_{21} , C''_{22} , C''_{23} (C'_{21} , C'_{22} and C''_{21} , C''_{22}), the vertical and dihedral reflections σ_{v1} , σ_{v2} , σ_{v3} and σ_{d1} , σ_{d2} , σ_{d3} , (σ_{v1} , σ_{v2} and σ_{d1} , σ_{d2}), respectively, the horizontal reflection σ_h , etc. Six (four) sets of four symmetry operations of the type $\{E, C_2, \sigma_h, \sigma\}$, namely the identity (E), one of the two-fold rotations, the horizontal reflection and the associated vertical or dihedral reflection, establish six (four) different C_{2v} subgroups—these are written with notations that remind of the rotations, i.e., $C_{2v}'1$, $C_{2v}'2$, $C_{2v}'3$ and $C_{2v}''1$, $C_{2v}''2$, $C_{2v}''3$ ($C_{2v}'1$, $C_{2v}'2$ and $C_{2v}''1$, $C_{2v}''2$), respectively. For example, $C_{2v}'1 = \{E, C'_{21}, \sigma_h, \sigma_{v1}\}$, $C_{2v}'2 = \{E, C'_{22}, \sigma_h, \sigma_{v2}\}$, \dots , $C_{2v}''1 = \{E, C''_{21}, \sigma_h, \sigma_{d1}\}$, \dots , etc. Analogous notations apply for other subgroups S of the point group $G = D_{6h}$ (D_{4h}) of the oriented benzene (Mg-porphyrin). Table 1 has a list of the symmetry operations, i.e., of the group elements g of the group $G = D_{6h}$ and various subgroups S , with specification of the selected subsets of elements g contained in S .

Table 1. Symmetry operations of point group D_{6h} and various subgroups for the oriented benzene ^(a).

D_{6h}	=	$\{E, 2C_6, 2C_3, C_2, 3C'_2, 3C''_2, i, 2S_6, 2S_6\sigma_h, 3\sigma_d, 3\sigma_v\}$
D'_{3h}	=	$\{E, 2C_3, 3C'_2\sigma_h, 2S_6, 3\sigma_v\}$
D''_{3h}	=	$\{E, 2C_3, 3C''_2\sigma_h, 2S_6, 3\sigma_d\}$
D'_{3d}	=	$\{E, 2C_3, 3C'_2, i, 2S_6, 3\sigma_d\}$
D''_{3d}	=	$\{E, 2C_3, 3C''_2, i, 2S_6, 3\sigma_v\}$
$D_{2h,k}$	=	$\{E, C_2, C'_{2k}, C''_{2k}, i, \sigma_h, \sigma_{dk}, \sigma_{vk}\}, k = 1, 2, 3$
$C'_{2v,k}$	=	$\{E, C'_{2k}, \sigma_h, \sigma_{vk}\}, k = 1, 2, 3, \subset D_{2h,k}, D'_{3h}$
$C''_{2v,k}$	=	$\{E, C''_{2k}, \sigma_h, \sigma_{vk}\}, k = 1, 2, 3, \subset D_{2h,k}, D''_{3h}$
C_{2h}	=	$\{E, C_2, i, \sigma_h\} \subset D_{2h,k}, k = 1, 2, 3$
C_s	=	$\{E, \sigma_h\} \subset C_{2h}$

^(a) Most of the related symmetry elements are illustrated in Figure 1.

It is also useful to define unit vectors $\mathbf{e}'_1, \mathbf{e}'_2, \mathbf{e}'_3$ and $\mathbf{e}''_1, \mathbf{e}''_2, \mathbf{e}''_3$ ($\mathbf{e}'_1, \mathbf{e}'_2$ and $\mathbf{e}''_1, \mathbf{e}''_2$) along the rotational axes $C'_{21}, C'_{22}, C'_{23}$ and $C''_{21}, C''_{22}, C''_{23}$ (C'_{21}, C'_{22} and C''_{21}, C''_{22}) of the oriented benzene (Mg-porphyrin) in the laboratory frame. These are listed in Table 2. Note that for benzene, $\mathbf{e}'_1 = \mathbf{e}_y$ and $\mathbf{e}''_1 = \mathbf{e}_x$ (this is a consequence of our adaption of the orientation of benzene used in Ref. [1], as in Refs. [2–4,6,9–12], cf. Figure 1), whereas for Mg-porphyrin, $\mathbf{e}'_1 = \mathbf{e}_x$ and $\mathbf{e}'_2 = \mathbf{e}_y$ (this is in accord with Refs. [13,15,16], cf. Figure 2). In the applications below, these unit vectors will serve as polarization vectors of the linearly polarized laser pulses, Equation (1).

Table 2. Linear polarizations of laser pulses for symmetry breaking of the electronic Hamiltonian of the oriented benzene and Mg-porphyrin ^(a).

	Benzene ($G = D_{6h}$) ^(b)							Mg-Porphyrin ($G = D_{4h}$)			
Polarization vectors	\mathbf{e}'_1	\mathbf{e}'_2	\mathbf{e}'_3	\mathbf{e}''_1	\mathbf{e}''_2	\mathbf{e}''_3	$\mathbf{e}'_1 \& \mathbf{e}''_1$	\mathbf{e}'_1	\mathbf{e}'_2	\mathbf{e}''_1	\mathbf{e}''_2
	e_y	$C_3 e_y$	$C_3^2 e_y$	e_x	$C_3 e_x$	$C_3^2 e_x$	$e_y \& e_x$	e_x	e_y	$C_8 e_x$	$C_8 e_y$
parallel to binary rotation axes	C'_{21}	C'_{22}	C'_{23}	C''_{21}	C''_{22}	C''_{23}	C'_{21}, C''_{21}	C'_{21}	C'_{22}	C''_{21}	C''_{22}
associated symmetry planes	σ_{v1}	σ_{v2}	σ_{v3}	σ_{d1}	σ_{d2}	σ_{d3}	σ_h	σ_{v1}	σ_{v2}	σ_{d1}	σ_{d2}
resulting subgroup $S(H_e(t))$	$C'_{2v,1}$	$C'_{2v,2}$	$C'_{2v,3}$	$C''_{2v,1}$	$C''_{2v,2}$	$C''_{2v,3}$	C_s	$C'_{2v,1}$	$C'_{2v,2}$	$C''_{2v,1}$	$C''_{2v,2}$
with symmetry operations	$C'_{2v,k} = \{E, C'_{2k}, \sigma_h, \sigma_{vk}\}, k = 1, 2, 3$						$\{E, \sigma_h\}$	$C'_{2v,k} = \{E, C'_{2k}, \sigma_h, \sigma_{vk}\}, k = 1, 2$			
	$C''_{2v,k} = \{E, C''_{2k}, \sigma_h, \sigma_{dk}\}, k = 1, 2, 3$							$C''_{2v,k} = \{E, C''_{2k}, \sigma_h, \sigma_{dk}\}, k = 1, 2$			

^(a) The field-free electronic Hamiltonians H_e of the oriented benzene and Mg-porphyrin have molecular point group symmetries $G = D_{6h}$ and D_{4h} . The interaction with the laser pulses with polarization \mathbf{e} changes H_e to $H_e(t)$ and breaks G to the subgroup $S(H_e(t))$ depending on \mathbf{e} .

^(b) The symbol $\mathbf{e}'_1 \& \mathbf{e}''_1$ denotes sequential applications of two laser pulses with polarizations \mathbf{e}'_1 and \mathbf{e}''_1 .

2.4. Quantum Chemical Methods for the Electronic States with Their Energies, Wavefunctions, IRREPs, and Transition Dipole Matrix Elements

The present project calls for quantum chemical *ab initio* calculations of various properties of the oriented model systems benzene and Mg-porphyrin.

(i) The nuclear scaffolds are determined as global minimum structures in the electronic ground state. They confirm the familiar nuclear symmetries (D_{6h} and D_{4h} , respectively.) The scaffolds are oriented in the laboratory frame as shown in Figures 1 and 2, respectively (Section 2.2). With these orientations, the laboratory frame also serves as a molecular frame. The corresponding electronic Hamiltonians $H_e = T_e + V_e$ account for the kinetic energies T_e of all electrons and for the Coulomb interactions V_e of all particles (electrons and nuclei). Proper nuclear charges are assigned to the respective positions provided by the rigid nuclear scaffold. This rule avoids any labeling of the nuclei, in accord with Ref. [6], and at the same time, it imposes the respective nuclear symmetry on H_e , which means H_e

commutes with all symmetry operations (=group elements g) of the point groups $G = D_{6h}$ or D_{4h} of the oriented benzene or Mg-porphyrin, respectively,

$$[H_e, g] = 0 \text{ for } g \in G = D_{6h} \text{ (oriented benzene) or } D_{4h} \text{ (oriented Mg-porphyrin)}. \quad (3)$$

As consequence, H_e also commutes with the symmetry projection operators of the groups G of order $|G|$,

$$P^{\Gamma_m}(G) = (d^{\Gamma_m} / |G|) \sum_{g \in G} \chi^{\Gamma_m}(g)^* g \quad (4)$$

for the IRREPs Γ_m with dimension d^{Γ_m} and characters $\chi^{\Gamma_m}(g)$,

$$[H_e, P^{\Gamma_m}(G)] = 0. \quad (5)$$

(ii) The singlet ground and low-lying electronic excited states of the oriented model systems with rigid nuclear frames are evaluated with their eigenenergies E_m and eigenfunctions $|m\rangle$ (using Dirac notation) in the laboratory (\equiv molecular) frame. The Dirac notation $|m\rangle$ is a short-hand notation that specifies the energy and IRREP quantum numbers of the eigenstate; for example, the electronic ground state is denoted $|0\rangle = |1A_{1g}\rangle (\equiv |1^1A_{1g}\rangle$, dropping the notation “1” for singlet states). They are obtained as real-valued solutions of the time-independent electronic Schrödinger equation (TISE)

$$H_e |m\rangle = E_m |m\rangle. \quad (6)$$

For convenience, we set $E_0 = 0$ eV for the ground state, cf. Figures 3 and 4. For benzene, the computations are carried out as in Refs. [6,11,12], i.e., by means of the state-averaged CASSCF(6,6) method with an aug-cc-pVTZ basis [17] as implemented in MOLPRO [18]. The energies of the 22 lowest excited states are corrected by multireference configuration interaction with single and double excitations. The energies are found to be in fair agreement with the literature [19]. The IRREPs of the electronic eigenfunctions are assigned by means of the symmetry projection operators (4) for the point group $G = D_{6h}$,

$$|m\rangle \text{ transforms as IRREP } \Gamma_m \text{ of } G \leftrightarrow P^{\Gamma_m}(G) |m\rangle = |m\rangle. \quad (7)$$

The resulting electronic energy levels of the ground and lowest singlet states of the oriented benzene are shown in Figure 3, together with the IRREPs of $G = D_{6h}$.

For Mg-porphyrin, the 20 lowest-lying excited states up to 5.5 eV are calculated using linear-response time-dependent density functional theory with the CAM-B3LYP functional [20] and a correlation-consistent aug-cc-pVTZ basis [17,21] as implemented in Gaussian 16 [22]. The resulting energy levels of the ground and lowest singlet states of the oriented Mg-porphyrin are shown in Figure 4, together with the assignments of IRREPs of $G = D_{4h}$. The energies compare well with literature values [23].

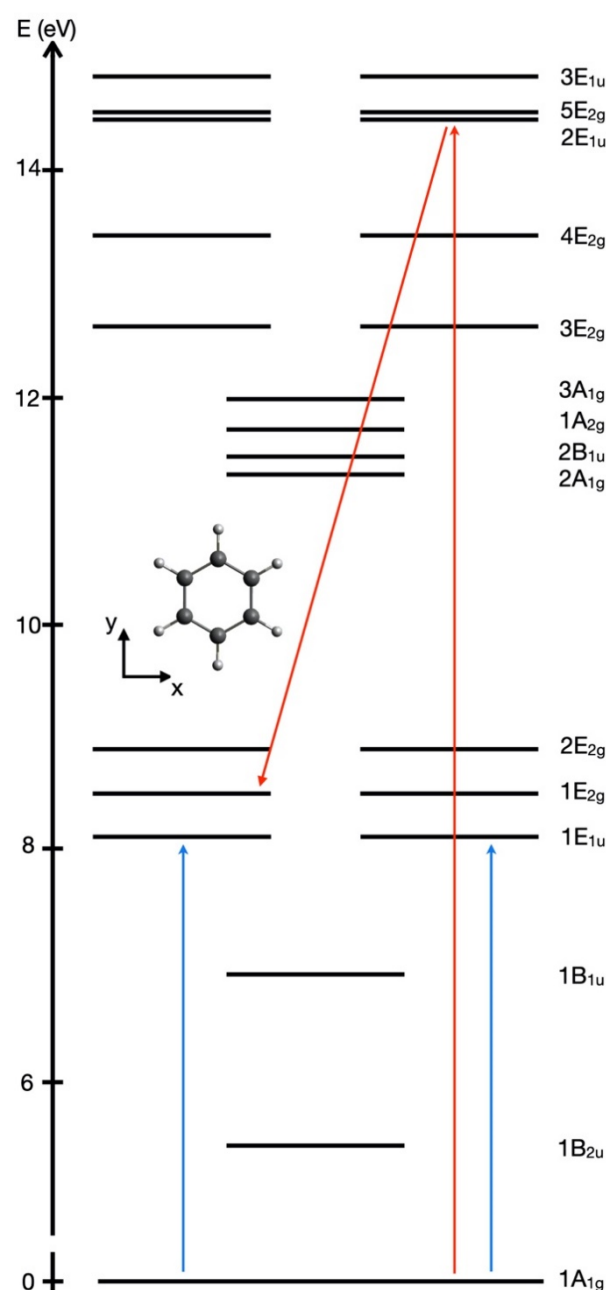


Figure 3. Level diagram of the singlet ground and lowest excited electronic states of the model benzene, with assignments of the irreducible representations (IRREPs). The rigid nuclear scaffold has D_{6h} symmetry and is oriented in the laboratory frame as shown in Figure 1. The doubly degenerate E_{1u} and E_{2g} states each consist of two orthogonal degenerate states which transform as the functions x and $x^2 - y^2$ (left column) and y and xy (right column), respectively. The preparation of superposition states of the electronic ground state $|1A_{1g}\rangle$ and selective excited singlet states with different IRREPs by linearly polarized laser pulses (or two sequential laser pulses) is illustrated schematically by arrows (or sequence of arrows) for the corresponding laser-induced target transitions. The blue arrows correspond to the laser excitations from the initial ($t = 0$) electronic ground state $|1A_{1g}\rangle$ to the superposition states $(1/\sqrt{2})(|1A_{1g}\rangle + |1E_{1u}^x\rangle)$ (left blue arrow, labeled $p = 1$) and $(1/\sqrt{2})(|1A_{1g}\rangle + |1E_{1u}^y\rangle)$ (right blue arrow, labeled $p = 2$), respectively. The sequence of two red arrows refers to excitation of the target superposition of the $|1A_{1g}\rangle$ and $|1E_{2g}^{x^2-y^2}\rangle$ states via the $|2E_{1u}^y\rangle$ state, by means of two sequential laser pulses, labeled $p = 7$ and 8 . See text for the details.

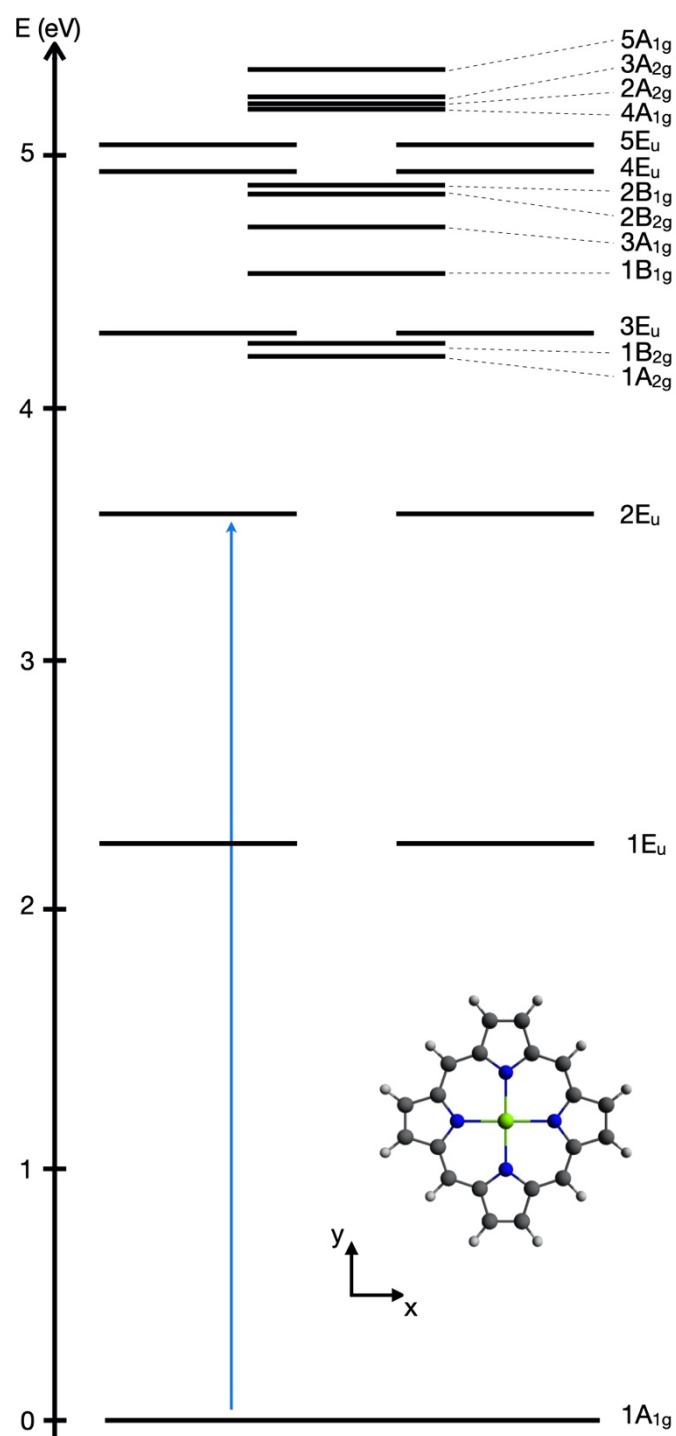


Figure 4. Level diagram of the singlet ground and lowest excited states of the model Mg-porphyrin with rigid nuclear scaffold oriented in the laboratory frame as shown in Figure 2. The notations are as in Figure 3, except for the D_{4h} symmetry of Mg-porphyrin instead of the D_{6h} symmetry of benzene. The blue arrow corresponds to the laser excitation from the electronic ground state $|1A_{1g}\rangle$ to the superposition states $(1/\sqrt{2})(|1A_{1g}\rangle + |1E_{1u}^x\rangle)$ labeled $p = 1$.

(iii) The electronic transition dipole matrix elements of the oriented model systems

$$\mathbf{d}_{mn} = \langle m | \mathbf{d} | n \rangle \quad (8)$$

are calculated with dipole operator

$$\mathbf{d} = -e \sum_j \mathbf{r}_j \quad (9)$$

where $-e$ denotes the electron charge. The sum \sum_j is over all electrons with coordinates $\mathbf{r}_j = (x_j, y_j, z_j)$ in the laboratory (\equiv molecular) frame. For the oriented benzene, the corresponding Cartesian components d_x , d_y and d_z of \mathbf{d} transform according to IRREPs E_{1u} (with basis E_{1u}^x, E_{1u}^y) and A_{2u} ; for the oriented Mg-porphyrin, they transform according to E_u (with basis E_u^x, E_u^y) and A_{2u} , respectively. Many x , y , or z -components of the transition dipole matrix elements (8) are equal to zero, due to the symmetry selection rules [1]. This supports selective laser-induced transitions between states $|m\rangle$ and $|n\rangle$ with non-zero matrix elements $\langle m | \mathbf{d} | n \rangle$, as illustrated in Figures 3 and 4. Detailed group theoretical derivations of symmetry rules for the transition dipole matrix elements are in Appendix B. The results of the quantum chemical calculations of selected non-zero values of the transition dipole matrix elements are listed in Table A2 therein. For the methods of calculating the integral (8), see Section 2.8.

2.5. Symmetry Breaking of the Electronic Hamiltonians for the Oriented Model Benzene or Mg-Porphyrin by Linearly Polarized Laser Pulses

The time-dependent total electronic model Hamiltonian $H_p(t)$ of the oriented molecule (benzene or Mg-porphyrin) interacting with the electric field $\mathcal{E}_p(t)$ of the linearly polarized laser pulse labeled “p” (Section 2.1) consists of two terms for the electronic Hamiltonian H_e and for the laser-dipole interaction— $\mathcal{E}_p(t) * \mathbf{d}$. In semiclassical dipole approximation

$$H_p(t) = H_e - \mathcal{E}_p(t) * \mathbf{d} = H_e - \mathbf{e}_p * \mathbf{d} * \mathcal{E}_p(t). \quad (10)$$

The scalar product $\mathbf{e}_p * \mathbf{d}$ breaks the symmetry of the point group $G = D_{6h}$ or D_{4h} for the oriented benzene or Mg-porphyrin) of H_e down to a subgroup $S(H_p(t))$ of G . For example, in the case of the oriented benzene interacting with the “first” ($p = 1$) laser pulse with polarization vector $\mathbf{e}_1 \equiv \mathbf{e}_x = \mathbf{e}''_1$, the full set of commutations (3) of the electronic Hamiltonian H_e with all symmetry operations ($=$ all group elements $g \in G$) is reduced to a much smaller set of commutations of the total Hamiltonian $H_p(t) \equiv H_{e''_1}(t)$ with only four symmetry operations of the subgroup $S(H_{p=1}(t)) \equiv S(H_{e''_1}(t)) = C_{2v}''_1$, specifically

$$[H_{e''_1}(t), g] = 0 \text{ for } g \in S(H_{e''_1}(t)) = C_{2v}''_1 = \{E, C_2'', \sigma_h, \sigma_{d1}\} \neq 0 \text{ else} \quad (11)$$

As consequence, the electronic Hamiltonian $H_{e''_1}(t)$ of the oriented benzene molecule interacting with the linearly \mathbf{e}''_1 polarized laser pulse conserves the symmetry elements $\{E, C_2'', \sigma_h, \sigma_{d1}\}$ of the subgroup $S(H_{e''_1}(t)) = C_{2v}''_1$ of the point group $G = D_{6h}$ of the Hamiltonian H_e of the non-interacting molecule. In brief, the \mathbf{e}''_1 polarized laser pulse breaks the symmetry $G = D_{6h}$ of the electronic Hamiltonian H_e down to $S(H_{e''_1}(t)) = C_{2v}''_1$ symmetry of $H_{e''_1}(t)$. This implies that $H_{e''_1}(t)$ also commutes with the symmetry projection operators $P^{\Gamma_m}(C_{2v}''_1) = (1/4) \sum_{g \in C_{2v}''_1} \chi^{\Gamma_m}(g) * g$ for the IRREPs $\Gamma_m = A_1, A_2, B_1, B_2$ of $C_{2v}''_1$,

$$[H_{e''_1}(t), P^{\Gamma_m}(C_{2v}''_1)] = 0 \text{ for } \Gamma_m = A_1, A_2, B_1, B_2. \quad (12)$$

By analogy, interactions of the oriented benzene (or Mg-porphyrin, in brackets) with laser pulses with linear polarization vectors $\mathbf{e} = \mathbf{e}'_1, \mathbf{e}'_2, \mathbf{e}'_3$ and $\mathbf{e}''_1, \mathbf{e}''_2, \mathbf{e}''_3$ ($\mathbf{e}'_1, \mathbf{e}'_2$ and $\mathbf{e}''_1, \mathbf{e}''_2$) along the rotational axes $C'_{21}, C'_{22}, C'_{23}$ and $C''_{21}, C''_{22}, C''_{23}$ (C'_{21}, C'_{22} and C''_{21}, C''_{22}) conserve the symmetry elements of the subgroups $S(H_e(t)) = C_{2v}'_1, C_{2v}'_2, C_{2v}'_3$ and $C_{2v}''_1, C_{2v}''_2, C_{2v}''_3$ ($C_{2v}'_1, C_{2v}'_2$ and $C_{2v}''_1, C_{2v}''_2$), respectively, with commutation relations analogous to Equations (11) and (12), or in brief, those \mathbf{e} polarized laser pulses break the symmetry $G = D_{6h}$ (D_{4h}) of H_e down to those C_{2v} -type symmetries $S(H_e(t))$. These results also hold for applications of two sequential laser pulses with the same polarization vectors $\mathbf{e}_p = \mathbf{e}_{p'}$. In contrast, interactions with laser pulses with other polarizations \mathbf{e}_p

perpendicular to \mathbf{e}_z , or two sequential laser pulses labeled p&p' (also called \mathbf{e}_p & $\mathbf{e}_{p'}$) with different polarizations $\mathbf{e}_p \neq \mathbf{e}_{p'}$, reduce the commutations (11) further to

$$\begin{aligned} [\mathbf{H}_e(t), \mathbf{g}] &= 0 \text{ for } \mathbf{g} \in S(\mathbf{H}_e(t)) = C_s = \{E, \sigma_h\} \\ &\neq 0 \text{ for laser polarizations } \mathbf{e}_p \text{ different from} \\ &\quad \mathbf{e}'_1, \mathbf{e}'_2, \mathbf{e}'_3 \text{ and } \mathbf{e}''_1, \mathbf{e}''_2, \mathbf{e}''_3 \text{ for oriented benzene} \\ &\quad (\mathbf{e}'_1, \mathbf{e}'_2 \text{ and } \mathbf{e}''_1, \mathbf{e}''_2 \text{ for oriented Mg-porphyrin}), \\ &\text{or for two sequential laser pulses with different polarizations} \end{aligned} \quad (13)$$

and this implies the commutations

$$[\mathbf{H}_{e'1}(t), P^{\Gamma_m}(C_s)] = 0 \text{ for } \Gamma_m = A', A'' \quad (14)$$

analogous to Equation (12).

The subgroup symmetries $S(\mathbf{H}_e(t))$ of the time-dependent Hamiltonians $\mathbf{H}_e(t)$ of the oriented molecules interacting with laser pulses with linear polarizations \mathbf{e} , or with two sequential laser pulses, are listed in Table 2.

2.6. Quantum Dynamical Methods for the Propagation of the Laser-Driven Electronic Superposition States

The laser pulse with linear polarization $\mathbf{e} = \mathbf{e}_p$, or two sequential linearly polarized laser pulses (Section 2.1) drive the electronic wave functions of the oriented model systems from their initial ($t = 0$) electronic ground state

$$|\Psi_e(t=0)\rangle = |1A_{1g}\rangle \equiv |0\rangle \quad (15)$$

to time-dependent excited states $|\Psi_e(t)\rangle = |\Psi_{ep}(t)\rangle = |\Psi_p(t)\rangle$. The different but equivalent notations are used below, depending on the context. The subscripts "e" and "p" remind of the polarization vectors $\mathbf{e} = \mathbf{e}_p$ of the laser pulse labeled p. The wavefunctions are expanded in terms of the electronic eigenstates (Section 2.4),

$$|\Psi_e(t)\rangle = \sum_m c_{em}(t) |m\rangle \quad (16)$$

with complex time-dependent coefficients $c_{em}(t)$. The initial state (15) corresponds to the initial coefficients

$$c_{em}(t=0) = \delta_{m0} \quad (17)$$

where δ denotes Kronecker's symbol. The coefficients $c_{em}(t)$ yield the time-dependent probabilities $P_{em}(t)$ of occupying the electronic eigenstates $|m\rangle$,

$$P_{em}(t) = |c_{em}(t)|^2. \quad (18)$$

These occupation probabilities are normalized,

$$\sum_m P_{em}(t) = 1. \quad (19)$$

Initially, the ground state is populated exclusively,

$$P_{em}(t=0) = \delta_{m0}. \quad (20)$$

The time evolution of the electronic wave function (16) is obtained as solution of the time-dependent Schrödinger equation (TDSE)

$$i\hbar \frac{d}{dt} |\Psi_e(t)\rangle = \mathbf{H}_e(t) |\Psi_e(t)\rangle \quad (21)$$

with initial value (15). The expansion in terms of electronic eigenstates (16) yields the equivalent algebraic version of the TDSE,

$$i\hbar \, d/dt \, \mathbf{c}_e(t) = \mathbf{H}_e(t) \, \mathbf{c}_e(t) \quad (22)$$

with initial values (17) of the components $c_{em}(t)$ of the vector $\mathbf{c}_e(t)$. In practice, Equation (22) is applied with a finite set of eigenstates in the expansion (16). The numerical results are converged with respect to the number of eigenstates shown in Figures 3 and 4. The Hamilton matrix $\mathbf{H}_e(t)$ for the oriented molecule interacting with the $\mathbf{e} = \mathbf{e}_p$ polarized laser pulse has elements

$$\mathbf{H}_{e,mn}(t) = \langle m | \mathbf{H}_e(t) | n \rangle = E_m \delta_{mn} - \mathbf{e}_p \cdot \mathbf{d}_{mn} \cdot \mathcal{E}_p(t), \quad (23)$$

cf. Equations (6), (8) and (10). The formal solution of Equation (22) is

$$\mathbf{c}_e(t) = \mathbf{U}_e(t) \, \mathbf{c}_e(0) \quad (24)$$

with unitary time evolution operator

$$\mathbf{U}_e(t) = \hat{T} \exp \left[-i \int_0^t dt' \, \mathbf{H}_e(t') / \hbar \right] \quad (25)$$

where \hat{T} is the time ordering operator. Equations (24) and (25) are propagated numerically by means of the methods and programs which were developed in Refs. [24–27]. In a nutshell, the lowest-lying eigenstates of the many-body electronic Hamiltonian are calculated as linear combinations of Slater determinants at a chosen level of theory (i.e., MRCISD for benzene, and LR-TDDFT for magnesium porphyrin). This step is performed using standard quantum chemistry programs (MOLPRO and Gaussian 16). All matrix elements required to represent the time-dependent Hamiltonian are computed using the open-source toolbox detCI@ORBIT [28–30]. Note that the many-body electronic Hamiltonian is considered diagonal in the basis at the chosen level of theory. The coefficients (i.e., the contributions of the different Slater determinants) extracted from the quantum chemistry programs as solutions of the time-independent many-body Hamiltonian are first pruned by removing all contributions below 0.001, and then renormalized. The matrix elements of the dipole moment operator are computed by numerical integration using these pseudo-eigenstate wave functions. Finally, the time-evolution of the coefficients $\mathbf{c}_e(t)$ in Equation (24) is performed by direct numerical integration of the time-dependent Schrödinger equation using a preconditioned adaptive step size Runge–Kutta algorithm [31]. For more detail on the implementation, the propagation, and the calculation of the required matrix elements, the reader is referred to the cited literature.

After the end of the laser pulse ($t \geq t_f$ where $t_f = \tau_p$ for a single pulse, or $t_f = \tau_p + \tau_{p'}$ for two pulses p, p') the wave functions (16) represent charge migration in the field-free systems, see the examples in Section 3. They evolve with constant amplitudes and with linearly increasing phases of the coefficients

$$c_{em}(t) = |c_{em}(t_f)| \cdot \exp[-i E_m (t - t_m) / \hbar] \text{ for } t \geq t_f \quad (26)$$

and with constant population probabilities of the electronic eigenstates $|m\rangle$,

$$P_{em}(t) = P_{em}(t_f) = |c_{em}(t_f)|^2 \text{ for } t \geq t_f. \quad (27)$$

The phase of the coefficient $c_{e0}(t)$ of the ground state is equal to zero because we set $E_0 = 0$ eV, cf. Figures 3 and 4. The phases of the coefficients (26) for the excited states ($E_m > 0$ eV) are written such that $\exp[\dots] = 1$ at $t = t_m, t_m + \hbar/E_m, t_m + 2\hbar/E_m$, etc. The specific choice of t_m is irrelevant; for convenience, one may choose the first event t_m after the end of the laser pulse, $t_f < t_m < t_f + \hbar/E_m$ which satisfies the equality $\exp[\dots] = 1$.

2.7. Some Symmetry Relations of the Wavefunctions Driven by Laser Pulses with Different Linear Polarizations

In the applications to electron symmetry breaking in oriented benzene below, we shall compare the effects of laser pulses with different polarizations. In this Section, we assume that they are labeled $p = 1$ and 2 , e.g., $\mathbf{e}_{p=1} \equiv \mathbf{e}_1 = \mathbf{e}_x = \mathbf{e}''_1$ and $\mathbf{e}_{p=2} \equiv \mathbf{e}_2 = C_3 \mathbf{e}_1 = \mathbf{e}''_2$, with the same amplitudes of the electric fields, $\mathcal{E}_1(t) = \mathcal{E}_2(t) \equiv \mathcal{E}(t)$. (Note that the real applications in Section 3.1. use different labels, as specified at the end of this Section.) The purpose of this Section is to prove that the laser-driven population dynamics is robust with respect to threefold rotations C_3 of the polarization vectors. The corresponding electronic wavefunctions are denoted $\Psi_{\mathbf{e}_1}(\{\mathbf{r}_i\}, t)$ and $\Psi_{\mathbf{e}_2}(\{\mathbf{r}_i\}, t)$, depending on the Cartesian coordinates $\{\mathbf{r}_i\}$ of all electrons in the laboratory frame. In Dirac notation,

$$\Psi_{\mathbf{e}_1}(\{\mathbf{r}_i\}, t) \equiv \langle \{\mathbf{r}_i\} | \Psi_{\mathbf{e}_1}(t) \rangle. \quad (28)$$

Analogous notations hold for the electronic eigenfunctions $\langle \{\mathbf{r}_i\} | m \rangle \equiv \Psi_m(\{\mathbf{r}_i\})$, e.g., the wave function of the ground state $|0\rangle = |1A_{1g}\rangle$ depending on $\{\mathbf{r}_i\}$ is written as $\langle \{\mathbf{r}_i\} | 1A_{1g} \rangle \equiv \Psi_{1A_{1g}}(\{\mathbf{r}_i\})$. The electronic wavefunctions also depend on the electronic spins, and they depend parametrically on the nuclear charges and coordinates at the proper places of the oriented nuclear scaffold, but these dependencies are not written explicitly in Equation (28).

The electronic wavefunctions (28) are obtained as solutions of the electronic TDSEs

$$i\hbar \frac{d}{dt} \Psi_{\mathbf{e}_1}(\{\mathbf{r}_i\}, t) = H_{\mathbf{e}_1}(t) \Psi_{\mathbf{e}_1}(\{\mathbf{r}_i\}, t) = [H_e(\{\mathbf{r}_i\}) + e \mathbf{e}_1 \cdot \sum_i \mathbf{r}_i \cdot \mathcal{E}(t)] \Psi_{\mathbf{e}_1}(\{\mathbf{r}_i\}, t), \quad (29)$$

$$\begin{aligned} i\hbar \frac{d}{dt} \Psi_{\mathbf{e}_2}(\{\mathbf{r}_i\}, t) &= H_{\mathbf{e}_2}(t) \Psi_{\mathbf{e}_2}(\{\mathbf{r}_i\}, t) = [H_e(\{\mathbf{r}_i\}) + e \mathbf{e}_2 \cdot \sum_i \mathbf{r}_i \cdot \mathcal{E}(t)] \Psi_{\mathbf{e}_2}(\{\mathbf{r}_i\}, t) \\ &= [H_e(\{\mathbf{r}_i\}) + e C_3 \mathbf{e}_1 \cdot \sum_i \mathbf{r}_i \cdot \mathcal{E}(t)] \Psi_{\mathbf{e}_2}(\{\mathbf{r}_i\}, t) \\ &= [H_e(\{\mathbf{r}_i(t)\})] \Psi_{\mathbf{e}_2}(\{\mathbf{r}_i\}, t) \\ &= [H_e(C_3^{-1} \mathbf{r}_i)] + e \mathbf{e}_1 \cdot \sum_i C_3^{-1} \mathbf{r}_i \cdot \mathcal{E}(t) \Psi_{\mathbf{e}_2}(\{\mathbf{r}_i\}, t) \end{aligned} \quad (30)$$

The last Equation (30) holds because of the D_{6h} symmetry of the electronic Hamiltonian H_e . The two wave functions have the same initial values,

$$\begin{aligned} \Psi_{\mathbf{e}_1}(\{\mathbf{r}_i\}, t=0) &= \Psi_{\mathbf{e}_2}(\{\mathbf{r}_i\}, t=0) = \Psi_{A_{1g}}(\{\mathbf{r}_i\}) \\ &= C_3 \Psi_{A_{1g}}(\{\mathbf{r}_i\}) = \Psi_{\mathbf{e}_1}(C_3^{-1} \mathbf{r}_i, t=0). \end{aligned} \quad (31)$$

The last Equation (31) holds because of the IRREP A_{1g} of the initial electronic wave function of the oriented benzene in its ground state, with all characters equal to 1. Comparison of the last Equations (30) and (29) together with Equation (31) shows that the solution of Equation (30) is

$$\Psi_{\mathbf{e}_2}(\{\mathbf{r}_i\}, t) = \Psi_{\mathbf{e}_1}(C_3^{-1} \mathbf{r}_i, t) = C_3 \Psi_{\mathbf{e}_1}(\{\mathbf{r}_i\}, t). \quad (32)$$

That means rotation of the linear polarization \mathbf{e}''_1 of the laser pulse by 120° to $C_3 \mathbf{e}''_1 = \mathbf{e}''_2$ without any changes of the electric field amplitude $\mathcal{E}(t)$ rotates the laser-driven electronic wave function by the same angle 120° . In brief $\mathbf{e}''_1 \rightarrow \mathbf{e}''_2 = C_3 \mathbf{e}''_1$ yields the rotation of the wave function $\Psi_{\mathbf{e}''_1}(\{\mathbf{r}_i\}, t) \rightarrow \Psi_{\mathbf{e}''_2}(\{\mathbf{r}_i\}, t) = C_3 \Psi_{\mathbf{e}''_1}(\{\mathbf{r}_i\}, t)$.

The expansion (16) of the time-dependent wave function in terms of the eigenfunction implies the relation

$$\begin{aligned} \Psi_{\mathbf{e}''_1}(\{\mathbf{r}_i\}, t) &= \sum_m c_{\mathbf{e}''_1 m}(t) \Psi_m(\{\mathbf{r}_i\}) \rightarrow \Psi_{\mathbf{e}''_2}(\{\mathbf{r}_i\}, t) = C_3 \Psi_{\mathbf{e}''_1}(\{\mathbf{r}_i\}, t) \\ &= \sum_m c_{\mathbf{e}''_1 m}(t) C_3 \Psi_m(\{\mathbf{r}_i\}). \end{aligned} \quad (33)$$

The third Equation (33) means that rotation of the laser pulse polarization vector \mathbf{e}''_1 by 120° to $C_3 \mathbf{e}''_1 = \mathbf{e}''_2$ yields the same coefficients for the expansion in terms of the rotated eigenfunctions. The relation (33) also implies that the quantum dynamics of the populations of the rotated eigenfunctions is the same as Equation (18) for the non-rotated eigenfunctions.

Analogous symmetry relations for laser-driven wavefunctions of the oriented benzene hold for analogous rotations of polarizations

$$\begin{aligned} \mathbf{e}'_1 \rightarrow \mathbf{e}'_2 = C_3 \mathbf{e}'_1 & \text{ yields the rotation } \Psi_{\mathbf{e}'_1}(\{\mathbf{r}_i\}, t) \rightarrow \Psi_{\mathbf{e}'_2}(\{\mathbf{r}_i\}, t) = C_3 \Psi_{\mathbf{e}'_1}(\{\mathbf{r}_i\}, t), \\ \mathbf{e}'_1 \rightarrow \mathbf{e}'_3 = C_3^2 \mathbf{e}'_1 & \text{ yields the rotation } \Psi_{\mathbf{e}'_1}(\{\mathbf{r}_i\}, t) \rightarrow \Psi_{\mathbf{e}'_3}(\{\mathbf{r}_i\}, t) = C_3^2 \Psi_{\mathbf{e}'_1}(\{\mathbf{r}_i\}, t), \end{aligned} \quad (34)$$

$$\begin{aligned} \mathbf{e}''_1 \rightarrow \mathbf{e}''_2 = C_3 \mathbf{e}''_1 & \text{ yields the rotation } \Psi_{\mathbf{e}''_1}(\{\mathbf{r}_i\}, t) \rightarrow \Psi_{\mathbf{e}''_2}(\{\mathbf{r}_i\}, t) = C_3 \Psi_{\mathbf{e}''_1}(\{\mathbf{r}_i\}, t), \\ \mathbf{e}''_1 \rightarrow \mathbf{e}''_3 = C_3^2 \mathbf{e}''_1 & \text{ yields the rotation } \Psi_{\mathbf{e}''_1}(\{\mathbf{r}_i\}, t) \rightarrow \Psi_{\mathbf{e}''_3}(\{\mathbf{r}_i\}, t) = C_3^2 \Psi_{\mathbf{e}''_1}(\{\mathbf{r}_i\}, t), \end{aligned} \quad (35)$$

with consequences for the expansions of the wavefunctions in terms of the rotated eigenfunctions analogous to Equation (33).

Likewise, rotations of the linear polarizations of the laser pulses for electron symmetry breaking in the oriented Mg-porphyrin, without any changes of the amplitude of the electric field, yield the following symmetry relations of the resulting electronic wave functions:

$$\mathbf{e}'_1 \rightarrow \mathbf{e}'_2 = C_4 \mathbf{e}'_1 \quad \text{yields the rotation } \Psi_{\mathbf{e}'_1}(\{\mathbf{r}_i\}, t) \rightarrow \Psi_{\mathbf{e}'_2}(\{\mathbf{r}_i\}, t) = C_4 \Psi_{\mathbf{e}'_1}(\{\mathbf{r}_i\}, t), \quad (36)$$

$$\mathbf{e}''_1 \rightarrow \mathbf{e}''_2 = C_4 \mathbf{e}''_1 \quad \text{yields the rotation } \Psi_{\mathbf{e}''_1}(\{\mathbf{r}_i\}, t) \rightarrow \Psi_{\mathbf{e}''_2}(\{\mathbf{r}_i\}, t) = C_4 \Psi_{\mathbf{e}''_1}(\{\mathbf{r}_i\}, t), \quad (37)$$

again with consequences for the expansions of the wavefunctions in terms of the rotated eigenfunctions analogous to Equation (33), except that the rotation C_3 is replaced by C_4 .

In Section 3.1 below, we shall show that six different laser pulses labeled $p = 1, \dots, 6$ with the same electric field amplitudes $\mathcal{E}_1(t) = \dots = \mathcal{E}_6(t)$ but with different polarizations yield the same population dynamics (cf. Figure 5 below) but different electron symmetry breakings and different attosecond charge migrations in benzene. This equality of all six population dynamics is proven in two steps. First, the Equations (34) and (35) prove the equality of the population dynamics of the laser pulses with polarization vectors $\mathbf{e}_1'', \mathbf{e}_2'', \mathbf{e}_3''$ (corresponding to $p = 1, 3, 4$) and independently also for the polarization vectors $\mathbf{e}_1', \mathbf{e}_2', \mathbf{e}_3'$ ($p = 2, 5, 6$). Second, Appendix B has additional group theoretical derivations for the transition dipole matrix elements which imply the equality of the population dynamics of the laser pulses with polarization vectors \mathbf{e}_1'' and \mathbf{e}_1' . Likewise, in Sections 3.2 and 3.4 we shall show that four different laser pulses labeled $p = 1, \dots, 4$ with the same electric field amplitudes $\mathcal{E}_1(t) = \dots = \mathcal{E}_4(t)$ but with different polarizations yield the same population dynamics (cf. Section 3.4) but different electron symmetry breakings and different attosecond charge migrations in Mg-porphyrin. The equality of all four population dynamics is again proven in two steps. First, the Equations (36) and (37) prove the equality of the population dynamics of the laser pulses with polarization vectors $\mathbf{e}_1', \mathbf{e}_2'$ (corresponding to $p = 1, 3$) and independently also for the polarization vectors $\mathbf{e}_1'', \mathbf{e}_2''$ ($p = 2, 4$). Second, Appendix B implies the proof for the equality of the population dynamics of the laser pulses with polarization vectors \mathbf{e}_1' and \mathbf{e}_1'' .

2.8. Calculation of the One-Electron Density of the Time-Dependent Electronic Superposition State

The electronic wavefunction (16) and (28) of the oriented model system driven by the laser pulse with linear polarization \mathbf{e}_p (or by two sequential laser pulses) yields the one-electron density

$$\rho_p(\mathbf{r}, t) = \int |\Psi_{\mathbf{e}_p}(\{\mathbf{r}_i\}, t)|^2 d\mathbf{r}_2 d\mathbf{r}_3 \dots |_{\mathbf{r}=\mathbf{r}_1} \quad (38)$$

The integration (38) is over the Cartesian coordinates $\{\mathbf{r}_i\}$ of all anti-symmetrized electrons but one. The integration is also over all electron spins, but this is not written explicitly in Equation (38). It is carried out numerically by means of detCI@ORBKIT [28–30] and plotted using Matplotlib [32]. This method is also used to calculate the integrals for transition dipole matrix elements (8).

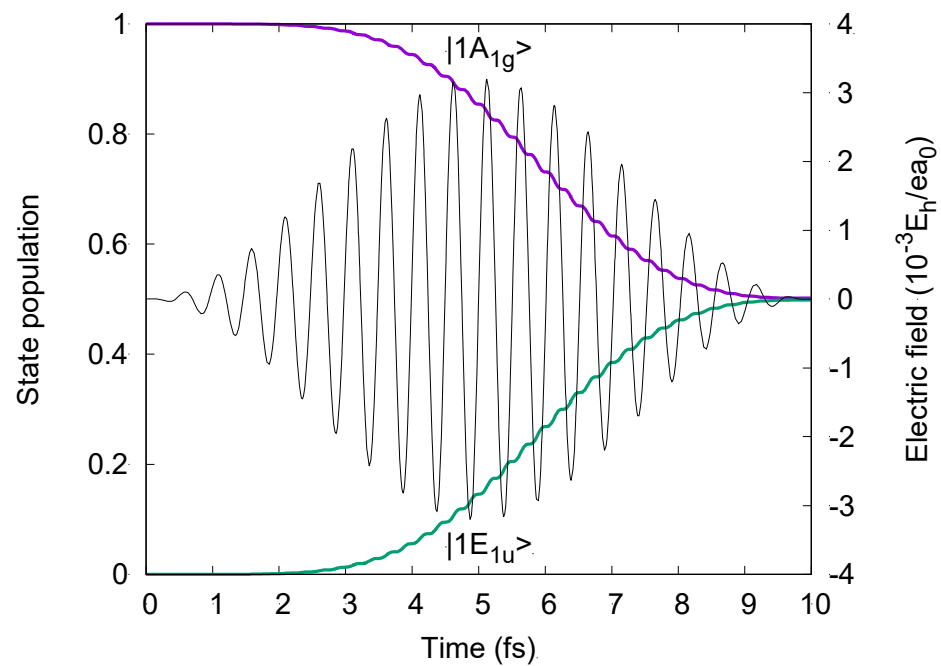


Figure 5. Electric field amplitude $\mathcal{E}(t) = \mathcal{E}_p(t)$ (Equation (1)) of six re-optimized $\pi/2$ laser pulses labeled $p = 1, \dots, 6$, and the resulting time evolutions of the population probabilities of selected eigenstates of the oriented model benzene. The $\mathcal{E}_p(t)$ are all the same, with the same laser parameters $\mathcal{E}_{0p} = 1.65 \times 10^7$ V/cm (corresponding to maximum intensity $I_{mp} = 3.616 \times 10^{11}$ W/cm²), $\tau_p = 10$ fs and $\omega_p = 8.17$ eV/ \hbar . The laser polarization vectors are different, however, specifically $\mathbf{e}_{p=1} = \mathbf{e}''_1 = \mathbf{e}_x$, $\mathbf{e}_{p=2} = \mathbf{e}'_1 = \mathbf{e}_y$, $\mathbf{e}_{p=3} = \mathbf{e}''_2 = C_3 \mathbf{e}''_1$, $\mathbf{e}_{p=4} = \mathbf{e}''_3 = C_3^2 \mathbf{e}''_1$, $\mathbf{e}_{p=5} = \mathbf{e}'_2 = C_3 \mathbf{e}'_1$ and $\mathbf{e}_{p=6} = \mathbf{e}'_3 = C_3^2 \mathbf{e}'_1$. All laser pulses $p = 1, \dots, 6$ yield the same population probability $P_{ep,m}(t)$ of the ground state $|m\rangle = |1A_{1g}\rangle$, and the same $P_{ep,m}(t)$ for the \mathbf{e}_p -selective excited target states, specifically for $|m\rangle = |1E_{1u}^x\rangle, |1E_{1u}^y\rangle, C_3|1E_{1u}^x\rangle, C_3^2|1E_{1u}^x\rangle, C_3|1E_{1u}^y\rangle, C_3^2|1E_{1u}^y\rangle$, respectively (Equations (33)–(35)). The populations of all other eigenstates are negligible.

The linear expansion of the electronic wavefunction (16) allows to decompose the one-electron density into “diagonal” (dia, $m = n$) and “off-diagonal” (odi, $m \neq n$) contributions,

$$\begin{aligned} \rho_p(\mathbf{r}, t) &= \rho_{p,\text{dia}}(\mathbf{r}, t) + \rho_{p,\text{odi}}(\mathbf{r}, t), \\ \rho_{p,\text{dia}}(\mathbf{r}, t) &= \sum_m |c_{ep,m}(t)|^2 \int |\Psi_m(\{\mathbf{r}_i\})|^2 d\mathbf{r}_2 d\mathbf{r}_3 \dots \big|_{\mathbf{r}=\mathbf{r}_1}, \\ \rho_{p,\text{odi}}(\mathbf{r}, t) &= \sum_{m < n} [c_{ep,m}(t)^* c_{ep,n}(t) \int \Psi_m(\{\mathbf{r}_i\})^* \Psi_n(\{\mathbf{r}_i\}) d\mathbf{r}_2 d\mathbf{r}_3 \dots \big|_{\mathbf{r}=\mathbf{r}_1} \\ &\quad + c_{ep,m}(t) c_{ep,n}(t)^* \int \Psi_m(\{\mathbf{r}_i\}) \Psi_n(\{\mathbf{r}_i\})^* d\mathbf{r}_2 d\mathbf{r}_3 \dots \big|_{\mathbf{r}=\mathbf{r}_1}]. \end{aligned} \quad (39)$$

For times t after the end t_f of the laser pulse, or of two sequential laser pulses, the field-free evolution of the expansion coefficients (26) renders these parts time-independent and time-dependent, respectively,

$$\begin{aligned} \rho_p(\mathbf{r}, t) &= \langle \rho_p(\mathbf{r}) \rangle + \Delta \rho_p(\mathbf{r}, t) \text{ for } t \geq t_f, \\ \langle \rho_p(\mathbf{r}) \rangle &= \rho_{p,\text{dia}}(\mathbf{r}, t_f) = \sum_m P_{ep,m}(t_f) \int |\Psi_m(\{\mathbf{r}_i\})|^2 d\mathbf{r}_2 d\mathbf{r}_3 \dots \big|_{\mathbf{r}=\mathbf{r}_1}, \\ &\equiv \sum_m P_{ep,m}(t_f) \rho_m(\mathbf{r}), \\ \Delta \rho_p(\mathbf{r}, t) &= \rho_{p,\text{odi}}(\mathbf{r}, t) = \sum_{m < n} |c_{ep,m}(t_f)|^* |c_{ep,n}(t_f)| \\ &\quad \times \{ \exp[i(E_m - E_n)t/\hbar] \int \Psi_m(\{\mathbf{r}_i\})^* \Psi_n(\{\mathbf{r}_i\}) d\mathbf{r}_2 d\mathbf{r}_3 \dots \big|_{\mathbf{r}=\mathbf{r}_1} \\ &\quad + \exp[i(E_n - E_m)t/\hbar] \int \Psi_m(\{\mathbf{r}_i\}) \Psi_n(\{\mathbf{r}_i\})^* d\mathbf{r}_2 d\mathbf{r}_3 \dots \big|_{\mathbf{r}=\mathbf{r}_1} \} \\ &= \sum_{m < n} |c_{ep,m}(t_f)|^* |c_{ep,n}(t_f)| \\ &\quad \times 2 \cos(\omega_{mn} t) \int \Psi_m(\{\mathbf{r}_i\}) \Psi_n(\{\mathbf{r}_i\})^* d\mathbf{r}_2 d\mathbf{r}_3 \dots \big|_{\mathbf{r}=\mathbf{r}_1} \end{aligned} \quad (40)$$

The notation in the first and second Equation (40) indicates that $\langle \rho_p(\mathbf{r}) \rangle$ is the long time mean average of $\rho_p(\mathbf{r}, t)$

$$\langle \rho_p(\mathbf{r}) \rangle = \lim_{t \rightarrow \infty} [1/(t - t_f)] \int_{t_f}^t \rho_p(\mathbf{r}, t') dt' \quad (41)$$

whereas $\Delta \rho_p(\mathbf{r}, t)$ is the time-dependent deviation from the mean. The $\rho_m(\mathbf{r})$ in Equation (40) is the one-electron densities of the eigenstates $|m\rangle$, e.g., $\rho_0(\mathbf{r}) = \rho_{1A_{1g}}(\mathbf{r})$ is the one-electron density of the ground state $|0\rangle = |1A_{1g}\rangle$, illustrated in Figures 1 and 2 for the oriented benzene and Mg-porphyrin, respectively. The last Equation (40) with transition frequencies

$$\omega_{mn} = (E_m - E_n)/\hbar \quad (42)$$

and transition periods

$$T_{mn} = 2\pi/\omega_{mn} \quad (43)$$

holds because we use real-valued electronic eigenfunctions.

2.9. Re-Optimized $\pi/2$ - and π -Laser Pulses for Control of Electron Symmetry Breaking and Charge Migration

The applications in Section 3 shall demonstrate electron symmetry breaking in the oriented model systems, benzene and Mg-porphyrin, by means of short linearly polarized laser pulses labeled $p = 1, 2, 3, \dots$, or by two sequential laser pulses. The total pulse duration should be below 10 fs so that the nuclear scaffolds are still frozen [7,8] with the conservation of nuclear symmetry. Initially, the systems are in the electronic ground state with IRREP A_{1g} . The initial electron symmetry is, therefore, the same as the nuclear symmetry, namely $G = D_{6h}$ and D_{4h} , respectively. After the laser pulse, or after two sequential laser pulses, the symmetry of the one-electron density (Section 2.8) is broken from G down to a subgroup $S(\rho_p(\mathbf{r}, t))$ of G . The subgroup $S(\rho_p(\mathbf{r}, t))$ depends on the one-electron density $\rho_p(\mathbf{r}, t)$ which is generated by the laser pulse labeled p . It is determined in the field-free environment immediately after the laser pulse, when the oriented model system still keeps the original nuclear symmetry of the frozen scaffold, but the electrons already exhibit charge migration, on typical time scales from a few hundred as to a few fs. One of the purposes of the applications is to demonstrate that the different linearly polarized laser pulses can prepare the electrons in a rather large variety of symmetries with different subgroups $S(\rho_p(\mathbf{r}, t))$ of G . This means that one can use the laser pulses to control electron symmetry while conserving nuclear symmetry. In many cases (but by no means in all cases), this type of laser control of electron symmetry is achieved by means of laser pulses which excite the oriented systems from the electronic ground state to a selective superposition of the ground plus one excited states, with equal population probabilities. The laser pulses which achieve this goal are so-called $\pi/2$ pulses, or re-optimized $\pi/2$ pulses.

The general theory for $\pi/2$ pulses is presented, e.g., in Ref. [33]; for applications, see, e.g., Refs. [1,2,10,15]. Here, we adapt the specific result for linearly polarized laser pulses with \sin^2 -shapes, electric field amplitude \mathcal{E}_0 and duration τ , cf. Section 2.1. Accordingly, the $\pi/2$ laser pulse for the selective transition from the initial state $|\Psi_i\rangle = |\Psi_{A_{1g}}\rangle$ to the superposition state $(1/\sqrt{2})(|\Psi_i\rangle + |\Psi_f\rangle)$ should be resonant to the energy gap between the states, i.e., the photon energy is tuned to

$$\hbar\omega = \hbar\omega_{if} \equiv E_f - E_i \quad (44)$$

with period

$$T = T_{if} = 2\pi/\omega_{if} \quad (45)$$

Moreover, the electric field amplitude \mathcal{E}_0 and the duration τ should satisfy the condition [10,15,33]

$$|d_{if}|^2 \mathcal{E}_0^2 \tau / (2\hbar) = \pi/2 \text{ for } \pi/2 \text{ pulses} \quad (46)$$

where $|d_{if}|$ denotes the absolute value of the transition dipole matrix element $\langle \Psi_i | \mathbf{d} | \Psi_f \rangle$ for the initial state $|\Psi_i\rangle$ and the target state $|\Psi_f\rangle$.

For a target transition $|\Psi_i\rangle \rightarrow (1/\sqrt{2})(|\Psi_i\rangle + |\Psi_f\rangle)$ with specific value of $|d_{if}|$, the rule (46) calls for the proper value of the product $\mathcal{E}_0 \cdot \tau$. Accordingly, large values of $|d_{if}|$ are favourable because they allow small values $\mathcal{E}_0 \cdot \tau$. The rule (46) allows some flexibility for the choice of the individual laser parameters, e.g., one could use either long weak pulses or short intense ones. The present applications call for a compromise, i.e., the laser pulses must be short ($\tau \leq 10$ fs) but not all too short, to avoid exceedingly large values of the maximum intensities I_m , cf. Section 2.1.

The rules (44)–(46) were derived for the ideal so-called two-state scenario with exclusive transitions between just two states, $|\Psi_i\rangle$ and $|\Psi_f\rangle$ [33]. Moreover, they hold for laser pulses with large numbers of optical cycles,

$$N_c = \tau/T \gg 1. \quad (47)$$

In contrast, the present multi-state quantum dynamics simulations (Section 2.6) allow—in principle, at least—many other transitions, and some of the pulses are just few-cycle pulses. For these more realistic scenarios, the rules (44)–(47) serve as a zero-order approximation. Systematic re-optimization of the laser parameters, e.g., slight detuning of the resonance frequency combined with variations of the field strength, then yields re-optimized $\pi/2$ pulses for the target transitions [15].

The subsequent discussions also refer to so-called π laser pulses. These achieve complete population transfer from the initial state $|\Psi_i\rangle$ to $|\Psi_f\rangle$. They require the same conditions (44) and (47) as for the $\pi/2$ pulses, but the condition (46) is replaced by [10,15,32].

$$|d_{if}| \cdot \mathcal{E}_0 \cdot \tau / (2 \cdot \hbar) = \pi \text{ for } \pi \text{ pulses.} \quad (48)$$

3. Results

This Section for the results is divided into three major parts: The first part has Sections 3.1 and 3.2. They demonstrate “empirical” numerical results for electron symmetry breaking by short linearly polarized laser pulses, from the groups G of the rigid nuclear scaffolds of the oriented model systems, benzene ($G = D_{6h}$) and Mg-porphyrin ($G = D_{4h}$), respectively, to various subgroups $S(\rho_p(\mathbf{r},t))$ of G . These results are based on the evidence of the symmetry elements of the one-electron density $\rho_p(\mathbf{r},t)$ which represents charge migration right after the laser pulses labeled p . The pulses are illustrated in the set of Figures 5–12, in particular in Figures 5, 9 and 11 below. Their mathematical expression is in Equation (1). The laser polarizations are listed in Table 2. All other laser parameters, i.e., the final values of the amplitudes, frequencies and pulse durations are in Figures 5, 9 and 11 below. The resulting one-electron densities are illustrated in Figures 6–8, 10 and 12 below. Their electron symmetries are listed in Tables 3 and 4 below. The second part has Sections 3.3 and 3.4. They present the theory of electron symmetry breaking, to explain the phenomena of Sections 3.1 and 3.2, respectively. The third part has Section 3.5—this discovers a simple general rule for electron symmetry breaking by short linearly polarized laser pulses which comprise all cases presented in Sections 3.1–3.4

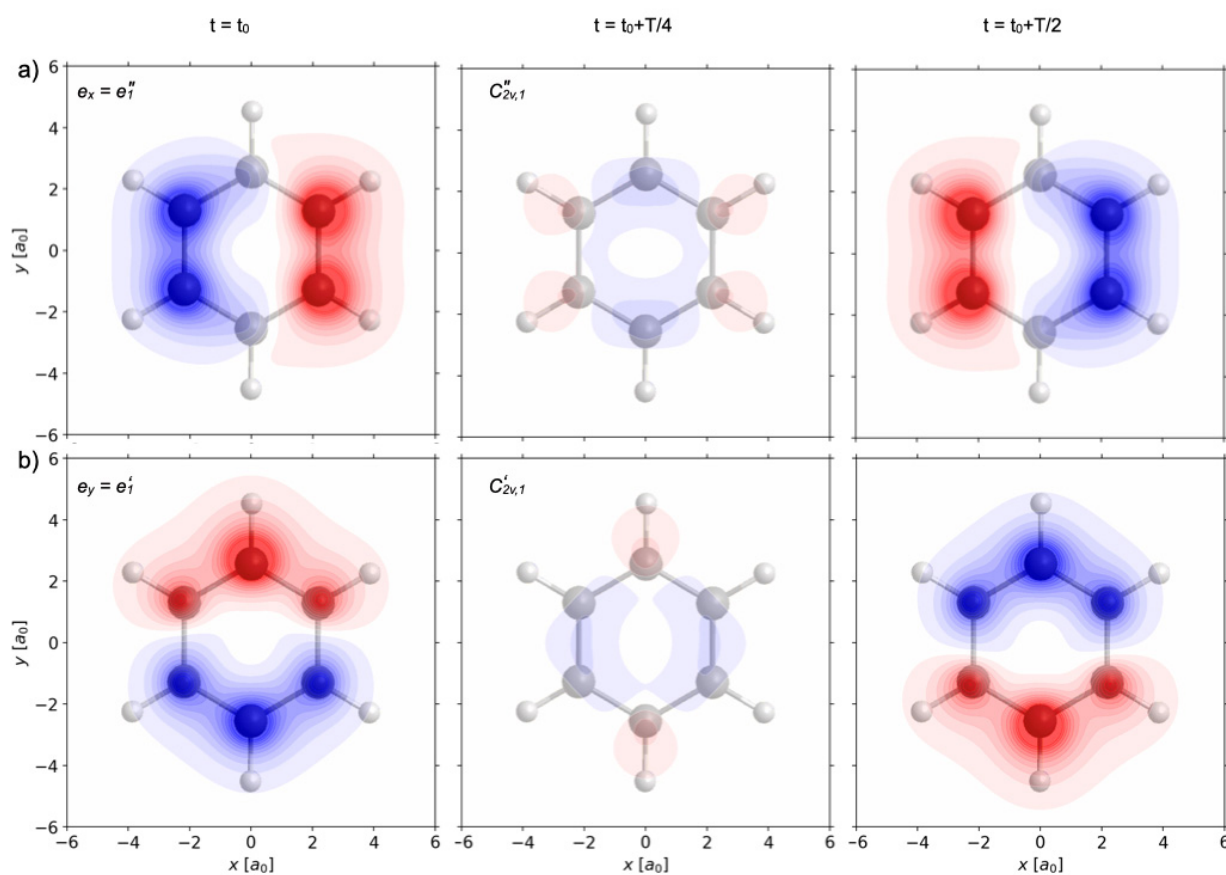


Figure 6. Time evolutions of the “swapping” one-electron densities $\rho_p(\mathbf{r},t) - \rho_{1A1g}(\mathbf{r})$ (cf. Equation (40)) in the oriented model benzene (cf. Figure 1), initiated by re-optimized $\pi/2$ laser pulses labeled $p = 1$ (panel a, top row) and $p = 2$ (panel b, bottom row). The electric fields amplitude $\mathcal{E}(t) = \mathcal{E}_p(t)$ of the pulses are shown in Figure 5. The polarization vectors are $\mathbf{e}_{p=1} = \mathbf{e}''_1 = \mathbf{e}_x$ and $\mathbf{e}_{p=2} = \mathbf{e}'_1 = \mathbf{e}_y$, respectively. The original ($t = 0$) one-electron density with D_{6h} symmetry is documented in Figure 1. The time evolutions of $\rho_p(\mathbf{r},t) - \rho_{1A1g}(\mathbf{r})$ are illustrated by three snapshots taken at $t = t_0$ (i.e., soon after the end of the laser pulses, left columns; see text for details), at $t = t_0 + T/4$ (middle columns) and at $t = t_0 + T/2$ (right columns). Equivalent snapshots at $t = t_0 + (3/4)T$ and at $t = t_0 + T$ look the same as those shown for $t = t_0 + T/4$ and for $t = t_0$, respectively. Each snapshot presents a colored contour plot of the integral $\int dz [\rho_p(\mathbf{r},t) - \rho_{1A1g}(\mathbf{r})]$ superimposed on the frozen nuclear scaffold. Red (blue) contours represent regions of electron density increase (depletion). The swapping one-electron densities in panels 6a and 6b document two different types of charge migration with period T , cf. Equation (43). They conserve three symmetry elements, namely $C''_{2v,1}$, σ_h , σ_{d1} (a) and $C'_{2v,1}$, σ_h , σ_{v1} (b), cf. Figure 1. Accordingly, the combined Figures 1 and 6a as well as Figures 1 and 6b document two different types of electron symmetry breaking induced by the \mathbf{e}''_1 and \mathbf{e}'_1 polarized laser pulses $p = 1$ and $p = 2$, namely $D_{6h} \rightarrow S(\rho_{p=1}(\mathbf{r},t)) = C''_{2v,1} = \{E, C''_{2v,1}, \sigma_h, \sigma_{d1}\}$ and $D_{6h} \rightarrow S(\rho_{p=2}(\mathbf{r},t)) = C'_{2v,1} = \{E, C'_{2v,1}, \sigma_h, \sigma_{v1}\}$, respectively.

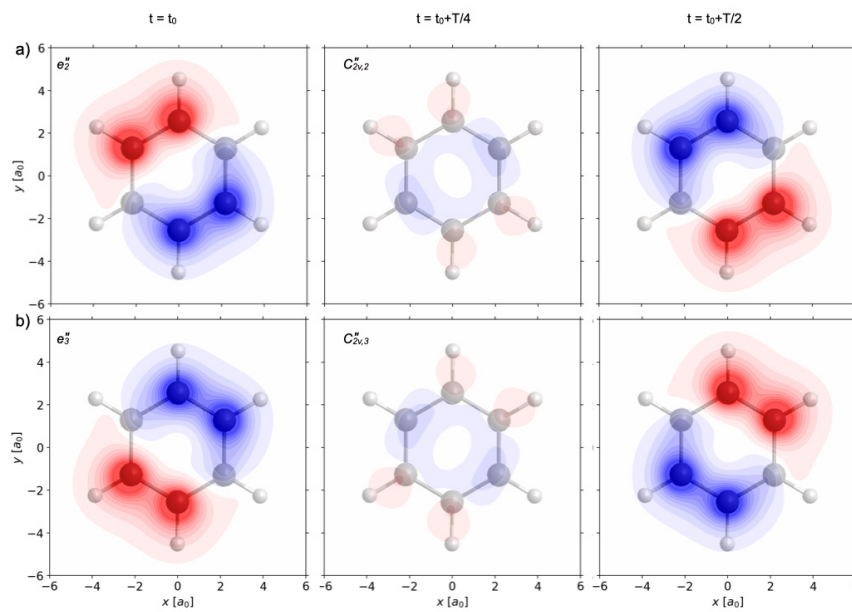


Figure 7. Same as Figure 6a, but for re-optimized $\pi/2$ laser pulses labeled $p=3,4$ with the same electric fields $\mathcal{E}_p(t) = \mathcal{E}(t)$ as shown in Figure 5, but with different polarizations $\mathbf{e}_{p=3} = \mathbf{e}''_2 = C_3 \mathbf{e}''_1$ (panel a) and $\mathbf{e}_{p=4} = \mathbf{e}''_3 = C_3^2 \mathbf{e}''_1$ (panel b), respectively. The resulting swapping one-electron densities appear as images of those shown in Figure 6a, rotated by 120° (C_3 , panel a) and by 240° (C_3^2 , panel b), respectively. By analyses analogous to those for Figure 6a, the combined Figures 1 and 7a as well as 1 and 7b document two different types of laser ($p = 3$ and $p = 4$)-induced electron symmetry breaking, namely $D_{6h} \rightarrow S(\rho_{p=3}(\mathbf{r},t)) = C_{2v}''_2 = \{E, C_2''_2, \sigma_h, \sigma_{d2}\}$ and $D_{6h} \rightarrow S(\rho_{p=4}(\mathbf{r},t)) = C_{2v}''_3 = \{E, C_2''_3, \sigma_h, \sigma_{d3}\}$, respectively. The nuclear symmetry D_{6h} is robust.

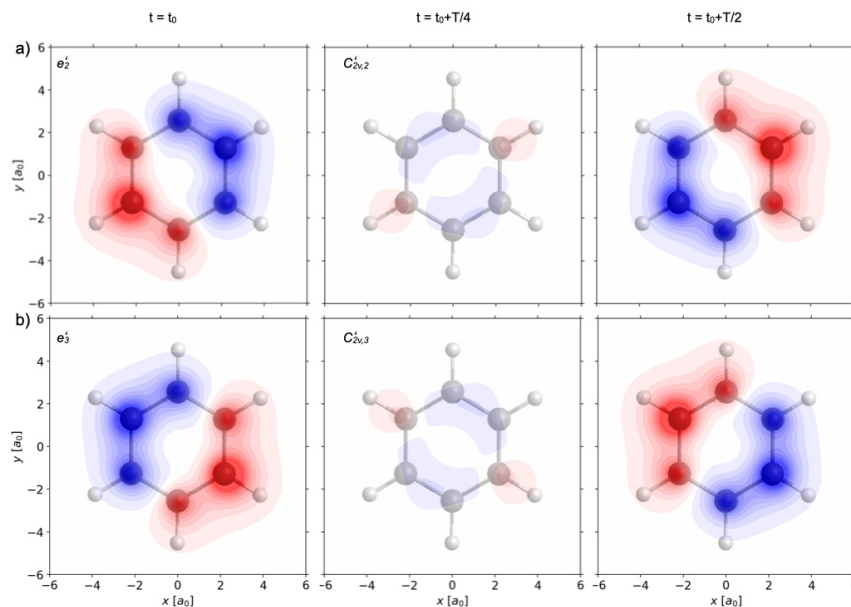


Figure 8. Same as Figure 6b, but for re-optimized $\pi/2$ laser pulses labeled $p = 5, 6$ with the same electric fields $\mathcal{E}_p(t) = \mathcal{E}(t)$ as shown in Figure 5, but with different polarizations $\mathbf{e}_{p=5} = \mathbf{e}'_2 = C_3 \mathbf{e}'_1$ (panel a) and $\mathbf{e}_{p=6} = \mathbf{e}'_3 = C_3^2 \mathbf{e}'_1$ (panel b), respectively. The resulting swapping one-electron densities appear as images of those shown in Figure 6b, rotated by 120° (C_3 , panel a) and by 240° (C_3^2 , panel b), respectively. By analyses analogous to those for Figure 6b, the combined Figures 1 and 8a as well as 1 and 8b document two different types of laser ($p = 5$ and $p = 6$)-induced electron symmetry breaking, namely $D_{6h} \rightarrow S(\rho_{p=5}(\mathbf{r},t)) = C_{2v}'_2 = \{E, C_2'_2, \sigma_h, \sigma_{v2}\}$ and $D_{6h} \rightarrow S(\rho_{p=6}(\mathbf{r},t)) = C_{2v}'_3 = \{E, C_2'_3, \sigma_h, \sigma_{v3}\}$, respectively. The nuclear symmetry D_{6h} is robust.

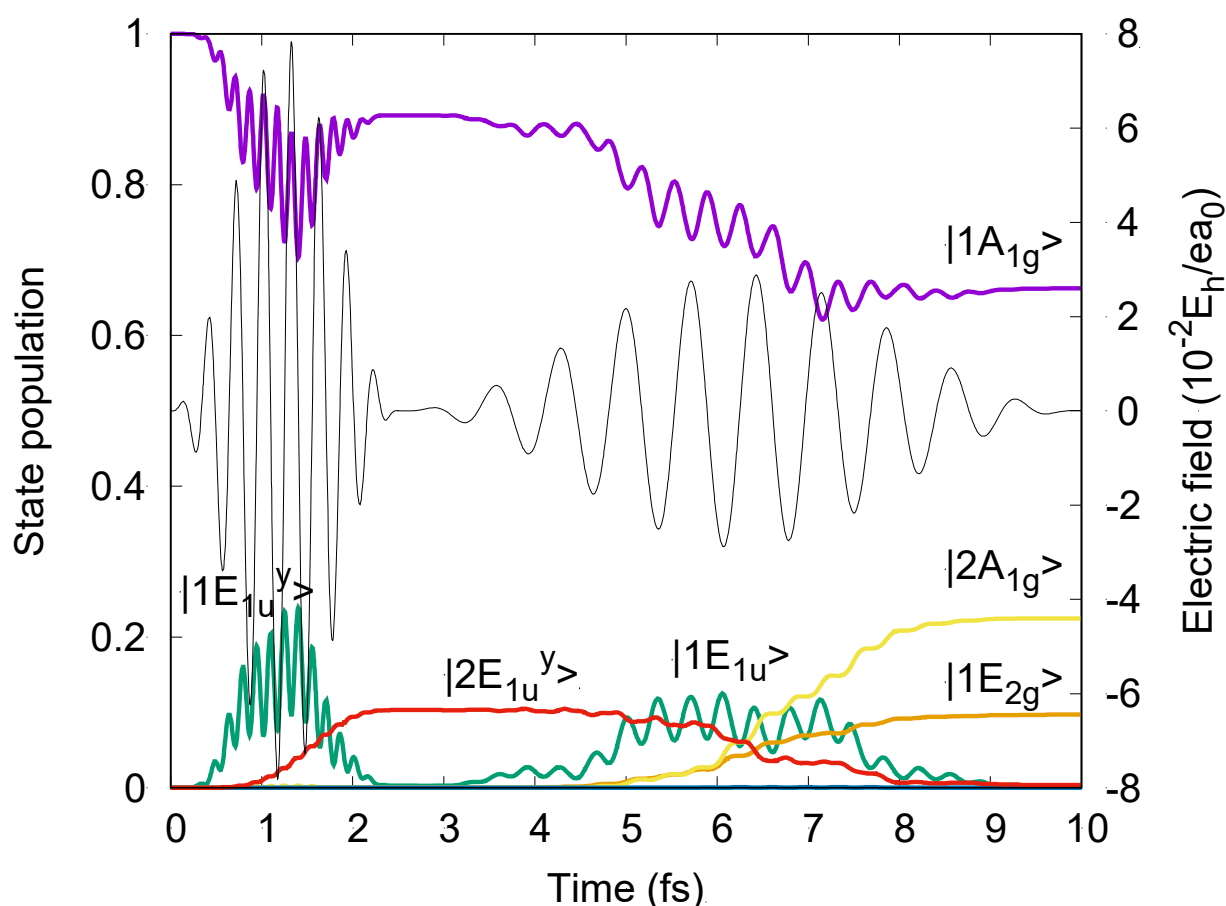


Figure 9. Electric field amplitude of two sequences of laser pulses labeled $p = 7$ and 8 and $p = 7$ and 9 , and the resulting time evolutions of the population probabilities of selected eigenstates of the oriented model benzene. The first laser pulse ($p = 7$) is the same in both cases. It has electric field amplitude $\mathcal{E}_7(t)$ with laser parameters $\mathcal{E}_{07} = 4.06 \times 10^8$ V/cm (corresponding to maximum intensity $I_{m7} = 2.19 \times 10^{14}$ W/cm²), $\tau_7 = 2.5$ fs and undertuned frequency $\omega_7 = 13.6$ eV/ \hbar . The laser polarization vector is $\mathbf{e}_{p=7} = \mathbf{e}'_1 = \mathbf{e}_y$. The second laser pulses have the same electric field amplitudes $\mathcal{E}_8(t) = \mathcal{E}_9(t)$ with the same laser parameters $\mathcal{E}_{08} = \mathcal{E}_{09} = 1.49 \times 10^8$ V/cm (corresponding to maximum intensity $I_{m8} = I_{m9} = 2.95 \times 10^{13}$ W/cm²), $\tau_8 = \tau_9 = 7.5$ fs and $\omega_8 = \omega_9 = 5.75$ eV/ \hbar . The polarization vectors are different, however, specifically $\mathbf{e}_{p=8} = \mathbf{e}'_1 = \mathbf{e}_y$ versus $\mathbf{e}_{p=9} = \mathbf{e}''_1 = \mathbf{e}_x$. The resulting populations $P_{\mathbf{e}_{7\&8,m}}(t)$ and $P_{\mathbf{e}_{7\&9,m'}}(t)$ of eigenstates $|m\rangle$ and $|m'\rangle$, respectively, show that at the end of the first laser pulse ($p=7$, $t = \tau_7 = 2.5$ fs), benzene is excited to a superposition of $|1A_{1g}\rangle$ and $|2E_{1u}^y\rangle$. At the end of the second laser pulses ($p = 8$ or 9 , $t = t_f = \tau_7 + \tau_8 = \tau_7 + \tau_9 \equiv \tau = 10$ fs), benzene is excited to different superpositions of three eigenstates, namely $|1A_{1g}\rangle$, $|2A_{1g}\rangle$, $|1E_{2g}\rangle = |1E_{2g}^{x^2-y^2}\rangle$ versus $|1A_{1g}\rangle$, $|2A_{1g}\rangle$, $|1E_{2g}\rangle = |1E_{2g}^{xy}\rangle$, respectively. Additionally shown are transient populations of states $|1E_{1u}^y\rangle$ (during pulse $p = 7$) and $|1E_{1u}\rangle = |1E_{1u}^y\rangle$ (during pulse $p = 8$) or $|1E_{1u}\rangle = |1E_{1u}^x\rangle$ (during pulse $p = 9$).

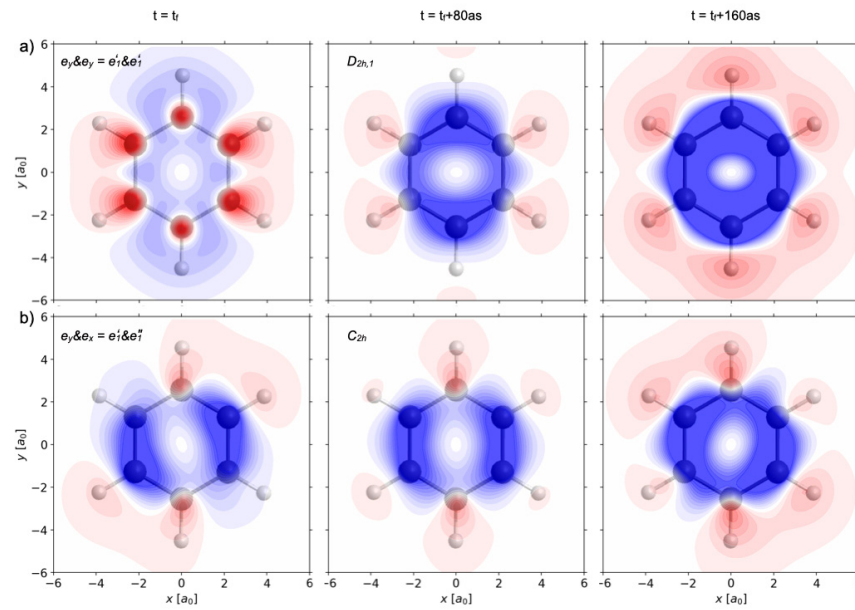


Figure 10. Time evolutions of the “swapping” one-electron densities $\rho_p(\mathbf{r},t) - \rho_{1A_{1g}}(\mathbf{r})$ (cf. Equation (40)) in the oriented model benzene (cf. Figure 1), initiated by two sequential laser pulses labeled $p = 7$ and 8 (panel **a**) and $p = 7$ and 9 (panel **b**). The electric field parameters are as in Figure 9. The time evolutions of $\rho_p(\mathbf{r},t) - \rho_{1A_{1g}}(\mathbf{r})$ are illustrated by three snapshots taken at $t = t_f = \tau_p = 10$ fs (i.e., at the end of the laser pulses, left columns), at $t = t_f + 0.080$ fs (middle columns) and at $t = t_f + 0.160$ fs (right columns). Each snapshot presents a colored contour plot of the integral $\int dz [\rho_p(\mathbf{r},t) - \rho_{1A_{1g}}(\mathbf{r})]$ superimposed on the frozen nuclear scaffold. The top and bottom panels document charge migration initiated using pulses with different polarizations, given in the leftmost panels.

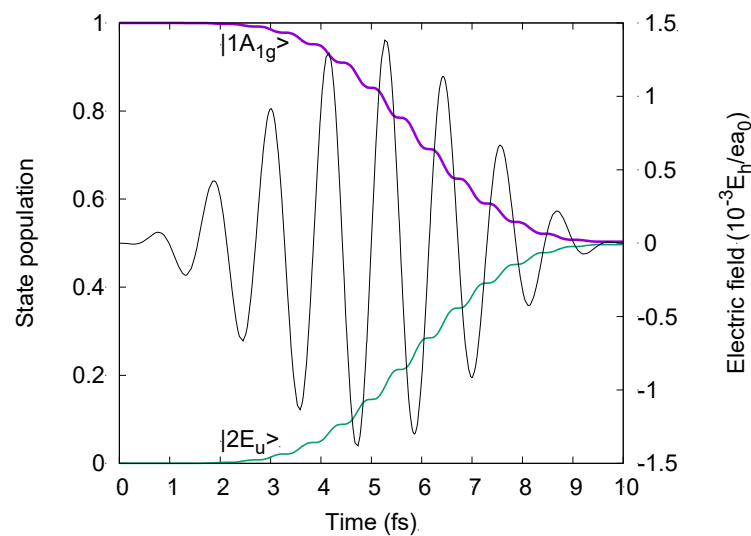


Figure 11. Electric field amplitude $\mathcal{E}(t) = \mathcal{E}_p(t)$ (Equation (1)) of two re-optimized $\pi/2$ laser pulses labeled $p = 1, 2$ and the resulting time evolutions of the population probabilities of selected eigenstates of the oriented model Mg-porphyrin. The $\mathcal{E}_p(t)$ are the same, with the same laser parameters $\mathcal{E}_{0p} = 7.20 \times 10^6$ V/cm (corresponding to maximum intensity $I_{mp} = 6.88 \times 10^{10}$ W/cm²), $\tau_p = 10$ fs and $\omega_p = 3.60$ eV/ \hbar . The laser polarization vectors are different, however, specifically $\mathbf{e}_{p=1} = \mathbf{e}'_1 = \mathbf{e}_x$ and $\mathbf{e}_{p=2} = \mathbf{e}''_1 = C_8 \mathbf{e}'_1$. The laser pulses $p = 1, 2$ yield the same population probability $P_{ep,m}(t)$ of the ground state $|m\rangle = |1A_{1g}\rangle$, and the same $P_{ep,m}(t)$ for the \mathbf{e}_p -selective excited target states, specifically for $|m\rangle = |1E_u^x\rangle \equiv |2E_u'^1\rangle$ and $|2E_u''_1\rangle$, respectively. The populations of all other eigenstates are negligible.

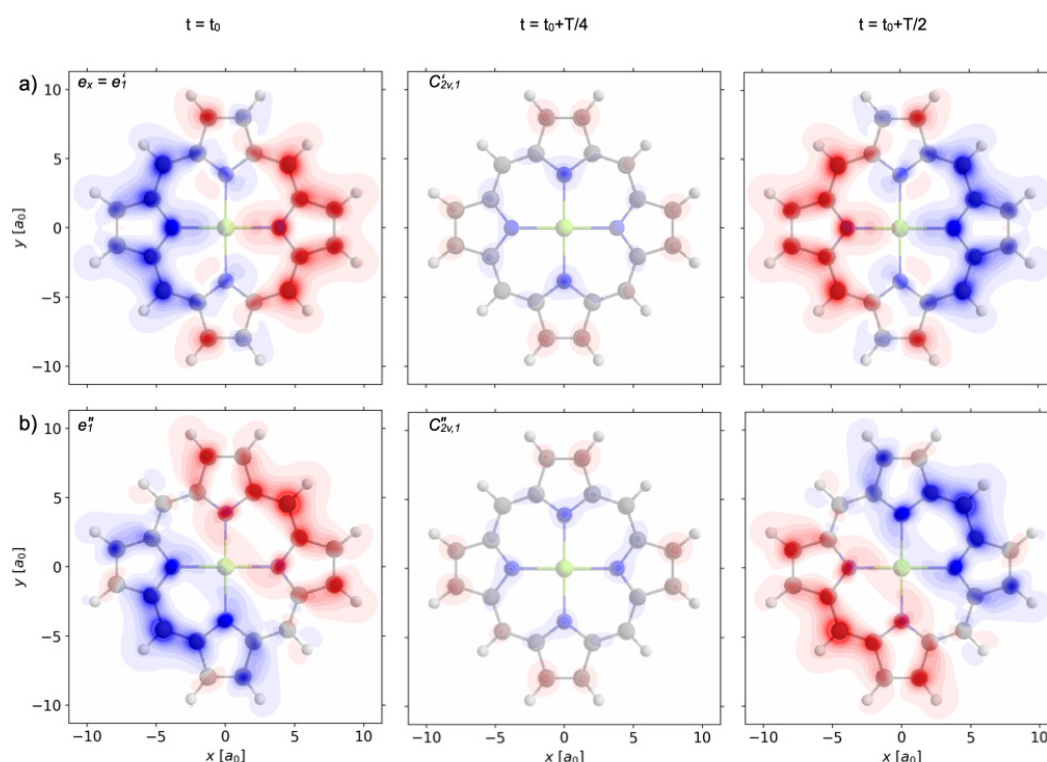


Figure 12. Time evolutions of the “swapping” one-electron densities $\rho_p(\mathbf{r},t) - \rho_{1A1g}(\mathbf{r})$ (cf. Equation (40)) in the oriented model Mg-porphyrin (cf. Figure 2), initiated by re-optimized $\pi/2$ laser pulses labeled $p = 1$ (panel a) and $p = 2$ (panel b). The electric fields amplitude $\mathcal{E}(t) = \mathcal{E}_p(t)$ of the pulses are shown in Figure 11. The polarization vectors are $\mathbf{e}_{p=1} = \mathbf{e}'_1 = \mathbf{e}_x$ and $\mathbf{e}_{p=2} = \mathbf{e}''_1 = (1/\sqrt{2})(\mathbf{e}_x + \mathbf{e}_y)$, respectively. The original ($t = 0$) one-electron density with D_{4h} symmetry is documented in Figure 2. The time evolutions of $\rho_p(\mathbf{r},t) - \rho_{1A1g}(\mathbf{r})$ are illustrated by three snapshots taken at $t = t_0$ (i.e., at the first occurrence of maximal phase coherence after the end of the laser pulses, left columns), at $t = t_0 + 0.287$ fs (middle columns) and at $t = t_0 + 0.574$ fs (right columns). Each snapshot presents a colored contour plot of the integral $\int dz [\rho_p(\mathbf{r},t) - \rho_{1A1g}(\mathbf{r})]$ superimposed on the frozen nuclear scaffold (the colors are chosen as in Figure 6). The swapping one-electron densities in Figure 12a,b document two different types of charge migration. They conserve three symmetry elements, namely $C_{2v,1}'$, σ_h , σ_{v1} (a) and $C_{2v,1}''$, σ_h , σ_{d1} (b), cf. Figure 1. Accordingly, the combined Figures 2 and 12a as well as Figures 2 and 12b document two different types of electron symmetry breaking induced by the \mathbf{e}'_1 and \mathbf{e}''_1 polarized laser pulses $p = 1$ and $p = 2$, namely $D_{4h} \rightarrow S(\rho_{p=1}(\mathbf{r},t)) = C_{2v,1}' = \{E, C_{2v,1}', \sigma_h, \sigma_{v1}\}$ and $D_{4h} \rightarrow S(\rho_{p=2}(\mathbf{r},t)) = C_{2v,1}'' = \{E, C_{2v,1}'', \sigma_h, \sigma_{d1}\}$, respectively.

3.1. Electron Symmetry Breaking and Charge Migration Induced by Linearly Polarized Laser Pulses in Oriented Benzene with D_{6h} Nuclear Scaffold

This Section presents the results of quantum dynamics simulations (cf. Section 2.6) of eight different examples of electron symmetry breaking in the oriented model benzene (cf. Section 2.2) induced by eight different linearly polarized laser pulses labeled $p = 1, 2, 3, \dots$, or two sequential laser pulses (cf. Section 2.1). The symmetry breakings $G = D_{6h} \rightarrow S(\rho_p(\mathbf{r},t))$ yield eight different point subgroups $S(\rho_p(\mathbf{r},t))$ of G for the one-electron densities $\rho_p(\mathbf{r},t)$ (cf. Section 2.8) which present eight different types of attosecond charge migration, right after the end of the laser pulse(s). The durations of the laser pulses, or two sequential laser pulses, are restricted to 10 fs, such that the nuclear scaffolds may be considered as frozen [7,8], implying conservation of nuclear D_{6h} symmetry.

The first two examples (labeled $p = 1, 2$) are motivated by the results of Ref. [10] which discovered quantum control of electronic fluxes during attosecond charge migration in superposition states of oriented benzene. The charge migration is illustrated in Ref. [10] by means of snapshots of the one-electron density. As a byproduct, but without explicit observation (even without mentioning the word “symmetry!”), Ref. [10] demonstrates two different C_{2v} -type symmetries of the time-dependent one-electron densities which are generated by two different linearly \mathbf{e}_x and \mathbf{e}_y polarized $\pi/2$ laser pulses with Gaussian

shapes. Here, we employ two similar re-optimized $\pi/2$ laser pulses with \sin^2 -shapes (cf. Sections 2.1 and 2.9), labeled $p = 1$ and 2, which are tailored to selective transitions from the initial ($t = 0$) electronic ground state $|1A_{1g}\rangle$ to the superposition states $(1/\sqrt{2})*(|1A_{1g}\rangle + |1E_{1u}^x\rangle)$ and $(1/\sqrt{2})*(|1A_{1g}\rangle + |1E_{1u}^y\rangle)$, respectively. The notation $\{|1E_{1u}^x\rangle, |1E_{1u}^y\rangle\}$ denotes the doublet of two orthogonal degenerate states with IRREP E_{1u} and with the lowest energy $E_{1E_{1u}}$ which transform as the functions x and y (in brief: as x and y), respectively [13]. The target transitions are illustrated schematically by vertical arrows from the energy level $E_{1A_{1g}}$ to $E_{1E_{1u}}$ in Figure 3. The energy gap between their eigenenergies is $\Delta E_{1A_{1g},1E_{1u}} = E_{1E_{1u}} - E_{1A_{1g}} = 8.17$ eV with corresponding transition frequency $\omega_{1A_{1g},1E_{1u}} = \Delta E_{1A_{1g},1E_{1u}} / \hbar$ and period $T = T_{1A_{1g},1E_{1u}} = 2\pi / \omega_{1A_{1g},1E_{1u}} = \hbar / \Delta E_{1A_{1g},1E_{1u}} = 506$ as, cf. Equations (42) and (43). The pulses have the same electric field amplitudes $\mathcal{E}_1(t) = \mathcal{E}_2(t) \equiv \mathcal{E}(t)$ which is shown in Figure 5, but different polarization vectors $\mathbf{e}_1 = \mathbf{e}_x = \mathbf{e}''_1$ and $\mathbf{e}_2 = \mathbf{e}_y = \mathbf{e}''_1$. The identical laser parameters are specified in Figure 5; the frequencies $\omega_1 = \omega_2$ are resonant with the transition frequency $\omega_{1A_{1g},1E_{1u}}$. Figure 5 also shows the resulting two-state population dynamics $P_{1A_{1g}}(t)$ and $P_{1E_{1u}^x}(t) = P_{1E_{1u}^y}(t) \equiv P_{1E_{1u}}(t)$, documenting perfect preparation of the target superposition states, with the same amplitudes ($= 1/\sqrt{2}$) of the ground and degenerate excited states at the end ($t = \tau_1 = \tau_2 \equiv \tau$) of the laser pulses. The populations of all other states are entirely negligible.

Table 3. Electronic superposition states of oriented benzene and the characters ($=1$) of the totally symmetric representations of their symmetry subgroups.

$ \Psi\rangle = 0\rangle + m\rangle$ (a)	$ A_{1g}\rangle + E_{1u}^x\rangle$	$ A_{1g}\rangle + E_{1u}^y\rangle$	$ A_{1g}\rangle + E_{1u}^z\rangle$	$ A_{1g}\rangle + E_{1u}^x\rangle$	$ A_{1g}\rangle + E_{1u}^y\rangle$	$ A_{1g}\rangle + E_{1u}^z\rangle$	$ A_{1g}\rangle + E_{2g}^{x^2-y^2}\rangle$	$ A_{1g}\rangle + E_{2g}^{xy}\rangle$	$ A_{1g}\rangle + B_{2u}\rangle$	$ A_{1g}\rangle + B_{1u}\rangle$
$g \in D_{6h}$ (b)										
E	1	1	1	1	1	1	1	1	1	1
$2C_6$										
$2C_3$									1	1
C_2^z							1	1		
C_{21}'				1			1			1
C_{22}'					1					1
C_{23}'						1				1
C_{21}''	1						1		1	
C_{22}''		1							1	
C_{23}''			1						1	
i							1	1		
$2S_3$									1	1
$2S_6$										
σ_h	1	1	1	1	1	1	1	1	1	1
σ_{v1}				1			1			1
σ_{v2}					1					1
σ_{v3}						1				1
σ_{d1}	1						1		1	
σ_{d2}		1							1	
σ_{d3}			1						1	
$S_\Psi \subseteq D_{6h}$	$C_{2v,1}'$	$C_{2v,2}'$	$C_{2v,3}'$	$C_{2v,1}'$	$C_{2v,2}'$	$C_{2v,3}'$	$D_{2h,1}$	C_{2h}	D_{3h}'	D_{3h}'
IRREP of S_Ψ (c)	A_1	A_1	A_1	A_1	A_1	A_1	A_g	A_g	A_1	A_1
$S_\rho \subseteq D_{6h}$	$C_{2v,1}''$	$C_{2v,2}''$	$C_{2v,3}''$	$C_{2v,1}''$	$C_{2v,2}''$	$C_{2v,3}''$	$D_{2h,1}$	C_{2h}	D_{3h}''	D_{3h}''
Laser pulses p (d)	1	3	4	2	5	6	7&8	7&9	Ref. [1]	Ref. [1]

(a) The expression $|A\rangle + |B\rangle$ denotes the superposition of two non-vanishing electronic wave functions with IRREP A_{1g} and another IRREP. The superposition states are prepared by selective laser pulses, and they depend on the laser polarizations and on the time after the laser pulses, cf. Section 3.1. (b) Some important symmetry elements corresponding to the symmetry operations g are illustrated in Figure 1.

(c) The electronic superposition state $|\Psi\rangle$ transforms according to the totally symmetric IRREP of the subgroup $S_\Psi \equiv S(\Psi)$ of D_{6h} . The subgroups are specified in Tables 1 and 2. (d) Cf. Section 3.1.

Table 4. Electronic superposition states of oriented Mg-porphyrin and the characters (=1) of the totally symmetric representations of their symmetry subgroups.

$g \in D_{4h}$ (b)	$ \Psi\rangle = 0\rangle + m\rangle$ (a) $ A_{1g}\rangle + E'_{u1}\rangle$ $ A_{1g}\rangle + E'_{u2}\rangle$ $ A_{1g}\rangle + E''_{u1}\rangle$ $ A_{1g}\rangle + E''_{u2}\rangle$			
E	1	1	1	1
C_4^+				
C_4^-				
C_2^z				
C_{21}'	1			
C_{22}'		1		
C_{21}''			1	
C_{22}''				1
i				
S_4^-				
S_4^+				
σ_h	1	1	1	1
σ_{v1}	1			
σ_{v2}		1		
σ_{d1}			1	
σ_{d2}				1
$S_\Psi \subseteq D_{4h}$ IRREP of S_Ψ (c)	$C'_{2v,1}$ A_1	$C'_{2v,2}$ A_1	$C''_{2v,1}$ A_1	$C''_{2v,2}$ A_1
$S_\rho \subseteq D_{4h}$	$C'_{2v,1}$	$C'_{2v,2}$	$C''_{2v,1}$	$C''_{2v,1}$
Laser pulses p (d)	1	2	3	4

(a) The expression $|A\rangle + |B\rangle$ denotes the superposition of two non-vanishing electronic wave functions with IRREP A_{1g} and another IRREP, e.g., $E'_{u1} \equiv E'_{u1}^x, E'_{u2} \equiv E'_{u2}^y$, etc. The superposition states are prepared by selective laser pulses, and they depend on the laser polarizations and on the time after the laser pulses, cf. Section 3.2. (b) Some important symmetry elements corresponding to the symmetry operations g are illustrated in Figure 2. (c) The electronic superposition state $|\Psi\rangle$ transforms according to the totally symmetric IRREP of the subgroup $S_\Psi \equiv S(\Psi)$ of. The subgroups are specified in Table 2. The corresponding one-electron density ρ has the same subgroup $S_\rho \equiv S(\rho) = S_\Psi$. (d) Cf. Sections 3.2 and 3.4.

Figure 6a,b illustrate the field-free time evolutions of the one-electron densities $\rho_p(\mathbf{r}, t)$ after the end of the re-optimized $\pi/2$ laser pulses labeled $p=1$ and 2, respectively. They are represented by three snapshots of $\rho_p(\mathbf{r}, t) - \rho_p(\mathbf{r}, t=0) = \rho_p(\mathbf{r}, t) - \rho_{1A_{1g}}(\mathbf{r})$ integrated over z , i.e., $\int [\rho_p(\mathbf{r}, t) - \rho_{1A_{1g}}(\mathbf{r})] dz$. The snapshots are taken at $t = t_0, t_0 + T/4$ and $t_0 + T/2$, with period $T = T_{1A_{1g}, 1E_{1u}}$. Here, t_0 is the first time after the end of the laser pulse when the phase factor $\exp[\dots]$ of $c_{e, 1E_{1u}}(t)$ is equal to 1, cf. Equation (26). This equality is obtained during the first period T after the end of the laser pulse, $t_f = \tau \leq t_0 \leq \tau + T$, such that the nuclei can still be considered as frozen, conserving nuclear symmetry. Sequel snapshots at $t = t_0 + (3/4)T$ and at $t_0 + T$ look the same as those at $t = t_0 + T/4$ and at t_0 , respectively. The subtraction of the initial one-electron density $\rho_p(\mathbf{r}, t=0) = \rho_{1A_{1g}}(\mathbf{r})$ from $\rho_p(\mathbf{r}, t)$ yields what may be called the “swapping one-electron density”, i.e., that part of the one-electron density which is driven by the laser pulse away from the original reference $\rho_{1A_{1g}}(\mathbf{r})$. It facilitates recognition of the time evolution and the symmetry of the one-electron density after the laser pulse; in contrast, the temporal changes of $\rho_p(\mathbf{r}, t)$ would be hardly recognizable. Appendix A proves that the electron symmetry of $\rho_p(\mathbf{r}, t)$ is the same as for the swapping one-electron density, $\rho_p(\mathbf{r}, t) - \rho_{1A_{1g}}(\mathbf{r})$.

Altogether, the time evolution of the laser-driven one-electron densities illustrated in Figure 6a,b demonstrate two different types of periodic charge migrations, essentially from the left to the right CC bonds (and back, $p = 1$), or from the domains of the bottom to the top C-atoms (and back, $p = 2$), respectively, with period $T = T_{1A_{1g}, 1E_{1u}}$. At time $t = t_0$, the swapping one-electron densities are accumulated in the left CC bond ($p = 1$), or

in the domain of the bottom C-atom ($p = 2$). At $t = t_0 + T/4$, they “tunnel” [34] between the sites, and at $t_0 + T/2$, they arrive on the opposite sites. At $t = t_0 + (3/4)T$, they tunnel back (snapshot identical to the one for $t = t_0 + T/4$), and at $t = t_0 + T$, they are back to the densities at $t = t_0$, completing the first cycle of periodic charge migration.

Inspection of the swapping one-electron density $\rho_{p=1}(\mathbf{r}, t) - \rho_{1A_{1g}}(\mathbf{r}) \equiv \rho_{\mathbf{e}''_1}(\mathbf{r}, t) - \rho_{1A_{1g}}(\mathbf{r})$ (Figure 6a) which is prepared by the $\mathbf{e}_1 = \mathbf{e}_x = \mathbf{e}''_1$ polarized re-optimized $\pi/2$ laser pulse reveals that it conserves three and only three symmetry elements of the frozen nuclear symmetry point group $G = D_{6h}$, namely the binary rotation axis $C_2''_1$, the related dihedral plane σ_{d1} , and the horizontal plane σ_h . The corresponding symmetry operations constitute the subgroup $S(\rho_{p=1}(\mathbf{r}, t)) = C_{2v}''_1 = \{E, C_2''_1, \sigma_h, \sigma_{d1}\}$. Accordingly, the one-electron density $\rho_{\mathbf{e}''_1}(\mathbf{r}, t)$ evolves with $C_{2v}''_1$ symmetry. In conclusion, the $\mathbf{e}_1 = \mathbf{e}_x = \mathbf{e}''_1$ polarized re-optimized $\pi/2$ laser pulse yields electron symmetry breaking $G = D_{6h} \rightarrow S(\rho_{p=1}(\mathbf{r}, t)) = C_{2v}''_1$.

By analogy, inspection of the swapping one-electron density $\rho_{p=2}(\mathbf{r}, t) - \rho_{1A_{1g}}(\mathbf{r})$ (Figure 6b) which is prepared by the $\mathbf{e}_2 = \mathbf{e}_y = \mathbf{e}'_1$ polarized re-optimized $\pi/2$ laser pulse reveals that it conserves a different set of three symmetry elements. The corresponding symmetry operations constitute the subgroup $S(\rho_{p=2}(\mathbf{r}, t)) = C_{2v}'_1 = \{E, C_2'_1, \sigma_h, \sigma_{v1}\}$ of $G = D_{6h}$. In conclusion, the $\mathbf{e}_2 = \mathbf{e}_y = \mathbf{e}'_1$ polarized re-optimized $\pi/2$ laser pulse yields electron symmetry breaking $G = D_{6h} \rightarrow S(\rho_{p=2}(\mathbf{r}, t)) = C_{2v}'_1$.

Figure 7a,b show the effects of two other re-optimized $\pi/2$ laser pulses labeled $p = 3, 4$. They have the same electric field amplitudes $\mathcal{E}_3(t) = \mathcal{E}_4(t) = \mathcal{E}(t)$ with the same laser parameters as the previous ones ($p = 1, 2$, cf. Figure 5), but different polarizations, $\mathbf{e}_3 = \mathbf{e}''_2 = C_3 \mathbf{e}''_1$ and $\mathbf{e}_4 = \mathbf{e}''_3 = C_3^2 \mathbf{e}''_1$, respectively. As shown in Section 2.7 (cf. the rule (35)), the rotations of the laser polarizations cause corresponding rotations of the laser-driven wave functions which may be expanded in terms of corresponding rotated eigenfunctions. The resulting population dynamics is the same as for the non-rotated wave functions, cf. Figure 5. Accordingly, the resulting time evolutions of the one-electron densities appear as images of the one shown in Figure 6a, rotated by 120° (C_3) and by 240° (C_3^2), respectively. By analogy with the previous analyses, inspection of the resulting swapping one-electron densities $\rho_3(\mathbf{r}, t) - \rho_{1A_{1g}}(\mathbf{r}) \equiv \rho_{\mathbf{e}''_2}(\mathbf{r}, t) - \rho_{1A_{1g}}(\mathbf{r})$ and $\rho_4(\mathbf{r}, t) - \rho_{1A_{1g}}(\mathbf{r}) \equiv \rho_{\mathbf{e}''_3}(\mathbf{r}, t) - \rho_{1A_{1g}}(\mathbf{r})$ show that the laser pulses labeled $p = 3$ and 4 yield electron symmetry breaking from $G = D_{6h}$ to two subgroups $S(\rho_{p=3}(\mathbf{r}, t)) = C_{2v}''_2 = \{E, C_2''_2, \sigma_h, \sigma_{d2}\}$ and $S(\rho_{p=4}(\mathbf{r}, t)) = C_{2v}''_3 = \{E, C_2''_3, \sigma_h, \sigma_{d3}\}$ —these are different from the previous subgroups $S(\rho_{p=1}(\mathbf{r}, t))$ and $S(\rho_{p=2}(\mathbf{r}, t))$.

Likewise, Figure 8a,b show the effects of two other re-optimized $\pi/2$ laser pulses labeled $p = 5, 6$. They have the same electric field amplitudes $\mathcal{E}_5(t) = \mathcal{E}_6(t) = \mathcal{E}(t)$ and the same laser parameters as the previous ones ($p = 1, 2, 3, 4$, cf. Figure 5), but different polarizations, $\mathbf{e}_5 = \mathbf{e}'_2 = C_3 \mathbf{e}'_1$ and $\mathbf{e}_6 = \mathbf{e}'_3 = C_3^2 \mathbf{e}'_1$, respectively. The resulting time evolutions of the swapping one-electron densities appear as images of the one shown in Figure 6b, rotated by 120° (C_3) and by 240° (C_3^2), respectively, in accord with the rule (34). By analogy with the previous analyses, inspection of the resulting swapping one-electron densities $\rho_5(\mathbf{r}, t) - \rho_{1A_{1g}}(\mathbf{r}) \equiv \rho_{\mathbf{e}'_2}(\mathbf{r}, t) - \rho_{1A_{1g}}(\mathbf{r})$ and $\rho_6(\mathbf{r}, t) - \rho_{1A_{1g}}(\mathbf{r}) \equiv \rho_{\mathbf{e}'_3}(\mathbf{r}, t) - \rho_{1A_{1g}}(\mathbf{r})$ show that the re-optimized $\pi/2$ laser pulses labeled $p=5$ and 6 yield electron symmetry breaking $G = D_{6h} \rightarrow S(\rho_{p=5}(\mathbf{r}, t)) = C_{2v}'_2 = \{E, C_2'_2, \sigma_h, \sigma_{v2}\}$ and $S(\rho_{p=6}(\mathbf{r}, t)) = C_{2v}'_3 = \{E, C_2'_3, \sigma_h, \sigma_{v3}\}$, different from the previous ones.

Finally, we present two additional electron symmetry breakings in the oriented benzene, which are achieved by two different sequences of two linearly polarized laser pulses. The first example is motivated by a specific result of Ref. [1] for laser preparation of oriented benzene in selective non-aromatic (“na”) superposition states

$$|\Psi_{na,1}\rangle = (1/\sqrt{2}) * (|1A_{1g}\rangle + |1B_{2u}\rangle) \quad (49)$$

or

$$|\Psi_{na,2}\rangle = (1/\sqrt{2}) * (|1A_{1g}\rangle + |1B_{1u}\rangle). \quad (50)$$

For the orientation of benzene adapted from Ref. [1], cf. Figure 1, the excited states $|1B_{2u}\rangle$ and $|1B_{1u}\rangle$ transform as $x(x^2 - 3y^2)$ and $y(3x^2 - y^2)$, respectively [13]. Symmetry selection rules do not allow direct excitations of the ground state to these target states [1,13], but Ulusoy and Nest succeeded in designing sequences of three e_x and e_y linearly polarized laser pulses, or alternative re-optimized pulses which reach the goals. Our first example is stimulated by their series of three e_y polarized laser pulses which prepare the target state (50) by means of three transitions which are all symmetry allowed. The first one is a $\pi/2$ laser pulses which excites the aromatic ground state $|1A_{1g}\rangle$ to the superposition state $(1/\sqrt{2})(|1A_{1g}\rangle + |1E_{1u}^y\rangle)$, analogous to the present laser pulse labeled $p = 2$. The second one is a π laser pulse which transfers the excited state $|1E_{1u}^y\rangle$ into $|1E_{2g}^{x^2-y^2}\rangle$. This state is one of two degenerate $1E_{2g}$ states $\{|1E_{2g}^{x^2-y^2}\rangle, |1E_{2g}^{xy}\rangle\}$ with energy $E_{1E_{2g}}$ which transform as $x^2 - y^2$ and xy , respectively [13]. The third one is another π laser pulse which transfers $|1E_{2g}^{x^2-y^2}\rangle$ into $|1B_{1u}\rangle$. Consequently, at the ends of the second and third laser pulses, the oriented benzene is in the superposition state $(1/\sqrt{2})(|1A_{1g}\rangle + |1E_{2g}^{x^2-y^2}\rangle)$ and finally in the target state (50), respectively.

As set off in the Introduction, Ulusoy and Nest already noted that their three-step approach to laser control of aromaticity in oriented benzene breaks electron symmetry [1]. Our original plan was to investigate laser-induced electron symmetry breaking already after two steps, i.e., after excitation of the ground state ($|1A_{1g}\rangle$ first to the superposition state $(1/\sqrt{2})(|1A_{1g}\rangle + |1E_{1u}^y\rangle)$ and then to $(1/\sqrt{2})(|1A_{1g}\rangle + |1E_{2g}^{x^2-y^2}\rangle)$, by means of two e_y polarized $\pi/2$ and π laser pulses, but now under the constraint of the conservation of nuclear symmetry. In the context of this manuscript, these laser pulses shall be labeled $p = 7$ and 8 , or briefly $7\&8$. The constraint requires that their durations should add up to $\tau_7 + \tau_8 \leq 10$ fs. [7,8].

Unfortunately, however, the plan cannot be realized, because of the following dilemma: Ulusoy and Nest's "intermediate" excited states $|1E_{1u}^y\rangle$ and $|1E_{2g}^{x^2-y^2}\rangle$ are near-degenerate, cf. Figure 3. The narrow energy gap $E_{1E_{1u}} - E_{1E_{2g}} = \hbar\omega_{1E_{1u},1E_{2g}} = 0.306$ eV implies the rather long period $T_{1E_{1u},1E_{2g}} = 2\pi/\omega_{1E_{1u},1E_{2g}} = 13.52$ fs, cf. Equation (45). The condition (47) thus requires that the second π laser pulse should take too long to transfer the "intermediate" excited state $|1E_{1u}^y\rangle$ into $|1E_{2g}^{x^2-y^2}\rangle$. This is far beyond the upper limit, 10 fs, for the conservation of nuclear symmetry, i.e., for our purpose, it is unacceptable.

To overcome this problem, it is essential to get rid of the near degeneracy of the levels $E_{1E_{1u}}$ and $E_{1E_{2g}}$. For this purpose, we decided that the "first" intermediate state $|1E_{1u}^y\rangle$ should be replaced by the more excited state $|2E_{1u}^y\rangle$ with much higher energy $E_{2E_{1u}}$ compared to $E_{1E_{1u}}$. The corresponding sequence of two laser-induced target transitions is illustrated schematically by two sequential arrows in Figure 3. The previous near degeneracy is clearly lifted. Specifically, the energy gap between states $|2E_{1u}^y\rangle$ and $|1E_{2g}^{x^2-y^2}\rangle$ is $E_{2E_{1u}} - E_{1E_{2g}} = 5.75$ eV, with corresponding period $T_{2E_{1u},1E_{2g}} = 719$ as. Likewise, the energy gap between states $|2E_{1u}^y\rangle$ and $|1A_{1g}\rangle$ is $E_{2E_{1u}} - E_{1A_{1g}} = 14.23$ eV, with period $T_{2E_{1u},1A_{1g}} = 291$ as. These two periods are short enough to satisfy condition (47) for two laser pulses with durations $\tau_7 = 2.5$ fs and $\tau_8 = 7.5$ fs, respectively. Their durations add up to $t_f = \tau_7 + \tau_8 = 10$ fs, in accord with the constraint for the conservation of nuclear symmetry [7,8]. The smaller value of τ_7 compared to τ_8 is suggested by condition (47), due to the smaller value of $T_{2E_{1u},1A_{1g}}$ compared to $T_{2E_{1u},1E_{2g}}$.

The replacement of the intermediate state $|1E_{1u}^y\rangle$ by the more excited state $|2E_{1u}^y\rangle$ with the same IRREP raises another problem, however, namely the absolute values of the y -components of the transition matrix element $|\langle 1A_{1g} | d_y | 2E_{1u}^y \rangle| = 0.161$ e a_0 for the target transitions $|1A_{1g}\rangle \rightarrow |2E_{1u}^y\rangle$ via $|2E_{1u}^y\rangle$ is significantly smaller than $|\langle 1A_{1g} | d_y | 1E_{1u}^y \rangle| = 2.339$ e a_0 for Ulusoy and Nest's transitions via $|1E_{1u}^y\rangle$. At the same time, the required durations $\tau_7 = 2.5$ fs and $\tau_8 = 7.5$ fs are an order of magnitude smaller than the values used in Ref. [1]. Consequently, the conditions (46) and (48) for a hypothetical sequence of $\pi/2$ and π laser pulses for sequential transitions $|1A_{1g}\rangle \rightarrow |2E_{1u}^y\rangle \rightarrow |1E_{2g}^{x^2-y^2}\rangle$ call for exceedingly large field strengths and intensities—this is, again, unacceptable.

The way out of this dilemma is pointed by Ref. [2] which shows that for the present purpose, i.e., for laser-induced electron symmetry breaking, it is not really necessary to use $\pi/2$ and π laser pulses. Instead, it suffices to employ weaker pulses $p = 7$ and/or 8 which prepare superposition states such as $c_{e'1,1A1g}(\tau_7) |1A1g\rangle + c_{e'1,2E1uy}(\tau_7) |2E1u^y\rangle$ and subsequently $c_{e'1\&e'1,1A1g}(t_f) |1A1g\rangle + c_{e'1\&e'1,1E2g}(t_f) |1E2g^{x^2-y^2}\rangle$, with rather small populations of the excited states compared to the ground states, $P_{e'1,2E1uy}(\tau_7) = |c_{e'1,2E1uy}(\tau_7)|^2 \ll P_{e'1,1A1g}(\tau_7) = |c_{e'1,1A1g}(\tau_7)|^2$ and $P_{e'1\&e'1,1E2g^{x^2-y^2}}(t_f) = |c_{e'1\&e'1,1E2g^{x^2-y^2}}(t_f)|^2 \ll P_{e'1\&e'1,1A1g}(t_f) = |c_{e'1\&e'1,1A1g}(t_f)|^2$. Consequently, we employ two sequential linearly $e_7 = e_8 = e_y = e'_1$ polarized laser pulses with durations $\tau_7 = 2.5$ fs and $\tau_8 = 7.5$ fs, with the same form of the electric fields, Equation (1), as before, with the carrier frequencies slightly detuned from the resonance frequencies, yet with electric field strengths well below the values for hypothetical $\pi/2$ and π pulses. The electric fields $\mathcal{E}_p(t)$ of the laser pulses $p = 7, 8$ are illustrated in Figure 9. The laser parameters are listed in the Figure 9. The resulting population dynamics are also shown in Figure 9.

Figure 9 shows that at the end ($\tau_7 = 2.5$ fs) of the first $e_{p=7} = e'_1 = e_y$ polarized laser pulse $p = 7$, the oriented benzene is excited from the initial ground state $|1A1g\rangle$ to the intermediate target superposition state $c_{e'1,1A1g}(\tau_7) |1A1g\rangle + c_{e'1,1E1uy}(\tau_7) |1E1u^y\rangle$, with populations $P_{e'1,1E1uy}(\tau_7) = |c_{e'1,1E1uy}(\tau_7)|^2 = 0.105 \ll P_{e'1,1A1g}(\tau_7) = |c_{e'1,1A1g}(\tau_7)|^2 = 0.890$. Subsequently, at $t_f = \tau_7 + \tau_8 = 10$ fs, the second $e_{p=8} = e'_1 = e_y$ polarized laser pulse $p = 8$ yields the superposition of three eigenstates (cf. Equation (16))

$$|\Psi_{e'1\&e'1}(t_f = \tau_7 + \tau_8)\rangle = c_{e'1\&e'1,1A1g}(t_f) |1A1g\rangle + c_{e'1\&e'1,2A1g}(t_f) |2A1g\rangle + c_{e'1\&e'1,1E2g^{x^2-y^2}}(t_f) |1E2g^{x^2-y^2}\rangle \quad (51)$$

with populations $P_{e'1\&e'1,1A1g}(t_f) = |c_{e'1\&e'1,1A1g}(t_f)|^2 = 0.664$, $P_{e'1\&e'1,2A1g}(t_f) = |c_{e'1\&e'1,2A1g}(t_f)|^2 = 0.225$ and $P_{e'1\&e'1,1E2g^{x^2-y^2}}(t_f) = |c_{e'1\&e'1,1E2g^{x^2-y^2}}(t_f)|^2 = 0.098$. The subscript “ $e'1\&e'1$ ” indicates that the wavefunction (51) is prepared by a sequence of two polarized laser pulses with the same polarizations, e'_1 and again e'_1 . The population of state $|2A1g\rangle$ is added unexpectedly to those of the two target states $|1A1g\rangle$ and $|1E2g^{x^2-y^2}\rangle$. However, this does not harm the present purpose. What matters for the new example of electron symmetry breaking is that the final state (51) is prepared as superposition of states which transform according to two different IRREPs—here this is A_{1g} (the same for states $|1A1g\rangle$ and $|2A1g\rangle$) and $E_{2g}^{x^2-y^2}$ (for state $|1E2g^{x^2-y^2}\rangle$). Apparently, Figure 9 shows that the pulses $p = 7$ and 8 also cause transient populations of complementary states, in particular $|1E1u^y\rangle$. This is caused by non-linear effects—but this is irrelevant for the present purpose, and beyond the scope of this paper.

After the sequence of two laser pulses 7 and 8 with the same polarizations e'_1 and again e'_1 , for times $t \geq t_f = \tau_7 + \tau_8 = 10$ fs, the wavefunction (51) evolves in field-free environments, with coefficients specified in Equation (26). The corresponding swapping part of the one-electron densities $\rho_{e'1\&e'1}(\mathbf{r}, t) - \rho_{1A1g}(\mathbf{r})$ is illustrated in Figure 10a by snapshots analogous to those shown in Figures 6–8. Corresponding inspection and analyses of these snapshots reveal that $\rho_{e'1\&e'1}(\mathbf{r}, t)$ displays charge migration with conservation of the symmetry elements of the subgroup $D_{2h,1} = \{E, C_2, C_2', C_2'', i, \sigma_h, \sigma_v, \sigma_d\}$ of D_{6h} . Hence, as resume of the combined Figures 1 and 10a, the series of two laser pulses 7 and 8 , also called $e'_1\&e'_1$ (Figure 9) yield electron symmetry breaking $D_{6h} \rightarrow S(\rho_{e'1\&e'1}(\mathbf{r}, t)) = D_{2h,1}$ in the oriented model benzene, with conservation of nuclear symmetry. This is quite different from the six previous examples which are documented in the combined Figures 1 and 6, Figure 7 or Figure 8.

Our last example of electron symmetry breaking in oriented benzene is achieved by another sequence of two laser pulses—this time they are labeled 7 and 9 . The first laser pulse ($p = 7$) is the same as the first laser pulse in the previous series of laser pulses 7 and 8 , cf. Figure 9. The second pulse ($p = 9$) has the same electric field as the previous pulse labeled $p=8$, i.e., $\mathcal{E}_{p=9}(t) = \mathcal{E}_{p=8}(t)$, cf. Figure 9, but the laser polarization is $e_9 = e''_1 = e_x$ instead of $e_8 = e'_1 = e_y$. Hence the series of laser pulses 7 and 9 will also be denoted

\mathbf{e}'_1 and \mathbf{e}''_1 . The resulting population probabilities $P_{\mathbf{e}'_1 \& \mathbf{e}''_1, m}(t)$ of eigenstates $|m\rangle$ are shown in Figure 9. Since the two series of laser pulses 7 and 8 and 7 and 9 employ the same first pulse ($p = 7$), they yield the same populations during the time $0 \leq t < \tau_7 = 2.5$ fs of the first laser pulse. During the time $\tau_7 = 2.5$ fs $\leq t \leq t_f = \tau_7 + \tau_8 = \tau_7 + \tau_9 = 10$ fs of the second pulses, $p = 8$ or 9 , the equality of their electric fields $\mathcal{E}_{p=8}(t) = \mathcal{E}_{p=9}(t)$ but orthogonality of the laser polarizations $\mathbf{e}_8 = \mathbf{e}'_1 = \mathbf{e}_y \perp \mathbf{e}_9 = \mathbf{e}''_1 = \mathbf{e}_x$ yields the same populations $P_{\mathbf{e}'_1 \& \mathbf{e}''_1, m}(t) = P_{\mathbf{e}'_1 \& \mathbf{e}'_1, m}(t)$ for the non-degenerate states $|m'\rangle = |m'\rangle = |1A_{1g}\rangle$ and $|2A_{1g}\rangle$, but require proper modifications of the quantum numbers of the degenerate states, i.e., the series of pulses 7 and 8 excite the transient and final states $|1E_{1u}^y\rangle$ and $|1E_{2g}^{x^2-y^2}\rangle$ whereas pulses 7 and 9 excite $|1E_{1u}^x\rangle$ and $|1E_{2g}^{xy}\rangle$, respectively. Accordingly, at the end ($t = t_f = \tau_7 + \tau_9 = 10$ fs) of the sequence of laser pulses 7 and 9, also called \mathbf{e}'_1 & \mathbf{e}''_1 , the oriented benzene is prepared in the superposition state

$$|\Psi_{\mathbf{e}'_1 \& \mathbf{e}''_1}(t_f = \tau_7 + \tau_9)\rangle = c_{\mathbf{e}'_1 \& \mathbf{e}''_1, 1A_{1g}}(t_f) |1A_{1g}\rangle + c_{\mathbf{e}'_1 \& \mathbf{e}''_1, 2A_{1g}}(t_f) |2A_{1g}\rangle + c_{\mathbf{e}'_1 \& \mathbf{e}''_1, 1E_{2g}^{xy}}(t_f) |1E_{2g}^{xy}\rangle \quad (52)$$

with the same populations of the states $|1A_{1g}\rangle$, $|2A_{1g}\rangle$, $|1E_{2g}^{xy}\rangle$ as those ($|1A_{1g}\rangle$, $|2A_{1g}\rangle$, $|1E_{2g}^{x^2-y^2}\rangle$) for pulses 7 and 8.

The field-free time evolution of the wave function (52) after the sequence laser pulses 7 and 9, also called \mathbf{e}'_1 & \mathbf{e}''_1 , i.e., for $t \geq t_f = 10$ fs, yields the swapping one-electron density $\rho_{\mathbf{e}'_1 \& \mathbf{e}''_1}(\mathbf{r}, t) - \rho_{1A_{1g}}(\mathbf{r})$ which is illustrated in Figure 10b by snapshots, analogous to those shown in Figure 10a for the laser pulses 7 and 8. They reveal a new type of charge migration, with the conservation of the symmetry elements of the subgroup $C_{2h} = \{E, C_2, i, \sigma_h\}$ of D_{6h} . Hence, as a result of the combined Figures 1 and 10b, the series of laser pulses 7 and 9 with polarizations \mathbf{e}'_1 and \mathbf{e}''_1 (Figure 9) yield electron symmetry breaking $D_{6h} \rightarrow S(\rho_{\mathbf{e}'_1 \& \mathbf{e}''_1}(\mathbf{r}, t)) = C_{2h}$ in the oriented model benzene, with the conservation of nuclear symmetry.

To summarize, all the different electron symmetry breakings $D_{6h} \rightarrow S(\rho_p(\mathbf{r}, t))$ from the point group $G = D_{6h}$ to different subgroups $S(\rho_p(\mathbf{r}, t))$ of G , $p = 1, \dots, 9$ are achieved by means of different linearly polarized laser pulses, or two sequential laser pulses, which excite the initial electronic ground state $|1A_{1g}\rangle$ to different superpositions (16) of the electronic ground state plus one ($p = 1, \dots, 6$) or two different excited states ($p = 7 \& 8$ and $7 \& 9$). An important common property of the different sets of the electronic ground and excited states which constitute the different superpositions is that (at least) two of them have different IRREPs, e.g., A_{1g} and E_{1u} or A_{1g} and E_{2g} . In the case of doubly degenerate IRREPs, preparations of superposition states with different sets of basis functions yield different point subgroups $S(\rho_p(\mathbf{r}, t))$ of G .

3.2. Electron Symmetry Breaking and Charge Migration Induced by Linearly Polarized Laser Pulses in Oriented Mg-Porphyrin with D_{4h} Nuclear Scaffold

This Section heightens the impression which was gained in the previous Section 3.1, namely different well designed short linearly polarized laser pulses labeled $p = 1, 2, 3, \dots$ can achieve different types of charge migrations with different electron symmetry breakings, from the point group of the electronic ground state G to various subgroups $S(\rho_p(\mathbf{r}, t))$ of G . For this purpose, we present additional examples, with applications to another oriented molecule with nuclear point group symmetry G different from D_{6h} . Specifically, we choose oriented Mg-porphyrin with $G = D_{4h}$, cf. Figures 2 and 4, and demonstrate different electron symmetry breakings $D_{4h} \rightarrow S(\rho_p(\mathbf{r}, t))$ by means of different linearly polarized laser pulses. The oriented model Mg-porphyrin is suggested by Ref. [15] which discovers the stimulation of a specific type of charge migration, namely electron circulation, by means of a circularly polarized laser pulse. As a byproduct, Ref. [15] has a series of snapshots of the time-dependent one-electron density after the laser-pulse. In retrospect, those snapshots clearly document electron symmetry breaking $D_{4h} \rightarrow C_s = \{E, \sigma_h\}$ by a short laser pulse, with the conservation of the nuclear symmetry D_{4h} . However, this effect was not noted in Ref. [15]—the word “symmetry” is not even mentioned therein. In contrast with Ref. [15], here we are heading for the explicit discovery of electron symmetry breaking $D_{4h} \rightarrow S(\rho_p(\mathbf{r}, t))$ in

oriented Mg-porphyrin, by means of selective linearly polarized laser pulses. The effects are analogous to those for $D_{6h} \rightarrow S(\rho_p(\mathbf{r},t))$ electron symmetry breaking in oriented benzene, as documented in Section 3.1. This analogy allows a rather brief presentation of the results for Mg-porphyrin, without any repetition of the detailed derivations of Section 3.1. Moreover, we restrict the presentation to just two cases of electron symmetry breaking $D_{4h} \rightarrow S(\rho_p(\mathbf{r},t))$ by means of two different laser pulses labeled $p = 1, 2$. The rich examples $D_{6h} \rightarrow S(\rho_p(\mathbf{r},t))$, $p = 1, \dots, 9$, for benzene should then suffice to stimulate the reader's imagination to invent additional cases, also for oriented Mg-porphyrin.

As in Section 3.1, we start with the demonstration of electron symmetry breaking in oriented Mg-porphyrin, by means of a $\mathbf{e}_{p=1} = \mathbf{e}_x = \mathbf{e}'_1$ polarized re-optimized $\pi/2$ laser pulse. The laser pulse labeled $p = 1$ has the familiar form of the electric field $\mathcal{E}_{p=1}(t)$, Equation (1). It is illustrated in Figure 11, with the laser parameters in Figure 11. The resulting population dynamics are also shown in Figure 11. Apparently, the first laser pulse $p = 1$ with duration $\tau_1 = 10$ fs excites the oriented Mg-porphyrin from the initial ($t = 0$) electronic ground state $|1A_{1g}\rangle$ to the superposition state $(1/\sqrt{2})^*(|1A_{1g}\rangle + |2E_u^x\rangle)$. The notation $|2E_u^x\rangle$ refers to the doublet $\{|2E_u^x\rangle, |2E_u^y\rangle\} \equiv \{|2E_u'^1\rangle, |2E_u'^2\rangle\}$ of two orthogonal degenerate states with IRREP E_u with the second-lowest energy E_{2E_u} which transform as x and y , respectively [13]. The target transitions is illustrated schematically by the vertical arrow from the energy level $E_{1A_{1g}}$ to E_{2E_u} in Figure 4. The energy gap between their eigenenergies is $\Delta E_{1A_{1g},2E_u} = E_{2E_u} - E_{1A_{1g}} = 3.60$ eV with corresponding transition frequency $\omega_{1A_{1g},2E_u} = \Delta E_{1A_{1g},2E_u} / \hbar$ and period $T = T_{1A_{1g},2E_u} = 2\pi / \omega_{1A_{1g},2E_u} = \hbar / \Delta E_{1A_{1g},2E_u} = 1.147$ fs, cf. Equations (42) and (43).

The subsequent ($t \geq \tau_1 = 10$ fs) time evolution of the swapping one-electron density $\rho_{p=1}(\mathbf{r},t) - \rho_{1A_{1g}}(\mathbf{r})$ is illustrated in Figure 12a by three snapshots, analogous to the previous Figure 6 for oriented benzene. Apparently, the oriented Mg-porphyrin exhibits periodic charge migration from the left to the right, and back, with period T . Analogous inspection and analyses show that the migrating one-electron density conserves three symmetry elements, namely $C_{2v}^{'1}, \sigma_h, \sigma_{v1}$, cf. Figure 2. Accordingly, the combined Figures 2 and 12a document electron symmetry breaking induced by the \mathbf{e}'_1 polarized laser pulse $p = 1$, namely $D_{4h} \rightarrow S(\rho_{p=1}(\mathbf{r},t)) = C_{2v}^{'1} = \{E, C_{2v}^{'1}, \sigma_h, \sigma_{v1}\}$.

The second example for electron symmetry breaking in oriented Mg-porphyrin employs another re-optimized $\pi/2$ laser pulse labeled $p = 2$. It has the same electric field as the first pulse $p = 1$, i.e., $\mathcal{E}_2(t) = \mathcal{E}_1(t)$, cf. Figure 11, but different polarization $\mathbf{e}_2 = \mathbf{e}''_1 = (1/\sqrt{2})^*(\mathbf{e}_x + \mathbf{e}_y) = C_8 \mathbf{e}''_1$. It prepares the superposition state $(1/\sqrt{2})^*(|1A_{1g}\rangle + |2E_u''^1\rangle)$, analogous to the superposition state $(1/\sqrt{2})^*(|1A_{1g}\rangle + |2E_u'^1\rangle)$ which is prepared by the \mathbf{e}'_1 polarized pulse $p = 1$. The \mathbf{e}'_1 ($p = 1$) and \mathbf{e}''_1 ($p = 2$) polarized pulses yield the same population dynamics, cf. Figure 11. The periodic charge migration which is initiated by the \mathbf{e}''_1 ($p = 2$) polarized pulse is illustrated in Figure 12b. It has the same period T as for the charge migration initiated by pulse $p = 1$, but it is from the lower left to the upper right of the oriented scaffold, and back. Apparently, it conserves three symmetry elements, namely $C_{2v}''^1, \sigma_h, \sigma_{d1}$, cf. Figure 2. Accordingly, the combined Figures 2 and 12b document electron symmetry breaking induced by the \mathbf{e}''_1 polarized laser pulse $p = 2$, namely $D_{4h} \rightarrow S(\rho_{p=2}(\mathbf{r},t)) = C_{2v}''^1 = \{E, C_{2v}''^1, \sigma_h, \sigma_{d1}\}$.

The summary of this Section 3.2 with application to oriented Mg-porphyrin is analogous to the summary for Section 3.1 for oriented benzene. Different electron symmetry breakings $D_{4h} \rightarrow S(\rho_p(\mathbf{r},t))$ from the point group $G = D_{4h}$ to different subgroups $S(\rho_p(\mathbf{r},t))$ of G , $p = 1, 2$ are achieved by means of different linearly polarized laser pulses which excite the initial electronic ground state $|1A_{1g}\rangle$ to different superpositions (16) of the electronic ground state plus an excited state with different IRREP E_u . Preparations of superposition states with different basis functions yield different point subgroups $S(\rho_p(\mathbf{r},t))$ of G .

3.3. Symmetry of One-Electron Densities of Superposition States in Oriented Benzene

Section 3.1 shows that different short laser pulses, or two sequential laser pulses with linear polarization(s) \mathbf{e} and with total durations $t_f = 10$ fs, initiate different charge migrations

in the oriented benzene which are represented by different one-electron densities $\rho_e(t > t_f)$ with different electron symmetries $S(\rho_e(t))$ depending on e . All those electron symmetry breakings $G = D_{6h} \rightarrow S(\rho_e(t))$ conserve nuclear symmetry D_{6h} . Until now, the symmetries $S(\rho_e(t))$ were determined by inspection of the symmetry elements of G which are conserved in $\rho_e(t > t_f)$.

The purpose of this Section is to derive a recipe for the rigorous determination of the subgroup $S(\rho_e(t > t_f))$, starting from the superposition state (16) which was prepared by the laser pulse, or two sequential laser pulses with polarization(s) e , without any empirical inspection of the symmetry elements of $\rho_e(t)$. For this purpose, to simplify the notation, we rewrite the superposition state (16) as

$$|\Psi_e(t > t_f)\rangle \equiv |\Psi\rangle = \sum_m c_m |m\rangle = \sum_{n,k} c_{n,k} |n,k\rangle = \sum_k |\Psi_k\rangle \quad (53)$$

i.e., we keep in mind that the wavefunctions $|\Psi\rangle$ and $|\Psi_k\rangle$ as well as the expansion coefficients c_m and $c_{n,k}$ depend on the laser polarization(s) e and on the time after the laser pulse, $t > t_f$, cf. Equation (26), but this dependence is no longer written explicitly. Equation (53) also replaces the energy quantum number m by two quantum numbers n, k . Here, k denotes the IRREP $\Gamma_k = \Gamma_k$ of the basis function $|m\rangle = |n, k\rangle \equiv |n, \Gamma_k\rangle$, and n specifies the energetic order of the basis functions with IRREP Γ_k . The wave functions

$$|\Psi_k\rangle = \sum_n c_{n,k} |n, \Gamma_k\rangle \quad (54)$$

in Equation (53) are in general linear combinations of basis functions $|n, \Gamma_k\rangle$ which have the same IRREP Γ_k and non-zero coefficients $c_{n,k}$. The wave function $|\Psi\rangle$ and the basis functions $|m\rangle = |n, \Gamma_k\rangle$ in Equations (53) and (54) are normalized, whereas the $|\Psi_k\rangle$ are not normalized. In fact, normalization of the $|\Psi_k\rangle$ is not necessary, for the present purpose.

The derivation of the subgroup $S(\rho_e(t > t_f))$ of the one electron density for $t > t_f$ after the laser pulse(s) with polarization(s) e proceeds in three steps, cf. Appendix A: First we determine the subgroup $S(|\Psi_e(t > t_f)\rangle)$ of the superposition state (53). Next we derive the subgroup $S(\Psi_e(t > t_f)^* \Psi_e(t > t_f))$ of the electron density $\Psi_e(t > t_f)^* \Psi_e(t > t_f)$, and finally the target subgroup $S(\rho_e(t > t_f))$ of the one-electron density $\rho_e(t > t_f)$. The derivations are general, in principle, but the presentation focuses on the present applications (cf. Section 3.1) where the laser pulses prepare superposition states (16), (53) with non-vanishing contributions of the ground state $|1A_{1g}\rangle$ plus possibly excited states $|nA_{1g}\rangle$ with the same IRREP A_{1g} plus one excited basis function $|n, k\rangle \equiv |n, \Gamma_k \neq A_{1g}\rangle$ with IRREP $\Gamma_k \neq A_{1g}$, thus

$$|\Psi_e(t > t_f)\rangle \equiv |\Psi_{A_{1g}}\rangle + |\Psi_{\Gamma_k \neq A_{1g}}\rangle. \quad (55)$$

The Appendix A proves that for such cases (and also for various other cases), the subgroups are all identical,

$$S(\rho_e(t > t_f)) = S(\Psi_e(t > t_f)^* \Psi_e(t > t_f)) = S(|\Psi_e(t > t_f)\rangle), \quad (56)$$

and the IRREP of $\rho_e(t > t_f)$ in the subgroup $S(\rho_e(t > t_f))$ is always the totally symmetric one. For this reason, the subsequent presentation focuses on the derivation of the subgroup $S(|\Psi_e(t > t_f)\rangle)$. Once $S(|\Psi_e(t > t_f)\rangle)$ is determined, the theorem (56) tells us that the target subgroup $S(\rho_e(t > t_f))$ is the same as $S(|\Psi_e(t > t_f)\rangle)$.

The general theory is presented in Appendix A. It ends up with a simple recipe. It is demonstrated here for the cases which were presented in Section 3.1. The results are summarized in Table 3. This Table 3 may be recognized as a collection of special parts of the character tables of the subgroups $S(|\Psi_e(t > t_f)\rangle)$ of the superpositions $|\Psi_e(t > t_f)\rangle$, Equation (55), namely for the characters of the totally symmetric IRREPs. These characters are all equal to 1. Thus Table 3 lists the number “1” for all symmetry operations $g \in S(|\Psi_e(t > t_f)\rangle)$. Turning the table, the task is to determine the symmetry elements g with “marks 1”

in Table 3. These sets of symmetry operations identify the subgroups $S(|\Psi_e(t > t_f)\rangle)$. At the same time, the theorem (56) for superpositions (55) makes those subgroups $S(|\Psi_e(t > t_f)\rangle)$ equal to the target subgroup $S(\rho_e(t > t_f))$ of the one-electron density $\rho_e(t > t_f)$.

Here we present step-by-step applications of the general theory (cf. Appendix A) to two (out of eight) examples which were presented in Section 3.1. Table 3 also lists analogous results for the other six cases of Section 3.1, and also for the non-aromatic states (49), (50) of the oriented benzene which are prepared by three linearly polarized laser pulses or by re-optimized laser pulses designed by Ulusoy and Nest [1].

Our first example is for the electronic superposition state $|\Psi_{e''1}(t > t_f)\rangle = c_{e''1,A1g}(t)|1A1g\rangle + c_{e''1,E1ux}(t)|1E1ux\rangle$ which is prepared by the $e''_1 = e_x$ polarized $\pi/2$ laser pulse shown in Figure 5, cf. Section 3.1. Using the simplified notation of Equations (53) and (55), this superposition state is rewritten

$$|\Psi\rangle = |A1g\rangle + |E1ux\rangle. \quad (57)$$

It consists of two partial waves with IRREPs $A1g$ and $E1ux$ of the group $G=D_{6h}$. According to the general theory (cf. Appendix A), the subgroup $S(|\Psi\rangle)$ of $|\Psi\rangle$ is the subset of the symmetry operations g of G which satisfy the same symmetry properties for all components,

$$S(|\Psi\rangle) = \{g \in G \mid g|\Psi_k\rangle = \chi(g)|\Psi_k\rangle\} \quad (58)$$

with the same characters $\chi(g)$ for all wave functions $|\Psi_k\rangle$ in the expansion (53). In the present case (57), $S(|\Psi\rangle)$ consists of all g which satisfy $g|A1g\rangle = \chi(g)|A1g\rangle$ as well as $g|E1ux\rangle = \chi(g)|E1ux\rangle$. The characters $\chi(g)$ of the totally symmetric IRREP $A1g$ are all equal to 1. Hence the operations g of G must satisfy the symmetry property $g|E1ux\rangle = |E1ux\rangle$,

$$S(|\Psi\rangle) = \{g \in G \mid g|E1ux\rangle = |E1ux\rangle\} \text{ for the case (57)}. \quad (59)$$

Since the electronic wave function $|E1ux\rangle$ transforms as x , the operations g of G must satisfy $gx = x$, or $g e_x = e_x$. There are only four operations g of G which map x on x , or the unit vector e_x on e_x , namely $g = E, C_{21}'', \sigma_h$ and σ_{d1} , cf. Figure 1. The set of operations $\{E, C_{21}'', \sigma_h, \sigma_{d1}\}$ is the subgroup $C_{2v}''1$, cf. Table 1. Hence $S(|\Psi\rangle) = C_{2v}''1$. Accordingly, the entry $|\Psi\rangle = |A1g\rangle + |E1ux\rangle$ in Table 3 marks the characters “1” for the operations $g = E, C_{21}'', \sigma_h$ and σ_{d1} , and these yield the subgroup $S(|\Psi\rangle) = C_{2v}''1$ with totally symmetric IRREP $A1g$. The theorem (56) implies that the corresponding one-electron density $\rho_e(t > t_f)$ has the same symmetry $C_{2v}''1$.

Our second example is for the superposition state $|\Psi_{e'1\&e''1}(t > t_f)\rangle = c_{e'1\&e''1,1A1g}(t)|1A1g\rangle + c_{e'1\&e''1,2A1g}(t)|2A1g\rangle + c_{e'1\&e''1,E2g^{xy}}(t)|1E2g^{xy}\rangle$, cf. Equation (52), which is prepared by the series of two laser pulses with different polarizations e'_1 and e''_1 , cf. Figure 9. Using again the simplified notation of Equations (53) and (55), this superposition state is rewritten

$$|\Psi\rangle = |A1g\rangle + |E2g^{xy}\rangle. \quad (60)$$

where

$$\begin{aligned} |A1g\rangle &= c_{e'1\&e''1,1A1g}(t)|1A1g\rangle + c_{e'1\&e''1,2A1g}(t)|2A1g\rangle, \\ |E2g^{xy}\rangle &= c_{e'1\&e''1,E2g^{xy}}(t)|1E2g^{xy}\rangle. \end{aligned} \quad (61)$$

It consists of two partial waves with IRREPs $A1g$ and $E2g^{xy}$ of the group $G=D_{6h}$. According to the general theory (cf. Appendix A), and by analogy with the first example, the subgroup $S(|\Psi\rangle)$ of $|\Psi\rangle$ is the subset of the symmetry operations g of G which satisfy the symmetry property $g|E2g^{xy}\rangle = |E2g^{xy}\rangle$,

$$S(|\Psi\rangle) = \{g \in G \mid g|E2g^{xy}\rangle = |E2g^{xy}\rangle\} \text{ for the case (60)}. \quad (62)$$

Since the electronic wave function $|E2g^{xy}\rangle$ transforms as xy , the operations g of G must satisfy $gxy = xy$. There are only four operations g of G which map xy on xy , namely $g = E, C_2^z, i$ and σ_h , cf. Figure 1. The set of operations $\{E, C_2^z, i, \sigma_h\}$ is the subgroup

C_{2h} , cf. Table 1. Hence $S(|\Psi\rangle) = C_{2h}$. Accordingly, the entry $|\Psi\rangle = |A_{1g}\rangle + |E_{2g}^{xy}\rangle$ in Table 3 marks the characters “1” for the operations $g = E, C_2^z, i, \sigma_h$, and these yield the subgroup $S(|\Psi\rangle) = C_{2h}$ with totally symmetric IRREP A_g . The theorem (56) implies that the corresponding one-electron density $\rho_e(t > t_f)$ has the same symmetry $S(\rho_e(t > t_f)) = C_{2h}$.

To summarize, the applications of the general theory (cf. Appendix A) to the cases (57) and (60) demonstrate a simple recipe for the approach from the laser-driven electronic superposition state (53) via its symmetry subgroup (58) to the same symmetry subgroup of the one-electron density. The same approach can be applied to all other cases which were presented in Section 3.1. The resulting electron symmetry breakings due to laser pulses p are also listed in Table 3. They are in perfect agreement with the empirical results which were obtained in Section 3.1, by inspection of the symmetry elements of the one-electron densities.

Table 3 also presents analogous results for the symmetry subgroups of the one-electron densities of two non-aromatic superposition states (49) and (50) which are prepared by laser pulses designed by Ulusoy and Nest [1]. Accordingly, our result $S(|A_{1g}\rangle + |B_{1u}\rangle) = D_{3h}'$ for the superposition state $|A_{1g}\rangle + |B_{1u}\rangle$ and for its one-electron density confirms their assignment. However, for the other case, our approach yields $S(|A_{1g}\rangle + |B_{2u}\rangle) = D_{3h}''$, different from their result D_{3d} [1]. In retrospect, close inspection of their cartoons of the one-electron density and of the corresponding Lewis structures verifies the present result.

3.4. Symmetry of One-Electron Densities of Superposition States in Oriented Mg-Porphyrin

This Section for the derivation of the symmetries of one-electron densities of laser-driven superposition states in oriented Mg-porphyrin (D_{4h}) is entirely analogous to the corresponding Section 3.3 for oriented benzene (D_{6h}). The previous Section 3 has detailed presentations of two applications of the general theory (cf. Appendix A) to two different superposition states which are prepared by a linearly polarized laser pulse, or by two sequential linearly polarized pulses, as illustrated in Figures 5 and 9, respectively, cf. Section 3.1. The results are summarized in Table 3, together with the results for six additional cases. The present Section 3.4 summarizes the corresponding results for four applications to laser-driven superposition states in Mg-porphyrin in Table 4, complemented by the analogous step-by-step presentation of one example.

Specifically, let us derive the symmetry subgroup of the one-electron density of the superposition state $|\Psi_{e'1}(t > t_f)\rangle = c_{e'1,A_{1g}}(t) |A_{1g}\rangle + c_{e'1,E_{u1}}(t) |E_{u1}\rangle$ which is prepared by the $\mathbf{e}'_1 = \mathbf{e}_x$ polarized $\pi/2$ laser pulse shown in Figure 11, cf. Section 3.2. Using the simplified notation of Equations (53) and (55), this superposition state is rewritten

$$|\Psi\rangle = |A_{1g}\rangle + |E_u^x\rangle \equiv |A_{1g}\rangle + |E_{u1}'\rangle \quad (63)$$

It consists of two partial waves with IRREPs A_{1g} and $E_u^x \equiv E_{u1}'$ of the group $G = D_{4h}$; the two equivalent notations remind of the two notations of the laser polarizations, $\mathbf{e}_x = \mathbf{e}'_1$. According to the general theory (cf. Appendix A) and its application in Section 3.3, the symmetry subgroup $S(|\Psi\rangle)$ of the wavefunction (63) consists of the operations g of G which satisfy the symmetry property $g|E_u^x\rangle = |E_u^x\rangle$,

$$S(|\Psi\rangle) = \{g \in G \mid g|E_u^x\rangle = |E_u^x\rangle\} \text{ for the case (63).} \quad (64)$$

Since the electronic wave function $|E_{u1}^x\rangle \equiv |E_{u1}'\rangle$ transforms as x , the operations g of G must satisfy $g x = x$, or $g \mathbf{e}'_1 = \mathbf{e}'_1$. There are four operations g of G which map x on x , or the unit vector \mathbf{e}'_1 on \mathbf{e}'_1 , namely $g = E, C_{21}', \sigma_h$ and σ_{v1} , cf. Figure 2. Accordingly, the entry $|\Psi\rangle = |A_{1g}\rangle + |E_{u1}'\rangle$ in Table 4 marks the characters “1” for the operations $g = E, C_{21}', \sigma_h$ and σ_{v1} , and these yield the subgroup $S(|\Psi\rangle) = C_{2v}'$ with totally symmetric IRREP A_{1g} . The theorem (56) implies that the corresponding one-electron density $\rho_{e'1}(t > t_f)$ has the same symmetry C_{2v}' . Table 4 summarizes this result, together with three additional applications. The empirical results which were derived by inspection of the

symmetry elements of the one-electron densities of two laser-driven superposition states in Section 3.2 (cf. Figure 12) are confirmed by the group-theoretical results of Table 4.

Table 4 also comprises the results for two cases of electron symmetry breaking in the oriented Mg-porphyrin which have not been demonstrated in Section 3.2. We use these cases to explain two applications of the general approach (cf. Appendix A) which was exemplified in Sections 3.3 and 3.4. First, it provides an efficient and firm method to determine the subgroup $S(\rho_e(t > t_f))$ of electron symmetry breaking $G \rightarrow S(\rho_e(t > t_f))$ by a laser pulse. As example, consider the (hypothetical) preparation of the superposition state $|\Psi_{e''2}(t > t_f)\rangle = c_{e''2,A1g}(t) |1A_{1g}\rangle + c_{e''2,1Eu2''}(t) |1Eu_{2''}\rangle$ by means of a e''_2 polarized $\pi/2$ laser pulse, labeled $p = 3$. It would represent a new type of charge migration. The traditional way of determining the related electron symmetry breaking $G = D_{4h} \rightarrow S(\rho_{e''2}(t > t_f))$ would cost quantum dynamics simulations of the laser excitation $|1A_{1g}\rangle \rightarrow |\Psi_{e''2}(t > t_f)\rangle$, calculation of the one-electron density $\rho_{e''2}(t > t_f)$, an inspection of $\rho_{e''2}(t > t_f)$ to determine the symmetry elements of G which are conserved in $\rho_{e''2}(t > t_f)$, and finally, the determination of the subgroup $S(\rho_{e''2}(t > t_f))$ as the set of the corresponding symmetry operations, cf. Sections 3.1 and 3.2. In contrast, the recipe which was exemplified in Sections 3.3 and 3.4 just calls for rewriting the target wavefunction as

$$|\Psi_{e''2}(t > t_f)\rangle = |\Psi\rangle = |A_{1g}\rangle + |Eu_{2''}\rangle \quad (65)$$

and then to determine the symmetry group of this wavefunction as the set of symmetry operations g which satisfy $g |Eu_{2''}\rangle = |Eu_{2''}\rangle$. The recipe of Sections 3.3 and 3.4 yields the result

$$\begin{aligned} S(\rho_{e''2}(t > t_f)) &= S(|\Psi_{e''2}(t > t_f)\rangle) = \{g \in D_{4h} \mid g |Eu_{2''}\rangle = |Eu_{2''}\rangle\} \\ &= \{g=E, C_{2v'}', \sigma_h, \sigma_{d2}\} = C_{2v'}' \end{aligned} \quad (66)$$

without any inspection of the one-electron density $\rho_{e''2}(t > t_f)$, cf. Table 4.

The second application is for laser control of electron symmetry. This task is motivated, e.g., by the Woodward–Hoffmann rules for the control of chemical reactions by preparations of the reactants with different electron symmetries in the electronic ground and excited states [35]. For example, let us assume that the goal is to design the laser pulse, or series of laser pulses with total duration $t_f \leq 10$ fs and polarization(s) e which achieve(s) electron symmetry breaking $G = D_{4h} \rightarrow S(\rho_e(t > t_f)) = C_{2v'}'$ in the oriented Mg-porphyrin. The recipe of Sections 3.3 and 3.4 suggests that for this purpose, the laser pulse(s) should prepare the superposition state

$$|\Psi_e(t > t_f)\rangle = |\Psi\rangle = |A_{1g}\rangle + |\Gamma_k\rangle \quad (67)$$

which consists of basis functions with IRREP A_{1g} and another IRREP $\Gamma_k \neq A_{1g}$ such that

$$\begin{aligned} S(\rho_e(t > t_f)) &= S(|\Psi_e(t > t_f)\rangle) = \{g \in D_{4h} \mid g |\Gamma_k\rangle = |\Gamma_k\rangle\} = C_{2v'}' \\ &= \{g=E, C_{2v'}', \sigma_h, \sigma_{v2}\} \end{aligned} \quad (68)$$

cf. Tables 1 and 4 and Figure 2.

The first challenge then is to determine the IRREP Γ_k of the wavefunction $|\Gamma_k\rangle$ which satisfies Equation (68). For this purpose, one should check the D_{4h} character Table for the characters for the one-dimensional (1d) IRREPs and—in the case of 2d IRREPs—also the diagonal elements of the 2×2 representation matrices for all symmetry operations of D_{4h} , see, e.g., Ref. [13]. The target IRREP Γ_k must have characters or diagonal elements of the representation matrices equal to “1” precisely for the symmetry elements $\{g=E, C_{2v'}', \sigma_h, \sigma_{v2}\}$. Table 4 shows that this condition is satisfied exclusively by the basis function $|nEu_{2'}\rangle$ for IRREP $\Gamma_k = Eu$. Hence the wavefunction $|\Gamma_k\rangle$ in the target superposition state (67) should be a linear combination of basis functions $|nEu_{2'}\rangle$. Likewise, the other wavefunction $|A_{1g}\rangle$ in the superposition state (67) should be a linear combination of

basis functions $|nA_{1g}\rangle$. These two conditions for Equation (67) allow many choices. The simplest linear combination is

$$|\Psi_e(t > t_f)\rangle = |A_{1g}\rangle + |\Gamma_k\rangle = c_{e,1A_{1g}} |1A_{1g}\rangle + c_{e,1Eu_2'} |1Eu_2'\rangle \quad (69)$$

with time-dependent coefficients, cf. Equation (26).

The second challenge is to design the laser pulse, or series of laser pulses, with polarization(s) \mathbf{e} which prepares the target state (69), within less than $t_f = 10$ fs. Again, there is no unique solution for this task. In the present case, experience with $|\Psi_{e'1}(t > t_f)\rangle = c_{e'1,1A_{1g}} |1A_{1g}\rangle + c_{e'1,Eu_1'} |1Eu_1'\rangle$ (cf. Section 3.2, Figure 11) suggests that one should employ the corresponding $\pi/2$ laser pulse, labeled $p = 4$, with polarization $\mathbf{e}_4 = \mathbf{e}'_2 = \mathbf{e}_y$ and with the same electric field $\mathcal{E}(t)$ as the one shown in Figure 11.

3.5. Symmetry of One-Electron Densities of Oriented Molecules Driven by One or Several Linearly Polarized Laser Pulses

The previous Section 3.1, Section 3.2, Section 3.3 and Section 3.4 contain ten plus four examples of electron symmetry breaking $G \rightarrow S(\rho_e(t > t_f))$ by short ($t_f = 10$ fs) laser pulses, or two sequential laser pulses with polarizations \mathbf{e} in the oriented benzene ($G = D_{6h}$) and Mg-porphyrin ($G = D_{4h}$). The results are summarized in Tables 3 and 4. Comparison with Table 2 reveals the rule

$$S(H_e(t)) \subseteq S(\rho_e(t > t_f)) = S(|\Psi_e(t > t_f)\rangle) \subseteq G \quad (70)$$

The corresponding orders $|\dots|$ of the groups and subgroups satisfy

$$|S(H_e(t))| \leq |S(\rho_e(t > t_f))| = |S(|\Psi_e(t > t_f)\rangle)| \leq |G|. \quad (71)$$

The equality in the middle of relations (70), (71) is adapted from Equation (56). It holds for superposition states (53) which are prepared by the laser pulse(s) such that they contain the ground state and/or an excited basis function with the IRREP A_{1g} of the initial state, plus one (or more) excited states with different IRREPs, see, e.g., Equation (55) and all the examples in Tables 3 and 4.

The right hand side of the relations (70), (71) simply means that $S(\rho_e(t > t_f)) = S(|\Psi_e(t > t_f)\rangle)$ is a subgroup of G . It may even be the same as G : In this case, the laser pulse does not break the symmetry G at all. This may be called the “largest case”, i.e., $|S(\rho_e(t > t_f))| = |S(|\Psi_e(t > t_f)\rangle)| = |G|$. This case holds for well-designed sequences of laser pulses with polarization vectors \mathbf{e} which break and restore electron symmetry [2–4], or which induce attosecond charge migration represented by superpositions of electronic eigenstates with the same IRREP as the ground state, see, e.g., Refs. [36–38]. The left hand side of the relations (70) and (71) is an important restriction. It means that the subgroup $S(\rho_e(t > t_f)) = S(|\Psi_e(t > t_f)\rangle)$ of laser-broken electron symmetry must contain the subgroup $S(H_e(t))$ of the time-dependent electronic Hamiltonian of the molecule interacting with the laser pulse(s), cf. Section 2.5 and Table 2. The subgroup $S(\rho_e(t > t_f)) = S(|\Psi_e(t > t_f)\rangle)$ may even be the same as $S(H_e(t))$. This may be called the “smallest case”, i.e., $|S(\rho_e(t > t_f))| = |S(|\Psi_e(t > t_f)\rangle)| = |S(H_e(t))|$. In general, however, the order of the subgroup $S(\rho_e(t > t_f)) = S(|\Psi_e(t > t_f)\rangle)$ can be larger than $S(H_e(t))$, and smaller than G . Comparison of all results in Tables 3 and 4 with Table 2 confirm the rule (70) and (71) for all ten plus four examples of Sections 3.1–3.4.

The purpose of this Section 3.5 is to prove the relation (70), and to discuss some consequences. The proof of the equality in the middle of relation (70) is in Appendix A, cf. Equation (56). The right-hand side of the relations (70) and (71) is proven by empirical evidence: The previous investigations [2–4] show that series of two laser pulses with the same polarizations can break and restore the original symmetry of the electronic ground state. From the viewpoint of this paper, Refs. [2–4] present the “largest cases” where $S(\rho_e(t > t_f)) = S(|\Psi_e(t > t_f)\rangle) = G$.

For the proof of the left-hand side of the relations (70) and (71), we use the fact that the Hamilton operator $H_e(t)$ commutes with the group elements $g \in S(H_e(t))$

$$[H_e(t), g] = 0 \text{ for } g \in S(H_e(t)) \quad (72)$$

cf. Section 2.5, Equations (11) and (13). The initial ($t = 0$) wavefunction is the electronic ground state, Equation (15). Since it is totally symmetric with respect to all symmetry elements of the group G ,

$$g |\Psi_e(t=0)\rangle = g |1A_{1g}\rangle = |1A_{1g}\rangle = |\Psi_e(t=0)\rangle \text{ for } g \in S(H_e(t)). \quad (73)$$

After the laser pulse ($t > t_f$), the laser-driven wave function has evolved to

$$|\Psi_e(t)\rangle = U_e(t) |\Psi_e(t=0)\rangle \quad (74)$$

with time evolution operator

$$U_e(t) = \hat{T} \exp[-i \int_0^t dt' H_e(t')/\hbar] \quad (75)$$

cf. Equation (25). Since the symmetry operations $g \in S(H_e(t))$ commute with $H_e(t)$, cf. Equation (72), they also commute with $U_e(t)$. Hence

$$\begin{aligned} g |\Psi_e(t)\rangle &= g U_e(t) |\Psi_e(t=0)\rangle \\ &= U_e(t) g |\Psi_e(t=0)\rangle \\ &= U_e(t) |\Psi_e(t=0)\rangle \\ &= |\Psi_e(t)\rangle \text{ for } g \in S(H_e(t)). \end{aligned} \quad (76)$$

This means that $|\Psi_e(t)\rangle$ has *at least* the symmetry $S(H_e(t))$ of the time-dependent Hamilton operator $H_e(t)$. However, at times $t \geq t_f$ after the laser pulse, the relation (76) may also hold for additional group elements $g^- \in G$ which do not belong to $S(H_e(t))$. Let $S(|\Psi_e(t > t_f)\rangle) = \{g, g^-\}$ be the subgroup of G which contains the elements $g \in S(H_e(t))$ and $g^- \notin S(H_e(t))$ which satisfy the relation (76). Now there may be two cases: either there are such “additional elements” g^- , or not. Accordingly, either $|S(H_e(t))| = |S(|\Psi_e(t > t_f)\rangle)|$ and $S(H_e(t)) = S(|\Psi_e(t > t_f)\rangle)$, or $|S(H_e(t))| < |S(|\Psi_e(t > t_f)\rangle)|$ and $S(H_e(t)) \subsetneq S(|\Psi_e(t > t_f)\rangle)$, respectively. This completes the proof of the left hand side of the relations (70) and (71). In any case, the IRREP of $|\Psi_e(t)\rangle$ is always the totally symmetric IRREP of the subgroup $S(|\Psi_e(t)\rangle)$, because all elements $g \in S(H_e(t))$ and the other ones (if any) g^- satisfy the equation (76), i.e., all the characters of $|\Psi_e(t)\rangle$ are equal to 1.

The rule (70) and (71) has (at least) two consequences, not only for the present examples, electron symmetry breaking by short (typically $t_f \leq 10$ fs) laser pulses, or two sequential laser pulses with polarization(s) \mathbf{e} in the oriented benzene of Mg-porphyrin, but by analogy also in other oriented molecules with symmetry group G of the nuclear scaffold. On the one hand, if one starts from the electronic ground state with totally symmetric IRREP and applies laser pulse(s) with polarization vector(s) \mathbf{e} , then the knowledge of the symmetry $S(H_e(t))$ of the time-dependent electronic Hamilton operator $H_e(t)$ of the molecule interacting with the laser pulse(s) (in semiclassical dipole approximation), does *not* suffice to determine the electron symmetry breaking $G \rightarrow S(\rho_e(t > t_f)) = S(|\Psi_e(t > t_f)\rangle)$. On the other hand, one has some important information about $S(\rho_e(t > t_f)) = S(|\Psi_e(t > t_f)\rangle)$, namely it has to be a subgroup of G , *and* it must contain the symmetry group $S(H_e(t))$ as a subgroup. For example, if one applies an $\mathbf{e} = \mathbf{e}_y = \mathbf{e}_1'$ polarized laser pulse (or series of pulses) on the oriented benzene, then $S(H_e(t)) = C_{2v'}1$, cf. Table 2. Hence it is impossible to design any electric fields $\mathcal{E}(t)$ of \mathbf{e}_y polarized laser pulses which would achieve electron symmetry breakings $D_{6h} \rightarrow C_s, C_2$, or C_i because these hypothetical target subgroups have order 2, below the order 4 of $S(H_e(t))$, which is the minimum according to the rule (71). Instead, there is a large variety of possible symmetry breakings $D_{6h} \rightarrow S(\rho_e(t > t_f)) =$

$S(|\Psi_e(t > t_f)\rangle)$ which satisfy the rule (70), (71), from the “smallest” case $S(\rho_e(t > t_f)) = S(|\Psi_e(t > t_f)\rangle) = C_{2v}''_1$ (cf. Table 3, entry for $|\Psi_e(t > t_f)\rangle = |A_{1g}\rangle + |E_{1u}^y\rangle$) via larger subgroups $D_{2h,1}$ (cf. Table 3, $|\Psi_e(t > t_f)\rangle = |A_{1g}\rangle + |E_{1u}^{x^2-y^2}\rangle$) or D_{3h}' (cf. Table 3, $|\Psi_e(t > t_f)\rangle = |A_{1g}\rangle + |B_{1u}\rangle$) to $G = D_{6h}$, in the extreme case of symmetry restoration—these examples are all in accord with the rule (70), (71). Likewise, if one applies an $\mathbf{e} = \mathbf{e}_x = \mathbf{e}_1$ polarized laser pulse (or series of pulses) on the oriented benzene, then $S(H_e(t)) = C_{2v}''_1$, and the rule (70), (71) again opens many possibilities, from the smallest possible subgroup $C_{2v}''_1$ (cf. Table 3, entry for $|\Psi_e(t > t_f)\rangle = |A_{1g}\rangle + |E_{1u}^x\rangle$) via the larger subgroup D_{3h}'' (cf. Table 3, $|\Psi_e(t > t_f)\rangle = |A_{1g}\rangle + |B_{2u}\rangle$) to $G = D_{6h}$. However, the rule (70), (71) also excludes many hypothetical cases, not only the subgroups of order 2 which must be discarded because this is below the order 4 of the minimum group $C_{2v}''_1$, but also larger ones such as D_{3d}' or D_{3d}'' —such symmetry groups (suggested in Ref. [1]) are excluded because they do not contain the subgroup $S(H_e(t)) = C_{2v}''_1$, i.e., they violate the theorem (70).

4. Conclusions

This work does not only confirm the discovery of Refs. [1–5], namely short laser pulses, or series of laser pulses can break electron symmetry during attosecond charge migration while conserving the symmetry group G of the nuclear scaffold, but it provides also important extensions:

- (a) Specific designs of laser pulses with selective polarization vectors and electric fields yield a large variety of electron symmetry breakings, from the original symmetry point group G of the electron density for the electronic ground state to various subgroups of G for excited superposition states. This is demonstrated here by eight plus four examples for different laser pulses applied to oriented benzene and Mg-porphyrin, cf. Tables 3 and 4, respectively. The target subgroups of the electron symmetry breaking are determined by two different approaches. First, the laser pulse(s) induce(s) intramolecular charge migration which is represented by the time-dependent one-electron density. Its symmetry can be determined by inspection of its symmetry elements, cf. Sections 3.1 and 3.2 and Figures 6–8, Figures 10 and 12. Alternatively, the symmetry subgroup can be determined by means of a systematic group-theoretical approach which is developed in Appendix A and exemplified in Sections 3.3 and 3.4. The results of the two approaches agree perfectly with each other.
- (b) One can make use of this variety (a) for laser control of electron symmetry.
- (c) Laser control of electron symmetry is, however, not *ad libitum*: For any chosen polarization(s) of the laser pulse, or series of laser pulses, the target electron symmetry must obey the theorem (70), (71), cf. Section 3.5, which means it must be a subgroup of G , and it must contain the symmetry elements of the symmetry group of the time-dependent electronic Hamiltonian for the oriented molecule interacting with the laser pulse. All examples in Tables 3 and 4 in Sections 3.3 and 3.4 satisfy this rule. It may also be used to check previous assignments of laser-driven symmetry breakings, see the discussion at the end of Section 3.5.

In retrospect, electron symmetry breaking can also be recognized in snapshots of the laser-driven one-electron densities presented in various previous publications, see, e.g., Refs. [15,36,39], but those publications centered attention on different phenomena, without any analyses or any methods for rigorous assignments of the laser-selective symmetry breaking from the original molecular point group G to specific subgroups.

The present advances should stimulate various additional extensions of the field:

- (d) The present examples are for linearly polarized laser pulses which prepare superpositions of electronic basis functions with two different IRREPs. One of these IRREPs is the totally symmetric one, cf. Tables 3 and 4 in Sections 3.3 and 3.4. This scenario makes the symmetry of the superposition state equal to the symmetry of the one-electron density, and this facilitates the applications. The general group-theoretical derivation in Appendix A is, however, ready for applications to more general cases. It

is thus a challenge to design laser pulse(s) which break electron symmetry by preparation of superpositions of basis functions that do not belong to the totally symmetry IRREP, and/or with more than two IRREPs.

- (e) Another challenge is to extend the present approach to applications of circularly polarized laser pulses, see, e.g., Refs. [2–4,15], or to laser pulses with different, preferably commensurable frequencies for two orthogonal components, see, e.g., Ref. [40].
- (f) At longer times, typically for $t > 10$ fs, the laser-driven electron density representing attosecond charge migration with broken electron symmetry will induce nuclear motions away from their initial equilibrium positions. As a working hypothesis, the nuclear and electron symmetries should adapt to each other, somewhat analogous to dynamical Jahn–Teller distortion on much longer time scales [14]. The underlying fundamental point group analyses for coupled electron and nuclear quantum dynamics driven by short laser pulses in the time domain from a few hundred to a few fs is largely *terra incognita*.
- (g) The literature has fascinating concepts for monitoring electron symmetry breaking in oriented molecules by short laser pulses, e.g., by attosecond photoionization of the superposition state [41], by time-resolved measurements of the asymmetries in photoelectron angular distributions [36,42], by high harmonic spectroscopy which is sensitive to electron symmetry [40,43,44] or by electron diffraction induced by ultrashort X-ray pulses [6,45,46]. The present predictions call for experimental applications or extensions of the concepts. The pioneering Ref. [47] points even to practical applications, i.e., photodissociation of molecules with broken electron symmetry may cause asymmetric distributions of the photoproducts in the laboratory—ultimately this could pave the way to photo-separation of the products.

Author Contributions: D.H. derived the fundamental theorems for point group analyses of laser driven attosecond charge migration (Appendices A and B) with applications to benzene and Mg-porphyrin (Sections 3.3 and 3.4), including all Tables. J.M. suggested the concepts, developed part of the theory (Sections 2.7 and 3.5) and wrote the zero order draft. J.C.T. carried out the quantum dynamics simulations and analyses (Sections 3.1 and 3.2), including Figures 5–12. The work was developed in continuous feedback between D.H., J.M., and J.C.T. including the joint preparation of the final version of the manuscript. G.H. and V.P. contributed the basic quantum chemistry calculations of the electronic energy levels and dipole transition matrix elements (Section 2.4, Figures 1–4, Table A2). All authors have read and agreed to the published version of the manuscript.

Funding: This work profits from financial support, in part by the National Key Research and Development Program of China (2017YFA0304203), the Program for Changjiang Scholars and Innovative Research Team (IRT_17R70), the National Natural Science Foundation of China (11904215), the 111 project (Grant No. D18001), the Fund for Shanxi 1331 Project Key Subjects Construction, and the Hundred Talent Program of Shanxi Province.

Data Availability Statement: Not applicable.

Acknowledgments: We are grateful to Beate Paulus (Freie Universität Berlin) for continuous support of our cooperation.

Conflicts of Interest: The authors declare no conflict of interest.

Appendix A

Symmetry Classification of Electronic Superposition States and Their Densities

Let G be the symmetry group of the electronic Hamiltonian H_e and $|\Psi_k\rangle$ be an eigenstate of H_e or a linear combination of eigenstates which transform according to the n -dimensional IRREP Γ_k of G where $n \geq 1$. It is shown (i) that a superposition $|\Psi\rangle = \sum_k |\Psi_k\rangle$ (cf. Equation (53)) transforms according to a one-dimensional IRREP Γ of a unique and maximum subgroup S of G , (ii) that by using the totally symmetric transformation behavior of $|\Psi\rangle \langle\Psi|$ under S (iii) the one-electron density $\rho(r)$ as well as (iv) $\rho(r)$ referred to the density $\rho_0(r)$ of the non-degenerate electronic ground state of H_e through $\rho(r) - \rho_0(r)$

have symmetry S too. Spin effects and time inversion invariance are ignored here. The different notation for the application of g to a function and to coordinates is ignored here too.

For the proof of proposition (i) we assume that the transformation behavior of $\Sigma_k |\Psi_k\rangle$ is determined by the behavior which is common to all $|\Psi_k\rangle$ [5]. For this purpose, those elements g are selected from G which satisfy the equation $g |\Psi_k\rangle = \chi(g) |\Psi_k\rangle$ for all k where $\chi(g)$ is independent of k so that $g |\Psi\rangle = \chi(g) |\Psi\rangle$. We show that the elements g with this property form a group $S \subseteq G$ and the $\chi(g)$ are the characters of a one-dimensional IRREP of S . Theorem A1 concerns the case that all Γ_k are one-dimensional IRREPs and Theorem A2 that at least one Γ_k is a multi-dimensional IRREP. The proofs are based on simple properties of representations.

Theorem A1. Let Γ_k and $\Gamma_{k'}$ be one-dimensional IRREPs of G and $\Gamma_k(g)$ and $\Gamma_{k'}(g)$ the characters of $g \in G$. Then the set M of all elements g with the property $\Gamma_k(g) = \Gamma_{k'}(g) = \chi(g)$ forms a unique and maximum subgroup S of G and the $\chi(g)$ are the characters of a one-dimensional IRREP of S according to which $|\Psi\rangle = \Sigma_k |\Psi_k\rangle$ transforms.

Proof. According to $\Gamma_k(E) = \Gamma_{k'}(E) = 1$, it is $\Gamma_k(gg^{-1}) = \Gamma_{k'}(gg^{-1}) = 1$ and from the property $\Gamma_k(gg^{-1}) = \Gamma_k(g) \Gamma_k(g^{-1})$ of a matrix representation, it follows that $\Gamma_k(g^{-1}) = \Gamma_{k'}(g^{-1}) = \chi(g^{-1})$. Thus, with E and g being elements of M , we obtain $g^{-1} \in M$ too. If there is a further element g' which fulfills $\Gamma_k(g') = \Gamma_{k'}(g') = \chi(g')$ then $\Gamma_k(gg') = \chi(g) \chi(g') = \Gamma_{k'}(gg')$ so that the product $gg' = g''$ and also its inverse are further elements of M . The largest set M forms the maximum subgroup S of G whose elements have the property cited. By restricting G to S the IRREPs Γ_k and $\Gamma_{k'}$ of G turn into the one-dimensional IRREP Γ of S with characters $\chi(g)$ and $\Sigma_k |\Psi_k\rangle$ transforms according to Γ . By construction, the group S is determined uniquely. \square

The result is also valid for more than two one-dimensional representations. If $|\Psi\rangle = |\Psi_k\rangle$ and Γ_k is one-dimensional then $S = G$.

Theorem A2. Let Γ_k be a multi-dimensional IRREP of G . If $\Gamma_k(g)_{pq}$ is the pq -element of the representation matrix $\Gamma_k(g)$ for $g \in G$, then the set M of all elements g with the property $\Gamma_k(g)_{pq} = \chi_k^q(g) \delta_{pq}$ forms a unique subgroup S of G . The $\chi_k^q(g)$ are the characters of a one-dimensional IRREP of S according to which the q -th basis function of Γ_k transforms.

Proof. Let the $|f_k^p\rangle$, $p = 1, \dots, n$, form a basis of the n -dimensional IRREP Γ_k of G . The transformation behavior of $|f_k^q\rangle$ is given by the elements of the columns of the representation matrix $\Gamma_k(g)$, i.e., by $g |f_k^q\rangle = \Sigma_p |f_k^p\rangle \Gamma_k(g)_{pq}$. If the elements of the q -th column vanish except for $\Gamma_k(g)_{qq}$, i.e., $\Gamma_k(g)_{pq} = \chi_k^q(g) \delta_{pq}$, then $g |f_k^q\rangle = \chi_k^q(g) |f_k^q\rangle$. Because the matrix $\Gamma_k(g)$ is unitary its q -th row also contains $\Gamma_k(g)_{qq}$ as the only non-vanishing element so that $\Gamma_k(g^{-1})_{pq} = \Gamma_k(g)^{-1}_{pq} = \chi_k^q(g)^* \delta_{pq} = \chi_k^q(g^{-1}) \delta_{pq}$. Thus, E , g , and g^{-1} are elements of M . If, additionally, the equation $\Gamma_k(g)_{pq} = \chi_k^q(g) \delta_{pq}$ is also valid for $g' \neq g$ then $[\Gamma_k(g) \Gamma_k(g')]_{rq} = \Sigma_s \Gamma_k(g)_{rs} \Gamma_k(g')_{sq} = \chi_k^q(g) \chi_k^q(g') \delta_{rq}$ so that the matrix elements of the q -th column of $\Gamma_k(g) \Gamma_k(g') = \Gamma_k(gg')$ for $gg' = g''$ vanish as well except for $\Gamma_k(g'')_{qq} = \chi_k^q(g'')$. The set of all $g \in G$ with this property forms again a unique and maximum subgroup S of G and the $\chi_k^q(g)$ are the characters of a one-dimensional IRREP of S according to which $|f_k^q\rangle$ transforms. \square

If $|\Psi\rangle = \Sigma_k |\Psi_k\rangle$ contains a $|\Psi_k\rangle$ which transforms according to a multi-dimensional IRREP Γ_k then, at first, the group S has to be determined according to which $|\Psi_k\rangle$ transforms one-dimensionally. In the subsequent procedure according to Theorem A1, this group S is used as starting point G' instead of G where the other summands must also be classified according to G' .

For proposition (ii) the transformation behavior of a product of two states $|\Psi_1\rangle|\Psi_2\rangle$ according to the Kronecker product representation $\Gamma_1 \otimes \Gamma_2$ is considered.

Theorem A3. *If state $|\Psi\rangle$ transforms according to a one-dimensional IRREP Γ of group S then the product $|\Psi\rangle\langle\Psi|$ transforms totally symmetric under S .*

Proof. The product $|\Psi\rangle\langle\Psi|$ transforms according to $\Gamma \otimes \Gamma^*$. The character of $g \in S$ in the Kronecker product representation is given by the product of the characters, $\chi(g)\chi(g)^*$, of the IRREPs Γ and Γ^* . Because $\chi(g)$ can only have the value 1 or -1 or $\exp(2\pi i/n)$, $n \geq 3$, then $\chi(g)\chi(g)^* = 1$ for all $g \in S$, i.e., $\Gamma \otimes \Gamma^*$ is the identity representation of S . \square

The proof of proposition (iii) takes into account the results for the behavior of the electronic wavefunction and the transformation behavior of a function $f(x)$ under g according to $g f(x) = f(g^{-1}x)$.

Theorem A4. *Let the electronic wavefunction $\Psi(r_1, r_2, \dots, r_N)$ transform one-dimensionally under $S \subseteq G$, i.e., $g \Psi\Psi^* = \Psi\Psi^*$ for all $g \in S$. Then the one-electron density function, defined by $\rho(r_1) = N \int \Psi(r_1, r_2, \dots, r_N) \Psi^*(r_1, r_2, \dots, r_N) (r_1, r_2, \dots, r_N) dr_2 \dots dr_N$, has the same symmetry S as $\Psi\Psi^*$. (N = number of electrons).*

Proof. By using the abbreviations $f(r_1, r_2, \dots, r_N) = N \Psi(r_1, r_2, \dots, r_N) \Psi^*(r_1, r_2, \dots, r_N)$ and $d\tau = dr_2 \dots dr_N$ and the equation $g f = f$ for $g \in S$, we find

$$\begin{aligned} \rho(r_1) &= \int f(r_1, r_2, \dots, r_N) d\tau = \int g f(r_1, r_2, \dots, r_N) d\tau \\ &= \int f(g^{-1}r_1, g^{-1}r_2, \dots, g^{-1}r_N) d\tau = \rho(g^{-1}r_1) = g \rho(r_1). \end{aligned}$$

\square

Thus the spatial symmetry of the electron density function $\rho(r)$ derived from $\Psi\Psi^*$ is given by the maximum subgroup S of G as discussed above.

The purpose of proposition (iv) is to make the symmetry elements of the electronic density function clearly recognizable in the figures. For this purpose, it is convenient to use the difference $\rho(r) - \rho_0(r)$ where $\rho_0(r)$ is the density for the non-degenerate electronic ground state of H_e .

Theorem A5. *If the one-electron density $\rho(r)$ has symmetry $S \subseteq G$ (see D) then the difference $\rho(r) - \rho_0(r)$ has the same symmetry S .*

Proof. The function $\rho_0(r)$ has symmetry G , i.e., it transforms totally symmetric under G and, thus, totally symmetric under any subgroup S of G . A linear combination of totally symmetric functions is totally symmetric too. \square

It should be noted that the classification of superpositions of electronic states according to Theorems A1 and A2 or by direct inspection of the transformation behavior of the functions under discussion can also be deduced from a correlation scheme. Such a scheme is constructed by subducing the IRREPs of G to its subgroups and shows the “genealogy” of the symmetry classification. A correlation scheme for some IRREPs of D_{6h} is given in Table A1.

Table A1. Correlation scheme for some IRREPs of D_{6h} and some of the subgroups.

D_{6h} State	D_{6h}	D_{3h}''	D_{3h}'	$D_{2h,1}$	$C_{2v,1}''$	$C_{2v,1}'$	C_{2h}	C_s
$ E_{2g}^{xy}\rangle$	E_{2g}	E'	E'	B_{1g}	B_1	B_2	A_g	A'
$ E_{2g}^{x^2-y^2}\rangle$				A_g	A_1	A_1	A_g	A'
$ E_{1u}^y\rangle$	E_{1u}	E'	E'	B_{2u}	B_1	A_1	B_u	A'
$ E_{1u}^x\rangle$				B_{3u}	A_1	B_2	B_u	A'
$ B_{1u}\rangle$	B_{1u}	A_2'	A_1'	B_{2u}	B_1	A_1	B_u	A'
$ B_{2u}\rangle$	B_{2u}	A_1'	A_2'	B_{3u}	A_1	B_2	B_u	A'
$ A_{1g}\rangle$	A_{1g}	A_1'	A_1'	A_g	A_1	A_1	A_g	A'

For determining the maximum subgroup S under which a superposition transforms one looks for the group of highest order in the correlation scheme where the summands of the superposition all transform according to the same IRREP. As an example, for the superposition $|A_{1g}\rangle + |E_{2g}^{xy}\rangle$ we find $S = C_{2h}$ because the summands both transform according to IRREP A_g in this group.

Appendix B

Symmetry Properties of Transition Dipole Moments of Benzene and Mg-Porphyrin Interacting with Linearly Polarized Laser Pulses

Appendix B.1. Preliminary Remarks

The purpose of this Appendix B is to complete the group-theoretical proof of a phenomenon which is discovered in the main text: A variety of different electron symmetry breakings in the model benzene and Mg-porphyrin can be achieved by means of selective laser pulses which yield the same population dynamics. For convenience, these laser pulses are labeled by “p”. They have the same electric field amplitudes $\mathcal{E}_p(t)$ but different polarizations \mathbf{e}_p , cf. Equation (1). Examples are documented in Figures 5, 9 and 11.

Part of the proof for the phenomenon has already been presented in Section 2.7, namely for the special cases when the same population dynamics but different electron symmetry breakings in benzene (or in Mg-porphyrin; results presented in brackets) are achieved by means of laser pulses with the same electric field amplitudes but different sets of three (two) polarization vectors which are generated by rotating the first one, say \mathbf{e}_x or \mathbf{e}_y , by C_3 and C_3^2 (C_4). The proofs in Section 2.7 exploit the fact that these rotations are symmetry operations of the point groups $G = D_{6h}$ of the model benzene (D_{4h} for Mg-porphyrin). In this Appendix B, we add the proof for another case, namely for robust population dynamics achieved by two laser pulses with the same $\mathcal{E}_p(t)$ but different polarizations \mathbf{e}_x and $\mathbf{e}_y = C_4\mathbf{e}_x$ applied to benzene (\mathbf{e}_x and $\mathbf{e}_{x'} = C_8\mathbf{e}_x$ for Mg-porphyrin). The rotation C_4 (C_8) is *not* an element of D_{6h} (D_{4h}), calling for proof beyond Section 2.7.

For the derivation, we make use of Equations (16)–(18), (22) and (23) of the main text. Accordingly, the populations (18) are the absolute squares of time-dependent coefficients for the expansion of the laser-driven wavefunction (16) in terms of electronic eigenstates.

These coefficients are obtained as solutions of the algebraic version of the time-dependent Schrödinger equation (TDSE, (22)) subject to the initial condition (17). The algebraic TDSE depends on the diagonal and off-diagonal matrix elements of the Hamiltonian (23) which consist of the electronic eigenenergies and of the transition dipole matrix elements coupled to the laser pulse, respectively. The proof of the phenomenon thus reduces to the following task namely to show that one can find proper electronic eigenstates such that different laser polarizations yield the same matrix elements. Once the matrix elements are the same, then the resulting expansion coefficients are also the same, and this implies the same laser-driven population dynamics.

Explicitly, the off-diagonal matrix elements for the laser dipole coupling (23) can be written as

$$-\mathcal{E}_p(t) \mathbf{e}_p \mathbf{d}_{mn} = -\mathcal{E}_p(t) \mathbf{e}_p \langle m | \mathbf{d} | n \rangle.$$

For benzene, the equality of these matrix elements for \mathbf{e}_x and \mathbf{e}_y polarizations calls for the equality $\langle m | d_x | n \rangle = \langle m' | d_y | n' \rangle$ for suitable sets of eigenstates. Likewise, for Mg-porphyrine, the equality of the matrix elements for \mathbf{e}_x and $\mathbf{e}_{x'}$ polarizations calls for $\langle m | d_x | n \rangle = \langle m' | d_{x'} | n' \rangle$.

The subsequent proof uses group-theoretical notations for the eigenstates, $\langle m | d_j | n \rangle \equiv \langle \Psi_i^\alpha | d_j^\beta | \Phi_k^\gamma \rangle$. Here, $|\Psi_i^\alpha\rangle$ is the i -th real-valued basis function of the n -dimensional IRREP D^α of point group G , $|\Phi_k^\gamma\rangle$ is the k -th basis function of IRREP D^γ , d_j^β is the j -th component of the dipole operator d , it arises from the dipole interaction operator $-d \cdot \mathcal{E}$ and depends on the polarization direction of the electric vector \mathcal{E} with respect to which it is defined. In this note the polarization directions are x and y and d_j thus transforms like one of the Cartesian basis vectors e_x , e_y or one of the functions p_x , p_y and, thus, for $G = D_{6h}$ (D_{4h}), d_x , d_y transform according to the IRREP $D^\beta = E_{1u}$ (E_u).

The matrix element is discussed through the general relation [48]

$$\langle \Psi_i^\alpha | d_j^\beta | \Phi_k^\gamma \rangle = 0 \text{ unless } D^\beta \otimes D^\gamma \supset D^\alpha. \quad (\text{A1})$$

Thus, a transition is “symmetry allowed” if the Kronecker product $D^\beta \otimes D^\gamma$ contains D^α because $D^{\alpha*} \otimes D^\alpha$ contains the identity representation so that the integral can be non-zero. Otherwise, the transition is “forbidden”. The integral can be evaluated if that part of $d_j^\beta | \Phi_k^\gamma \rangle$ is known which transforms like $|\Psi_i^\alpha\rangle$. For this purpose the basis vectors of the reduced product $D^\beta \otimes D^\gamma = \sum_\delta n_\delta D^\delta$ have to be determined. The general procedure consists of introducing two bases $\{e_j^\beta\}$ and $\{e_k^\gamma\}$ which reflect the transformation behavior of the sets $\{d_j^\beta\}$ and $\{\Phi_k^\gamma\}$ without considering their physical nature. They are coupled together to linear combinations of the form $|e_i^\delta\rangle = \sum_{j,k,\mu} C_{\beta j, \gamma k}^{\delta i \mu} |e_j^\beta e_k^\gamma\rangle$ where $\mu = 1, \dots, n_\delta$. The coefficients $C_{\beta j, \gamma k}^{\delta i \mu}$ are called “coupling” or “Clebsch Gordan” coefficients and can be systematically constructed or determined by direct inspection of tables with basis functions for the IRREPs of G . In this note, we use real functions of s , p , d , or f type whose transformation behavior is given in character tables so that the linear combinations are determined by inspection.

Appendix B.2. Reduced Products and Their Bases

In case of D_{6h} we discuss the following Kronecker products $\otimes D^\gamma$:

$$\begin{aligned} E_{1u} \otimes E_{1u} &= A_{1g} \oplus A_{2g} \oplus E_{2g}, \\ E_{1u} \otimes E_{2g} &= B_{1u} \oplus B_{2u} \oplus E_{1u}. \end{aligned}$$

The basis for $E_{1u} \otimes E_{1u}$ is given by $(d_x | E_{1u}^x \rangle, d_x | E_{1u}^y \rangle, d_y | E_{1u}^x \rangle, d_y | E_{1u}^y \rangle)$ and the products $| e_j^\beta e_k^\gamma \rangle$ transform like $xx', xy', yx',$ and yy' where x and x' denote different functions with the same transformation behavior. The bases in the reduced product are:

$$\begin{array}{l} \text{Bases} \\ \text{transform like} \\ \text{with } \varphi \text{ parts} \end{array} \quad \begin{array}{l} E_{1u} \otimes E_{1u} \\ (xx', xy', yx', yy') \end{array} = \begin{array}{l} A_{1g} \\ xx' + yy' \\ x^2 + y^2 \end{array} \oplus \begin{array}{l} A_{2g} \\ xy' - yx' \\ R_Z \end{array} \oplus \begin{array}{l} E_{2g} \\ (xx' - yy', xy' + yx') \\ x^2 - y^2, xy \\ (\cos 2\varphi, \sin 2\varphi) \end{array} \quad (A2)$$

Likewise, the basis for $E_{1u} \otimes E_{2g}$ is given by $(d_x | E_{2g}^{x^2-y^2} \rangle, d_x | E_{2g}^{xy} \rangle, d_y | E_{2g}^{x^2-y^2} \rangle, d_y | E_{2g}^{xy} \rangle)$ and the products $| e_j^\beta e_k^\gamma \rangle$ transform like $x \cdot (x'^2 - y'^2), x \cdot 2x'y', y \cdot (x'^2 - y'^2), y \cdot 2x'y'$. Factor 2 is used for getting the same normalization of the functions as can be seen by their φ -parts $\cos 2\varphi$ and $\sin 2\varphi$. If the products are abbreviated to xX', xY', yX', yY' the bases in the reduced product are:

$$\begin{array}{l} \text{Bases} \\ \text{transform like} \\ \text{with } \varphi \text{ parts} \end{array} \quad \begin{array}{l} E_{1u} \otimes E_{2g} \\ (xX', xY', yX', yY') \end{array} = \begin{array}{l} B_{2u} \\ xX' - yX' \\ x(x^2 - 3y^2) \\ \cos 3\varphi \end{array} \oplus \begin{array}{l} B_{1u} \\ xY' + yX' \\ y(3x^2 - y^2) \\ \sin 3\varphi \end{array} \oplus \begin{array}{l} E_{1u} \\ (xX' + yY', xY' - yX') \\ \{x(x^2 + y^2), y(x^2 + y^2)\} \\ (\cos \varphi, \sin \varphi) \end{array} \quad (A3)$$

In case of D_{4h} the same procedure leads to

$$\begin{array}{l} \text{Bases} \\ \text{transform like} \\ \text{with } \varphi \text{ parts} \end{array} \quad \begin{array}{l} E_u \otimes E_u \\ (xx', xy', yx', yy') \end{array} = \begin{array}{l} A_{1g} \\ xx' + yy' \\ (x^2 + y^2) \end{array} \oplus \begin{array}{l} A_{2g} \\ xy' - yx' \\ R_Z \end{array} \oplus \begin{array}{l} B_{1g} \\ xx' - yy' \\ x^2 - y^2 \\ \cos 2\varphi \end{array} \oplus \begin{array}{l} B_{2g} \\ xy' + yx' \\ xy \\ \sin 2\varphi \end{array} \quad (A4)$$

It should be noted that the φ -parts of these functions for D_{6h} and D_{4h} systems determine their transformation behavior because the θ -parts are given by powers of $\sin \theta$ and, therefore, they are invariant with respect to the reflection σ_h across the x - y -plane and improper rotations $S_n = \sigma_h C_n = i\bar{C}_n$.

Appendix B.3. Some Transition Dipole Moments

For evaluating the integrals, the relations Ref. [48].

$$\langle \Psi_i^\alpha | \Phi_j^\delta \rangle = 0 \text{ unless } \alpha = \delta \text{ and } i = j, \quad (A5)$$

$$\langle \Psi_i^\alpha | \Phi_i^\alpha \rangle = \text{constant}, i = 1, 2, \dots, n \quad (A6)$$

are used. Equation (A5) reflects the orthogonality of basis functions of different IRREPs D^α and D^δ as well as that of the basis functions of one and the same n -dimensional IRREP, $n > 1$. Relation (A6) means that the scalar products $\langle \Psi_i^\alpha | \Phi_i^\alpha \rangle$ for all i have the same value if $|\Psi_i^\alpha\rangle$ and $|\Phi_i^\alpha\rangle$ transform exactly in the same way. Some examples are discussed where we use $\langle \Psi | \mathbf{d} \Phi \rangle = \langle \Phi | \mathbf{d} \Psi \rangle$ for real functions.

$$\langle A_{1g} | \mathbf{d} E_{1u} \rangle = \langle E_{1u} | \mathbf{d} A_{1g} \rangle$$

This expression represents the integrals $\langle A_{1g} | d_x E_{1u}^x \rangle, \langle A_{1g} | d_x E_{1u}^y \rangle, \langle A_{1g} | d_y E_{1u}^x \rangle, \langle A_{1g} | d_y E_{1u}^y \rangle$. From (A6), we have $\langle E_{1u}^x | d_x A_{1g} \rangle = \langle E_{1u}^y | d_y A_{1g} \rangle = \text{constant}$ and from (A5) $\langle E_{1u}^x | d_y A_{1g} \rangle = \langle E_{1u}^y | d_x A_{1g} \rangle = 0$. We show that Equation (A2) leads to the same results. From (A2) and (A6) we find $\langle A_{1g} | A_{1g} \rangle = \langle A_{1g} | xx' + yy' \rangle = \text{constant}$ and from $\langle A_{1g} | E_{2g} \rangle = 0$ it follows $\langle A_{1g} | xx' - yy' \rangle = 0$ so that $\langle A_{1g} | xx' \rangle = \langle A_{1g} | yy' \rangle = \text{constant}$ or $\langle A_{1g} | d_x E_{1u}^x \rangle = \langle A_{1g} | d_y E_{1u}^y \rangle = \text{constant}$. Additionally, from (A2) and (A5) $\langle A_{1g} | A_{2g} \rangle = \langle A_{1g} | E_{2g} \rangle = 0$ so that $\langle A_{1g} | xy' - yx' \rangle = \langle A_{1g} | xy' + yx' \rangle = 0$ and, therefore, $\langle A_{1g} | d_x E_{1u}^y \rangle = \langle A_{1g} | d_y E_{1u}^x \rangle = 0$.

In case of D_{4h} the analogous discussion of $\langle A_{1g} | d | E_u \rangle$ leads to the same results by using (A5), (A6) and Equation (A4) except for index u instead of $1u$.

$$\langle E_{1u} | d | E_{2g} \rangle = \langle E_{2g} | d | E_{1u} \rangle$$

Equations (A2) and Equations (A5) and (A6) yield $\langle E_{2g}^{x^2-y^2} | x^2-y^2 \rangle = \langle E_{2g}^{xy} | 2xy \rangle =$ constant and $\langle E_{2g}^{x^2-y^2} | x^2+y^2 \rangle = \langle E_{2g}^{x^2-y^2} | xy \rangle = 0$. Hence, e.g., $\langle E_{2g}^{x^2-y^2} | x^2 \rangle = -\langle E_{2g}^{x^2-y^2} | y^2 \rangle$ which can be interpreted as $\langle E_{1u}^x | d_x | E_{2g}^{x^2-y^2} \rangle = -\langle E_{1u}^y | d_y | E_{2g}^{x^2-y^2} \rangle$.

These results and analogous ones are summarized in Table A2. They follow from symmetry alone. Numerical values calculated by quantum chemical methods are added, cf. Section 2.4. The equality of the matrix elements yields the corresponding equality of the population dynamics, as documented in Figure 5, Figure 9, Figure 11, cf. the last column of Table A2.

Table A2. Transition dipole moments $\langle \Psi_i^{\alpha} | d_j^{\beta} | \Phi_k^{\gamma} \rangle$, $j = x, y$, for some D_{6h} and D_{4h} states.

Transition $ \Psi\rangle \rightarrow \Phi\rangle$ (a)	Integrals (b,c)	$ c_{mn}^{(i)} $ [ea ₀]	cf. Fig.
D_{6h}			
$ A_{1g}\rangle \rightarrow B_{2u}\rangle$	(f)		
$\rightarrow B_{1u}\rangle$	(f)		
$\rightarrow E_{1u}\rangle$	(a) $\langle mA_{1g} d_x nE_{1u}^x \rangle = \langle mA_{1g} d_y nE_{1u}^y \rangle = c_{mn}^{(1)}$ (d) (f) $\langle mA_{1g} d_x nE_{1u}^y \rangle = \langle mA_{1g} d_y nE_{1u}^x \rangle = 0$	$ c_{11}^{(1)} = 2.36$ $ c_{12}^{(1)} = 0.16$ $ c_{13}^{(1)} = 0.03$ $ c_{21}^{(1)} = 0.93$ $ c_{22}^{(1)} = 0.51$	5,9
$\rightarrow E_{2g}\rangle$	(f)		
$ E_{1u}\rangle \rightarrow B_{2u}\rangle$	(f)		
$\rightarrow B_{1u}\rangle$	(f)		
$\rightarrow E_{2g}\rangle$	(a) $\langle mE_{1u}^x d_x nE_{2g}^{x^2-y^2} \rangle = \langle mE_{1u}^x d_y nE_{2g}^{xy} \rangle = c_{mn}^{(2)}$ $= -\langle mE_{1u}^y d_y nE_{2g}^{x^2-y^2} \rangle = \langle mE_{1u}^y d_x nE_{2g}^{xy} \rangle$ (f) $\langle mE_{1u}^x d_y nE_{2g}^{x^2-y^2} \rangle = \langle mE_{1u}^x d_x nE_{2g}^{xy} \rangle$ $= \langle mE_{1u}^y d_x nE_{2g}^{x^2-y^2} \rangle = \langle mE_{1u}^y d_y nE_{2g}^{xy} \rangle = 0$	$ c_{11}^{(2)} = 0.38$ $ c_{21}^{(2)} = 0.67$	9

Table A2. Cont.

Transition $ \Psi\rangle \rightarrow \Phi\rangle$ (a)	Integrals (b,c)	$ c_{mn}^{(i)} $ [ea ₀]	cf. Fig.
D_{4h}			
$ A_{1g}\rangle \rightarrow E_{1u}\rangle$	(a) $\langle mA_{1g} d_x nE_u^x\rangle = \langle mA_{1g} d_y nE_u^y\rangle = c_{mn}^{(3)}$ (d) (f) $\langle mA_{1g} d_x nE_u^y\rangle = \langle mA_{1g} d_y nE_u^x\rangle = 0$	$ c_{11}^{(3)} = 5.41$	11

(a) For real-valued wavefunctions $\langle \Psi_i^\alpha | d_j^\beta | \Phi_k^\gamma \rangle = \langle \Phi_k^\gamma | d_j^\beta | \Psi_i^\alpha \rangle$. For the discussion of the integral on the right hand side the Kronecker product $D^\beta \otimes D^\gamma$ has to be replaced by $D^\beta \otimes D^\alpha$. (b) (a) = symmetry allowed, (f) = forbidden. (c) The present discrimination of symmetry allowed and forbidden transitions agrees with Ref. [1]. (d) The integrals are invariant under rotation of $d_j^\beta \Phi_k^\gamma$ about the z axis, in particular $\langle A_{1g}|d_x E_u^x\rangle = \langle A_{1g}|d_{x'} E_u^{x'}\rangle$ where $e_{x'} = C_8 e_x$; see Section 3.

Appendix B.4. The Invariance of $\langle A_{1g}|d_x E_{1u}^x\rangle$ with Respect to Rotation of $d_x E_{1u}^x$

The relations $\langle A_{1g}|d_x E_{1u}^x\rangle = \langle A_{1g}|d_y E_{1u}^y\rangle = c$ and $\langle A_{1g}|d_x E_{1u}^y\rangle = \langle A_{1g}|d_y E_{1u}^x\rangle = 0$ or the abridged version $\langle A_{1g}|x^2\rangle = \langle A_{1g}|y^2\rangle = c$ and $\langle A_{1g}|xy\rangle = 0$ are invariant under the rotation R of the functions x and y according to $x' = x \cos \alpha + y \sin \alpha$, $y' = -x \sin \alpha + y \cos \alpha$. This is verified by replacing x^2 , y^2 , and xy by x'^2 , y'^2 , and $x'y'$ in the matrix elements, respectively. The result is $\langle A_{1g}|x'^2\rangle = \langle A_{1g}|x^2\rangle$. This is the reason why the transition from the ground state to a laser-induced $|E_{1u}\rangle$ or $|E_u\rangle$ state has the same probability regardless of whether this state is induced in the direction of an edge or a vertex of a **D_{6h}** or **D_{4h}** nuclear framework. The behavior is valid not only for the point groups **D_{6h}** and **D_{4h}**, but for all point groups for which $x^2 - y^2$ and xy are basis functions for 1-dimensional IRREPs different from the identity representation, or for a 2-dimensional IRREP.

It should be noted that the equality $\langle A_{1g}|d_{x'} E_{1u}^{x'}\rangle = \langle A_{1g}|d_x E_{1u}^x\rangle$ is known if the rotation R is a symmetry operation $R = g \in G$ because then $R|A_{1g}\rangle = |A_{1g}\rangle$ and the invariance property $\langle R A_{1g} | R \mathbf{d} \Phi \rangle = \langle A_{1g} | \mathbf{d} \Phi \rangle$ leads to $\langle A_{1g} | R \mathbf{d} \Phi \rangle = \langle A_{1g} | \mathbf{d} \Phi \rangle$, see also Section 2.7.

References

1. Ulusoy, I.S.; Nest, M. Correlated Electron Dynamics: How Aromaticity Can Be Controlled. *J. Am. Chem. Soc.* **2011**, *133*, 20230–20236. [\[CrossRef\]](#)
2. Liu, C.; Manz, J.; Ohmori, K.; Sommer, C.; Takei, N.; Tremblay, J.C.; Zhang, Y. Attosecond Control of Restoration of Electronic Structure Symmetry. *Phys. Rev. Lett.* **2018**, *121*, 173201. [\[CrossRef\]](#) [\[PubMed\]](#)
3. Liu, C.; Manz, J.; Tremblay, J.C. Comment on not only breaking but also restoring the symmetry of the electronic structure of a small molecule by means of laser pulses. *Faraday Discuss.* **2018**, *212*, 598–600.
4. Liu, C.; Manz, J.; Tremblay, J.C. From Symmetry Breaking via Charge Migration to Symmetry Restoration in Electronic Ground and Excited States: Quantum Control on the Attosecond Time Scale. *Appl. Sci.* **2019**, *9*, 953. [\[CrossRef\]](#)
5. Haase, D.; Manz, J.; Tremblay, J.C. Attosecond Charge Migration Can Break Electron Symmetry While Conserving Nuclear Symmetry. *J. Phys. Chem. A* **2020**, *124*, 3329–3334. [\[CrossRef\]](#) [\[PubMed\]](#)
6. Bouakline, F.; Tremblay, J.C. Is it really possible to control aromaticity of benzene with light? *Phys. Chem. Chem. Phys.* **2020**, *22*, 15401–15412. [\[CrossRef\]](#)
7. Mineo, H.; Lin, S.H.; Fujimura, Y. Vibrational effects on UV/Vis laser-driven π -electron ring currents in aromatic ring molecules. *Chem. Phys.* **2014**, *442*, 103–110. [\[CrossRef\]](#)
8. Despré, V.; Marciniak, A.; Lorient, V.; Galbraith, M.C.E.; Rouzée, A.; Vrakking, M.J.J.; Lépine, F.; Kuleff, A.I. Attosecond Hole Migration in Benzene Molecules Surviving Nuclear Motion. *J. Phys. Chem. Lett.* **2015**, *6*, 426–431. [\[CrossRef\]](#)
9. Hermann, G.; Liu, C.; Manz, J.; Paulus, B.; Pérez-Torres, J.F.; Pohl, V.; Tremblay, J.C. Multidirectional Angular Electronic Flux during Adiabatic Attosecond Charge Migration in Excited Benzene. *J. Phys. Chem. A* **2016**, *120*, 5360–5369. [\[CrossRef\]](#)
10. Jia, D.; Manz, J.; Paulus, B.; Pohl, V.; Tremblay, J.C.; Yang, Y. Quantum control of electronic fluxes during adiabatic attosecond charge migration in degenerate superposition states of benzene. *Chem. Phys.* **2017**, *482*, 146–159. [\[CrossRef\]](#)

11. Hermann, G.; Liu, C.; Manz, J.; Paulus, B.; Pohl, V.; Tremblay, J.C. Attosecond angular flux of partial charges on the carbon atoms of benzene in non-aromatic excited state. *Chem. Phys. Lett.* **2017**, *683*, 553–558. [CrossRef]
12. Hermann, G.; Pohl, V.; Dixit, G.; Tremblay, J.C. Probing Electronic Fluxes via time-Resolved X-Ray Scattering. *Phys. Rev. Lett.* **2020**, *124*, 013002. [CrossRef] [PubMed]
13. Altmann, S.L.; Herzig, P. *Point-Group Theory Tables*; Clarendon: Oxford, UK, 1994; ISBN 0-19-855226-2.
14. Bunker, P.R.; Jensen, P. *Molecular Symmetry and Spectroscopy*; National Research Council: Ottawa, ON, Canada, 1998; ISBN 0-660-17519-3.
15. Barth, I.; Manz, J. Periodic Electron Circulation Induced by Circularly Polarized Laser Pulses: Quantum Model Simulations for Mg Porphyrin. *Angew. Chem. Int. Ed.* **2006**, *45*, 2962–2965. [CrossRef] [PubMed]
16. Barth, I.; Manz, J.; Shigeta, Y.; Yagi, K. Unidirectional electronic ring current driven by a few cycle circularly polarized laser pulse: Quantum model simulations for Mg-porphyrin. *J. Am. Chem. Soc.* **2006**, *128*, 7043–7049. [CrossRef] [PubMed]
17. Dunning, T.H., Jr. Gaussian basis sets for use in correlated molecular calculations. I. The atoms boron through neon and hydrogen. *J. Chem. Phys.* **1989**, *90*, 1007–1023. [CrossRef]
18. Werner, H.J.; Knowles, P.J.; Knizia, G.; Manby, F.R.; Schütz, M.; Celani, P.; Korona, T.; Lindh, R.; Mitrushenkov, A.; Rauhut, G.; et al. Molpro, Version 2012.1, A Package of Ab Initio Programs. 2012. Available online: <http://www.molpro.net> (accessed on 20 November 2020).
19. Hashimoto, T.; Nakano, H.; Hirao, K. Theoretical study of the valence $\pi \rightarrow \pi^*$ excited states of polyacenes: Benzene and naphthalene. *J. Chem. Phys.* **1996**, *104*, 6244–6258. [CrossRef]
20. Yanai, T.; Tew, D.P.; Handy, N.C. A new hybrid exchange–correlation functional using the Coulomb-attenuating method (CAM-B3LYP). *Chem. Phys. Lett.* **2004**, *393*, 51–57. [CrossRef]
21. Woon, D.E.; Dunning, T.H., Jr. Gaussian basis sets for use in correlated molecular calculations. III. The atoms aluminum through argon. *J. Chem. Phys.* **1993**, *98*, 1358–1371. [CrossRef]
22. Frisch, M.J.; Trucks, G.W.; Schlegel, H.B.; Scuseria, G.E.; Robb, M.A.; Cheeseman, J.R.; Scalmani, G.; Barone, V.; Petersson, G.A.; Nakatsuji, H.; et al. *Gaussian 16, Revision A.03*; Gaussian Inc.: Wallingford, CT, USA, 2016.
23. Sundholm, D. Density functional theory study of the electronic absorption spectrum of Mg-porphyrin and Mg-etiochlorophyll-a. *Chem. Phys. Lett.* **2000**, *317*, 392–399. [CrossRef]
24. Tremblay, J.C.; Klamroth, T.; Saalfrank, P. Time-Dependent Configuration-Interaction Calculations of Laser-Driven Dynamics in Presence of Dissipation. *J. Chem. Phys.* **2008**, *129*, 084302. [CrossRef]
25. Tremblay, J.C.; Krause, P.; Klamroth, T.; Saalfrank, P. The Effect of Energy and Phase Relaxation on Dynamic Polarizability Calculations. *Phys. Rev. A* **2010**, *81*, 063420. [CrossRef]
26. Tremblay, J.C.; Klinkusch, S.; Klamroth, T.; Saalfrank, P. Dissipative Many-Electron Dynamics of Ionizing Systems. *J. Chem. Phys.* **2011**, *134*, 044311. [CrossRef] [PubMed]
27. Klinkusch, S.; Tremblay, J.C. Resolution-of-Identity Stochastic Time-Dependent Configuration Interaction for Dissipative Electron Dynamics in Strong Fields. *J. Chem. Phys.* **2016**, *144*, 184108. [CrossRef] [PubMed]
28. Hermann, G.; Pohl, V.; Tremblay, J.C.; Paulus, B.; Hege, H.-C.; Schild, A. ORBKIT—A modular Python Toolbox for Cross-Platform Post-Processing of Quantum Chemical Wavefunction Data. *J. Comput. Chem.* **2016**, *37*, 1511–1520. [CrossRef]
29. Pohl, V.; Hermann, G.; Tremblay, J.C. An Open-Source Framework for Analyzing N-Electron Dynamics: I. Multideterminantal Wave Functions. *J. Comput. Chem.* **2017**, *38*, 1515–1527. [CrossRef]
30. Hermann, G.; Pohl, V.; Tremblay, J.C. An Open-Source Framework for Analyzing N-Electron Dynamics: II. Hybrid Density Functional Theory/Configuration Interaction Methodology. *J. Comput. Chem.* **2017**, *38*, 2378–2387. [CrossRef]
31. Tremblay, J.C.; Carrington, T., Jr. Using Preconditioned Adaptive Step Size Runge-Kutta Methods for Solving the Time-Dependent Schrödinger Equation. *J. Chem. Phys.* **2004**, *121*, 11535. [CrossRef]
32. Hunter, J.D. Matplotlib: A 2D graphics environment. *Comput. Sci. Eng.* **2007**, *9*, 90–95. [CrossRef]
33. Tannor, D.J. *Introduction to Quantum Mechanics: A Time-Dependent Perspective*; University Science Books: Sausalito, CA, USA, 2012.
34. Jia, D.; Manz, J.; Schild, A.; Svoboda, V.; Yang, Y. From Nuclear Fluxes during Tunnelling to Electronic Fluxes During Charge Migration, in *Tunnelling in Molecules: Nuclear Quantum Effects from Bio to Physical Chemistry*; Kästner, J., Kozuch, S., Eds.; Theoretical and Computational Chemistry Series No. 18; Royal Society of Chemistry: Cambridge, UK, 2021; Chapter 5; pp. 167–191.
35. Woodward, R.B.; Hoffmann, R. The Conservation of Orbital Symmetry. *Angew. Chem. Int. Ed.* **1969**, *8*, 781–853. [CrossRef]
36. Chelkowski, S.; Yudin, G.L.; Bandrauk, A.D. Observing electron motion in molecules. *J. Phys. B At. Mol. Opt. Phys.* **2006**, *39*, S409–S417. [CrossRef]
37. Kraus, P.M.; Mignolet, B.; Baykusheva, D.; Rupenyanyan, A.; Horný, L.; Penka, E.F.; Grassi, G.; Tolstikhin, O.I.; Schneider, J.; Jensen, F.; et al. Measurement and Laser Control of Attosecond Charge Migration in Ionized Iodoacetylene. *Science* **2015**, *350*, 790–795. [CrossRef] [PubMed]
38. Jia, D.; Manz, J.; Yang, Y. Generation of electronic flux during femtosecond $\pi/2$ laser pulse tailored to induce adiabatic attosecond charge migration in HCCI⁺. *J. Mod. Opt.* **2017**, *64*, 960–970. [CrossRef]
39. Remacle, F.; Kienberger, R.; Krausz, F.; Levine, R.D. On the feasibility of an ultrafast purely electronic reorganization in lithium hydride. *Chem. Phys.* **2007**, *338*, 342–347. [CrossRef]
40. Yuan, K.-J.; Bandrauk, A.D. Symmetry in Circularly Polarized Molecular High-Order Harmonic Generation with Intense Circular Laser Pulses. *Phys. Rev. A* **2018**, *97*, 023408. [CrossRef]

41. Yudin, G.L.; Chelkowski, S.; Itatani, J.; Bandrauk, A.D.; Corkum, P.B. Attosecond Photoionization of Coherently Coupled Electronic States. *Phys. Rev. A* **2005**, *72*, 051401. [[CrossRef](#)]
42. Ivanov, M.Y.; Corkum, P.B.; Dietrich, P. Coherent Control and Collapse of Symmetry in a Two-Level System in an Intense Laser Field. *Laser Phys.* **1993**, *3*, 375–380.
43. Baykusheva, D.; Ahsan, M.S.; Lin, N.; Wörner, H.J. Bicircular High-Harmonic Spectroscopy Reveals Dynamical Symmetries of Atoms and Molecules. *Phys. Rev. Lett.* **2016**, *116*, 123001. [[CrossRef](#)]
44. Liu, X.; Zhu, X.; Li, L.; Li, Y.; Zhang, Q.; Lan, P.; Lu, P. Selection Rules of High-Order-Harmonic Generation: Symmetries of Molecules and Laser Fields. *Phys. Rev. A* **2016**, *94*, 033410. [[CrossRef](#)]
45. Yuan, K.-J.; Bandrauk, A.D. Exploring Coherent Electron Excitation and Migration Dynamics by Electron Diffraction with Ultrashort X-ray Pulses. *Chem. Phys.* **2017**, *19*, 25846–25852. [[CrossRef](#)]
46. Popova-Gorelova, D. Imaging Electron Dynamics with Ultrashort Light Pulses: A Theory Perspective. *Appl. Sci.* **2018**, *8*, 318. [[CrossRef](#)]
47. Martín, F.; Fernández, J.; Havermeier, T.; Foucar, L.; Weber, T.; Kreidi, K.; Schöffler, M.; Schmidt, L.; Jahnke, T.; Jagutzki, O.; et al. Single Photon-Induced Symmetry Breaking of H₂ Dissociation. *Science* **2007**, *315*, 629–633. [[CrossRef](#)] [[PubMed](#)]
48. McWeeny, R. *Symmetry, an Introduction to Group Theory and Its Applications*; Pergamon: Oxford, UK, 1963; pp. 223–233.